TWO NOVEL ULTRASONIC LENSES

by
Alain J. Nicolle, rmc, B.Eng.(RMC)

Department of Electrical Engineering
McGill University
Montreal, Quebec
March, 1991

A thesis submitted to the Faculty of Graduate Studies and Research
in partial fulfillment of the requirements for the degree of
Master of Engineering

ABSTRACT

Experimental investigations of two ultrasonic lenses are presented, a graded acoustic index lens and a cylindrical lens. The first lens is a short rod which has a graded acoustic velocity profile in the radial direction giving it the ability to focus acoustic waves. Electron probe microanalyses, optical refractive index measurements and acoustic velocity measurements are used to characterize the lens. The ray acoustics approach is used for the theoretical interpretation and the focussing behavior is visualized with a Schlieren system. Potential applications of the lens are discussed.

The cylindrical lens consists of a lead zirconate titanate (PZT) coated wire or optical fibre. The fabrication and evaluation of the lens is described. Ultrasonic measurements of miniature transducers and electronically controllable deflection are demonstrated. A novel laser ablation patterning technique is used to make an interdigital transducer with a 20μm resolution on the outer electrode of the lens for special applications. Finally, possible applications of the cylindrical lens are outlined.

RESUME

On présente les études expérimentales de deux lentilles ultrasoniques, une qui possède un index acoustique gradué et l'autre qui a une géométrie cylindrique. La première lentille est une tige courte qui a un profil gradué de vitesse acoustique le long de son diamètre tel qu'elle lui donne la capacité de focaliser des ondes acoustiques. Des microanalyses électroniques, des mesures d'index de réfraction et des mesures de vitesses acoustiques caractérisent la lentille. On utilise un modèle à rayon acoustique pour l'interprétation théorique et un système de visualisation de Schlieren pour l'observation de l'effet. Les applications possibles de la lentille sont présentées.

La lentille cylindrique est un fil métallique ou une fibre optique recouverte de zirconate titanate de plomb (PZT). On décrit sa fabrication et son évaluation. On présente des mesures ultrasoniques de transducteurs miniatures ainsi que de la déflection controllable électroniquement. On utilise une technique d'ablation par laser pour fabriquer un transducteur interdigital avec une résolution de 20μm sur l'électrode externe de la lentille pour des applications spéciales. Enfin, on examine les applications possibles de cette lentille cylindrique.

ACKNOWLEDGEMENTS

I would first like to express my gratitude to my thesis supervisor, Dr. C.K. Jen, for his interest and support which has made this study possible. He has inspired me with and taught me philosophies which are crucial for successful research. I will be forever grateful for his timeless guidance.

Many thanks go to Dr. Ralph Hsu from Algonquin College in Ottawa, Ontario for his assistance in setting up the IBM PC controlled laser ablation system. His modifications to the GW-BASIC program which runs the stepping motor controller card were essential to the success of the experiment.

I would also like to thank Prof. Z. Wang for his guidance in the derivation of the ray acoustics theory for the graded index rod and assistance during the Schlieren visualization experiments.

Special thanks are given to Christian Néron for his scanning acoustic microscope measurements and very helpful and lengthy discussions with respect to instrumentation.

The graded index rods were supplied by Mr. L. Bonnell and Dr. K. Abe at National Optics Institute in Sainte-Foy, Quebec. PZT coated optical fibres and wires were provided by Prof. M. Sayer's research group at Queen's University in Kingston, Ontario.

Finally, I would like to salute my parents whom without their support throughout my entire course of study, I would not be where I am today. And so, I dedicate this thesis and all my other academic, artistic and military achievements, to my parents, Claire and François.

This research was partially supported by the Natural Sciences and Engineering Research Council of Canada (NSERC). Special appreciation is given to Industrial Materials Institute, National Research Council of Canada where the entire thesis research has been carried out.

TABLE OF CONTENTS

LIST OF FIGURES

LIST OF TABLES

Chapter 1: Introduction

The ability to image objects with radiation has always been an important task . measurement science. Unlike other forms of radiation, an acoustic wave interacts directly with the elastic properties of the material. By using the acoustic field which propagates through an object to form an image, we can study the spatial variations of these properties. In order to achieve high spatial resolution, various kinds of acoustic lenses which focus the acoustic energy have been used. The development of acoustic microscope lenses before 1979 has been reviewed briefly by Lemons and Quate [1]. Other types of acoustic imaging systems involving focussing may also be found in [2] and in the annual proceedings of IEEE Ultrasonics Symposiums and Acoustic Imaging Conferences.

In the past decade there has been a considerable amount of efforts made to further develop various acoustic lenses operating at very high frequency such as VHF or UHF, however, most of them use a spherical [1] or cylindrical [3] concave surface. It requires very high precision to fabricate such concave surfaces. Therefore some lenses with planar geometries such as acoustic Fresnel zone plates [4]-[6] and curved surface acoustic wave interdigital transducers [7]-[9] are used as alternatives. The planar lenses mentioned above can be fabricated with ease by the standard integrated circuits technology. It is very interesting to note that there exits at least an optical counterpart for nearly all the acoustic lenses developed. The origin of such a fact could be explained from the analogy between acoustics and electromagnetics [10].

In optics, there exists a type of planar lenses named graded index (GRIN) lenses [11] or SELFOC (self-focussing) rods [12]. They are mainly glass rods having a graded index of refraction along the radial direction. The parameters that define the index distribution provide valuable new degrees of freedom for designers of optical lens or imaging systems [11]. It appears that an acoustic counterpart has not been developed. Chapter 2 of this thesis is a report devoted to the development of rods having acoustically graded index (velocity) profiles which exhibit focussing behaviors in acoustics similar to those exhibited by optical GRIN rods in optics. The two end surfaces of such GRIN rods are flat. We name them "acoustic graded index (GRIN) rods or lenses" [13]. For lens applications, as an analogy, the phase velocity at the center of either optical or acoustic GRIN rod must be less than that at the edge. One application of acoustic GRIN rods is for long acoustic imaging probes [14]. The fabrication methods for optical GRIN rods may also be used to produce acoustic GRIN rods. It is noted that optically opaque materials may be employed for acoustic rods. Furthermore, in optics only transverse waves are involved, whereas in acoustics both transverse (shear) and longitudinal waves should be considered. In chapter 4, we will also show that acoustic Fresnel zone plates may also be achieved using different acoustic velocity profiles across the rod diameter.

In-line fibre optic signal processing devices which process guided light directly within the optical fibre are becoming more significant and attractive in fibre optic communication networks. Such devices can be simple, inexpensive and of small size. Many of these devices employ acousto-optic interactions [15]-[19]. Acoustic waves are generated by piezoelectric focussed thin film transducers directly deposited on the optical fibres. These acoustic waves which are focussed radially toward the fibre axis interact with guided optical waves in optical fibres. Basically, the focussed acoustic waves will perturb the refractive index of the optical fibres and modulate the guided light. Phase modulators [15]-[18] and phase shifters [19] were constructed and their role in the current expanding single mode optical fibre communication and sensor applications was reviewed in [20].

The piezoelectric thin film materials reported to fabricate such cylindrical type of acoustic lenses were polyvinylidene fluoride (PVDF) [15], [16] and zinc oxide (ZnO) [17], [18]. PVDF transducers are not efficient for operating frequencies higher than 50MHz [15], [16]. ZnO transducers are normally fabricated using vacuum sputtering techniques, and it is very difficult to coat it around the thin diameter (large curvature and convex shape) optical fibres and with a long coating length [21]. Recently, researchers at Queen's University and at Industrial Materials Institute, National Research Council of Canada have worked together to develop an alternative piezoelectric thin coating which is lead-zirconate-titanate (PZT) for such ultrasonic lens applications. Their coating technology uses a sol-gel process [22]. Good piezoelectric and acoustic properties of such films have been demonstrated [23]-[25]. PZT thin films have also been successfully deposited on multimode optical fibres [26]. In this thesis, chapter 3 will report the further developments of these PZT cylindrical lenses. A novel laser ablation technique is developed to fabricate a complex patterns of electrodes for such lenses. In addition, miniature ultrasonic transducers and electronically controllable deflectors made by the same technology are also demonstrated.

Conclusions and suggestions for future work will be given in chapter 4.

Chapter 2: Acoustic Graded Index Lens

2.1 Introduction:

Glass rods having a graded index of refraction along the radial direction have been widely used in optical lens design. As mentioned in chapter 1, they are referred to as graded index (GRIN) lenses [11] or SELFOC rods [12]. These rods can be produced by ion exchange [12], [27]-[30], chemical vapor deposition [27], sol-gel techniques [31]-[33], etc. It has been shown that rods having a graded refractive index profile also exhibit graded leaky surface acoustic velocity variations [34], [35]. It has also been found that there exists an analogy between weakly guiding optical and acoustic fibres [36]. It is therefore expected that rods having graded acoustic velocity profiles in the radial direction possess the same "focussing" behavior as the optical GRIN lens. This chapter presents the design, fabrication and verification of the acoustic GRIN lenses.

Section 2.2 presents the element concentration, optical refractive index and acoustic velocity profile measurements of the different samples used in the experiments. An acoustic ray theory to interpret the focussing behavior is derived in section 2.3 while section 2.4 explains two methods to visualize an acoustic field. Section 2.5 presents the results of Schlieren visualization experiments and section 2.6 proposes potential applications of acoustic graded index lenses. Section 2.7 summarizes the contents of the chapter.

2.2 Profile Measurements:

2.2.1 Sample Fabrication:

Three samples with a graded index and one sample with a step index were used in the experiments. They were fabricated by the National Optics Institute (NOI) using a modified chemical vapour deposition (MCVD) method [37] which is a standard technology to fabricate optical fibre preforms. So far, NOI has been the only supplier which can provide us the designed GRIN lenses. In addition to the two commercially purchased GRIN rods (please see Figs.2.32-2.33 in section 2.5.5), all the others presented here were made by the NOI's MCVD technology. Silica rods were doped with GeO_2 and P_2O_5 to form a core and cladding. These rods, as shown in Fig.2.1, have been made to lengths of up to 40cm.

2.2.2 Element Concentration Profile:

The element concentration profiles of silicon (Si), phosphorus (P) and germanium (Ge) of each sample were measured along a radius using an electron probe micro-analysis attached to a scanning electron microscope. The sample was scanned mechanically. The scan-line was across the center of each rod. The distance between each adjacent scanned point is 100μm in the core and much more in the cladding region. From Fig.2.2 it was found that the step index sample had an averaged concentration of 3% phosphorus and 8% germanium in the core. The GRIN samples had 8%, 17%, and 31% peak germanium concentrations and 3%, 1.5% and 1.5% phosphorus concentrations in the core respectively as illustrated in Figs.2.3-2.5. There exists a dip in the germanium and phosphorus doped region near the center (position 0) of each sample and also fine oscillations across the rod. These are due to the MCVD fabrication process of the GRIN rod [37]. GRIN rods made by other techniques do not normally have such dips and fine structures. From the element concentration profiles, the core diameters were estimated to be around 5mm. It is noted that all the GRIN rods except the 31% GeO_2 doped rod have a cladding either of a ~2.5mm thick pure silica or a uniform dopant concentration. The cladding of the 31% GeO_2 doped GRIN rod was removed by mechanical polishing.

2.2.3 Optical Refractive Index Profile:

The optical refractive index profiles of the samples were measured by a York Technology (Princeton, New Jersey) device which provides a 10μm spatial resolution. Figures 2.6-2.9 show the optical refractive index profiles of the 8% GeO_2 doped step index rod, and the 8%, 17% and 31% GeO_2 doped GRIN rods, respectively. As expected, the index profiles follow the same approximate shape as the element concentration profiles, including the dip in the center and the oscillations across the diameter of the samples.

2.2.4 Acoustic Velocity Profile:

Since it is very difficult to obtain the radial distribution of bulk longitudinal, v_L, and shear wave velocity, v_S, for small diameter rods, an approach which uses reflection scanning acoustic microscopy (SAM) and the V(z) technique to obtain leaky surface acoustic wave (LSAW) and leaky surface-skimming compressional wave (LSSCW) velocities is used [3],

[35]. Such measurements have been reported previously using a 775MHz point focus beam (PFB) SAM [34]; here, a 225MHz line focus beam (LFB) SAM [3] is used. The velocity measured was along the direction perpendicular to the LFB and parallel to the radial direction of the rod. The 775MHz PFB SAM offers better spatial resolution, but the 225MHz LFB SAM provides higher accuracy in velocity measurements due to the higher signal-to-noise ratio especially for LSSCW.

Due to the defocussing requirement of V(z) measurements, the measured velocity represents an average value over the defocussed area which is about 40μm by 1000μm for the LFB SAM. All the samples, as shown in Fig.2.10, for the LFB SAM were cut to approximately a 7mm thickness and then polished; the last and the finest polishing step was with a mechanical-chemical (0.06μm) polishing. The relative accuracy in v_{LSAW} (average value) profile measurements is better than 0.1%. Since the LSSCW is very weakly excited, the signal-to-noise ratio for such a wave is much less than that for LSAW, hence less accuracy is available in v_{LSSCW} measurements. More studies are required in order to understand the effects of graded velocity profiles on the measurement accuracy. However, detailed descriptions for the V(z) measurement of the LFB SAM is given in [3]. Because LSAW and LSSCW have predominantly shear and longitudinal wave components, respectively, their velocity profiles can be regarded as those of v_S and v_L.

The LSAW and LSSCW velocity profiles of the 8% GeO_2 doped step index rod and the 8%(*), 17%(o) and 31%(Δ) GeO_2 doped GRIN rods are shown in Figs.2.11 and 2.12, respectively. The scan-line was also across the rod center. Since the LFB SAM only measures the average velocity over a 40 by 1000μm area and the measurements have been taken at a distance of 0.1mm/step, the fine details appearing in the optical refractive index profiles cannot be seen in the corresponding acoustic measurements. However, with a high spatial resolution PFB SAM the abrupt change at the rod center can be seen in [34]. From Fig.2.12 we conclude that a higher concentration of GeO_2 decreases the acoustic wave velocity. It is also found that these silica rods which have been doped with GeO_2 and P_2O_5 exhibit quite a different percentage change acoustically and optically. For example, the 31% GeO_2 doped GRIN rod shows a 2% refractive index change but a 14% LSAW and LSSCW velocity change.

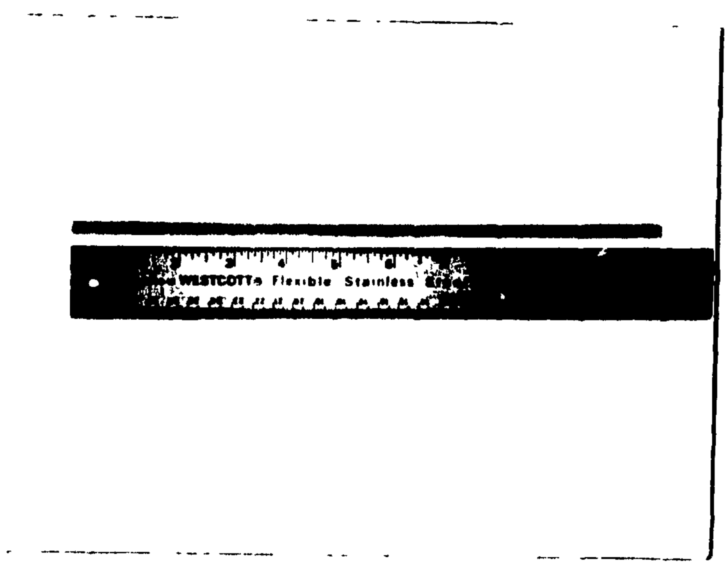

Figure 2.1 *Long GeO_2 and P_2O_5 doped preform fabricated by the National Optics Institute.*

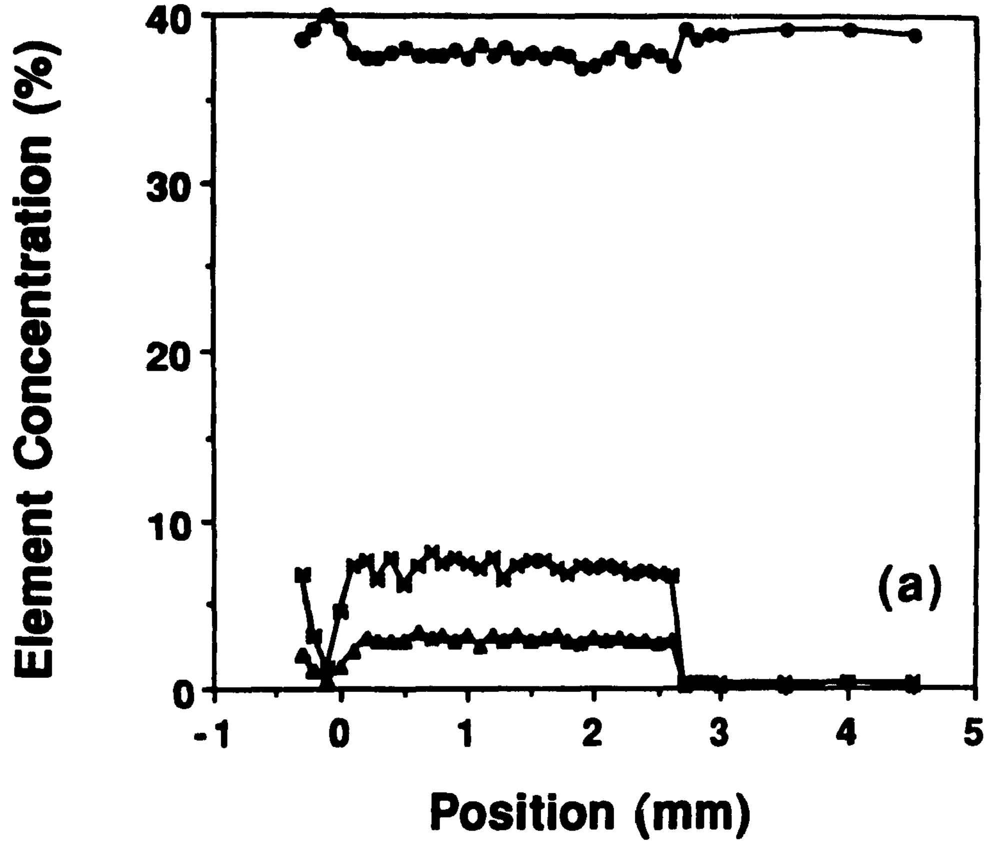

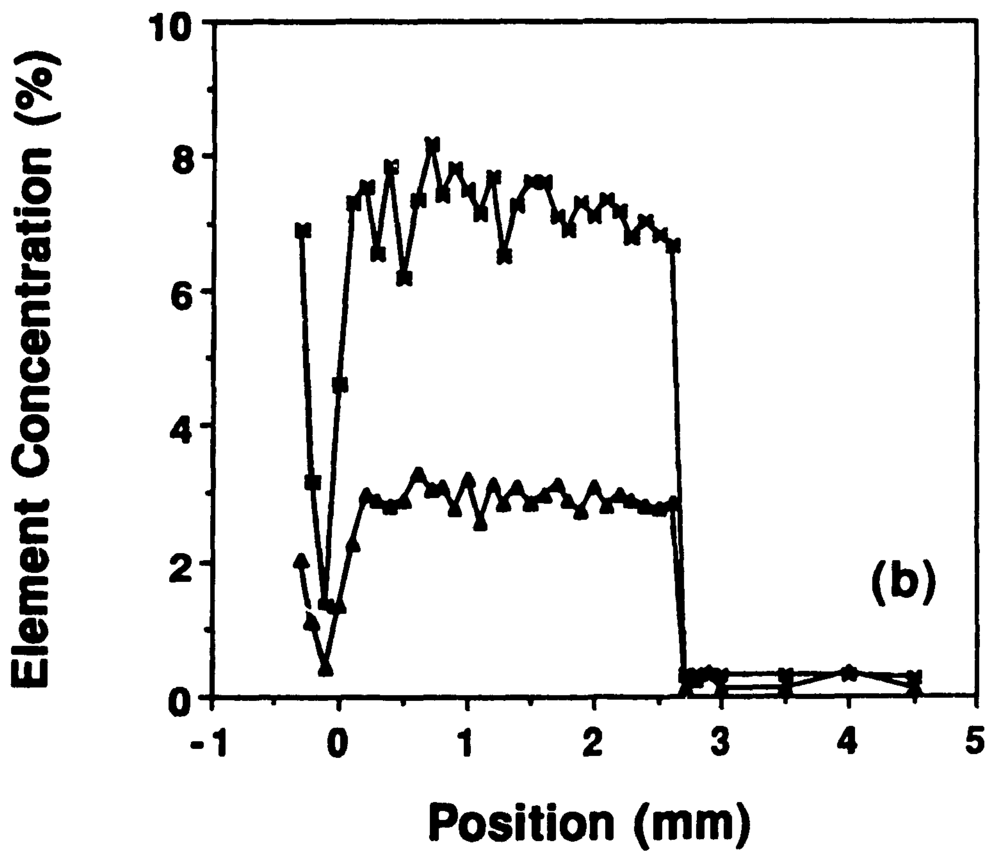

Figure 2.2 *Element concentration profiles of GeO_2 and P_2O_5 doped step index glass rod, (a) Si(•), Ge(*) and P(Δ) concentrations (b) Ge(*) and P(Δ) concentrations.*

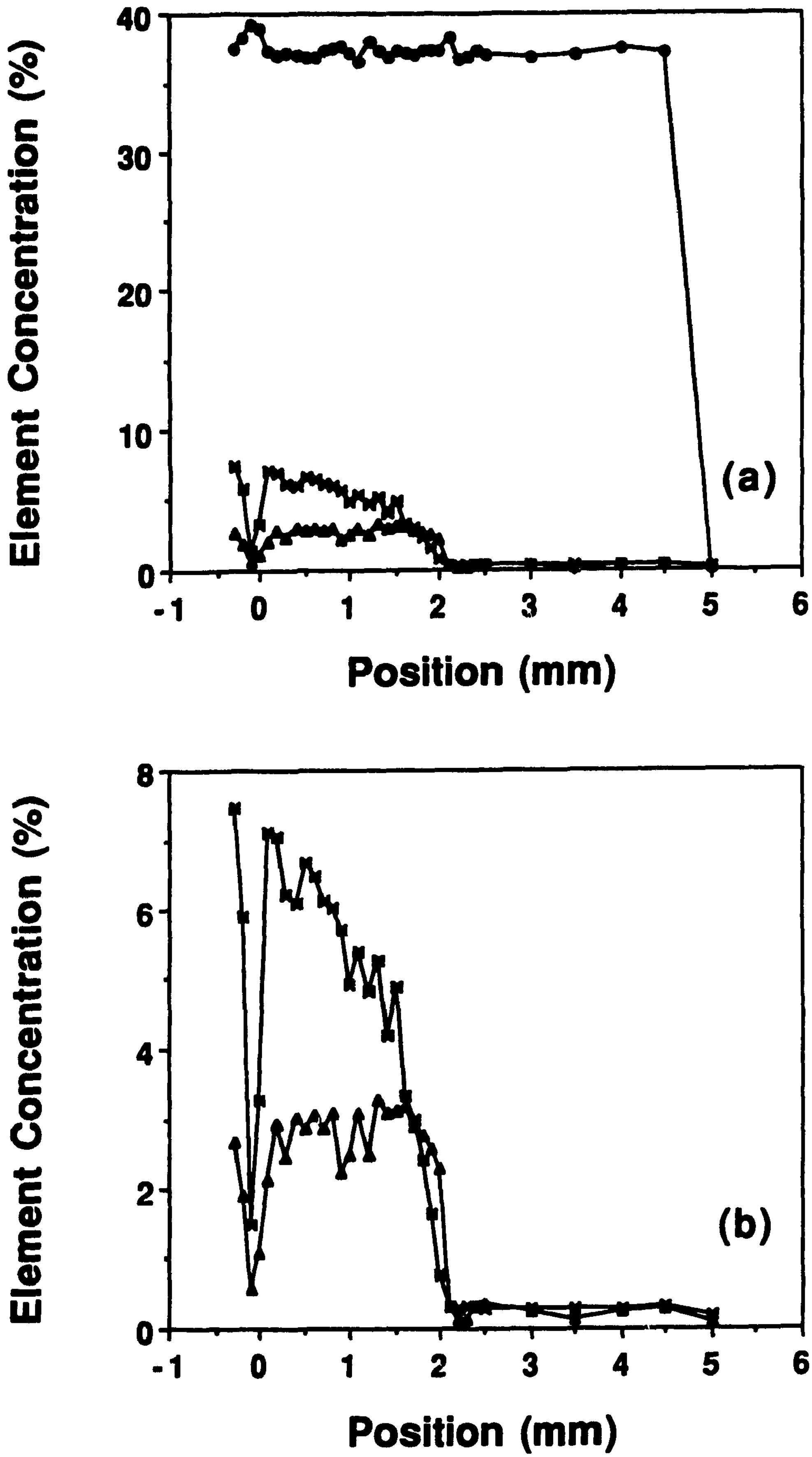

Figure 2.3 *Elem·ent concentration profiles of GeO_2 and P_2O_5 doped GRIN glass rod sample #1, (a) Si(●), Ge(*) and P(Δ) concentrations (b) Ge(*) and P(Δ) concentrations.*

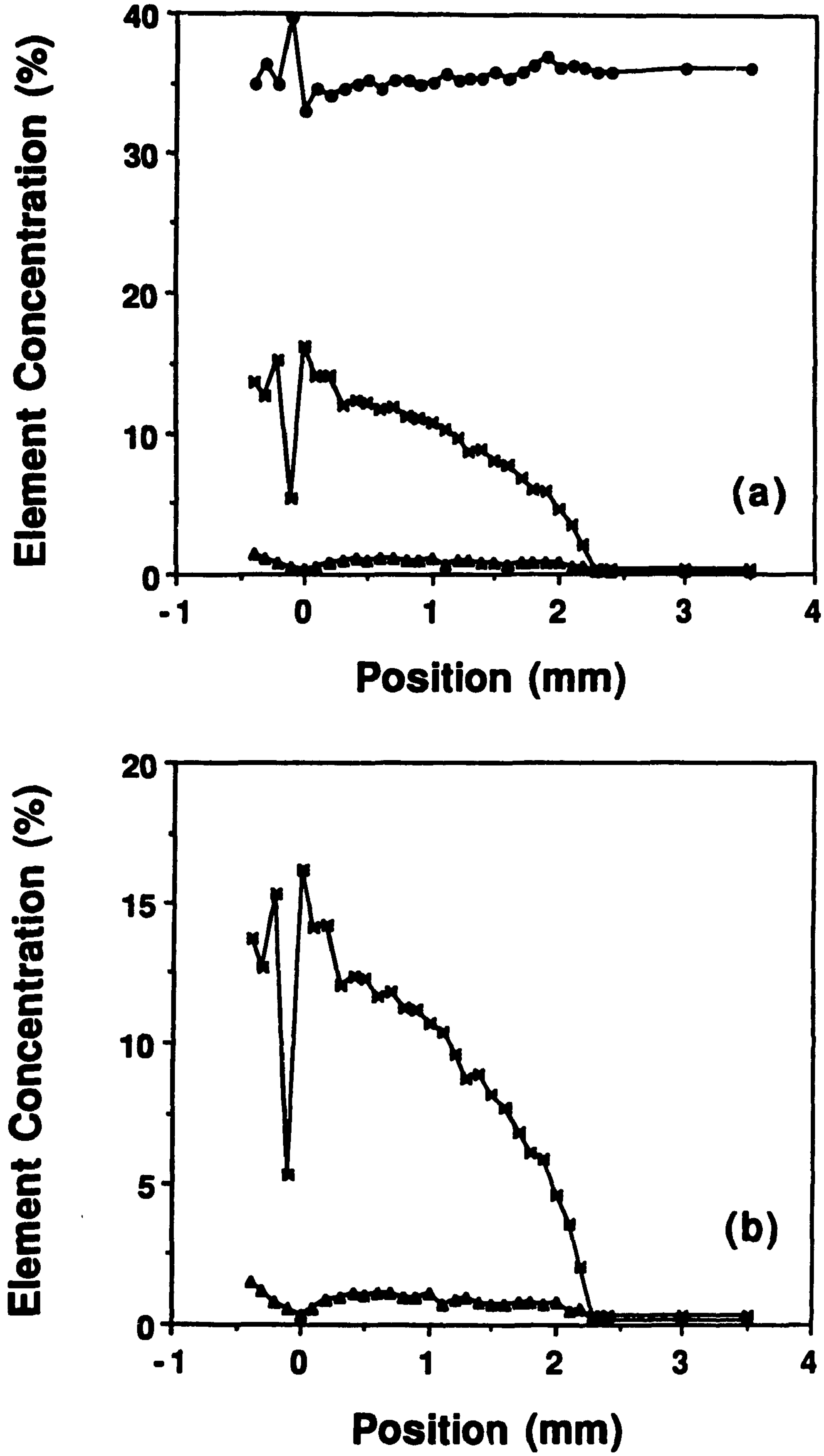

Figure 2.4 *Element concentration profiles of GeO_2 and P_2O_5 doped GRIN glass rod sample #2, (a) Si(●), Ge(*) and P(Δ) concentrations (b) Ge(*) and P(Δ) concentrations.*

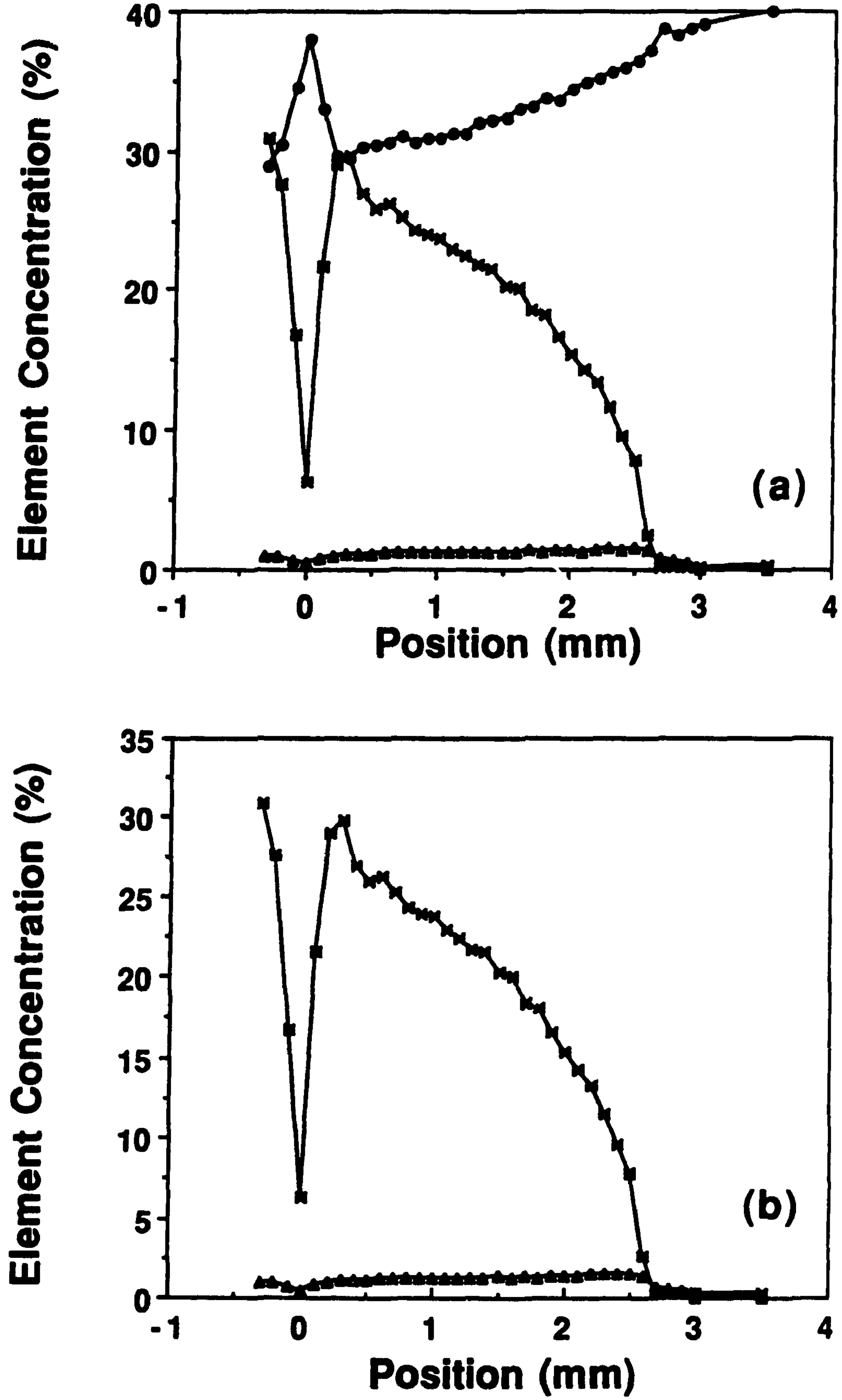

Figure 2.5 *Element concentration profiles of* GeO_2 *and* P_2O_5 *doped GRIN glass rod sample #3, (a) Si(•), Ge(*) and P(Δ) concentrations (b) Ge(*) and P(Δ) concentrations.*

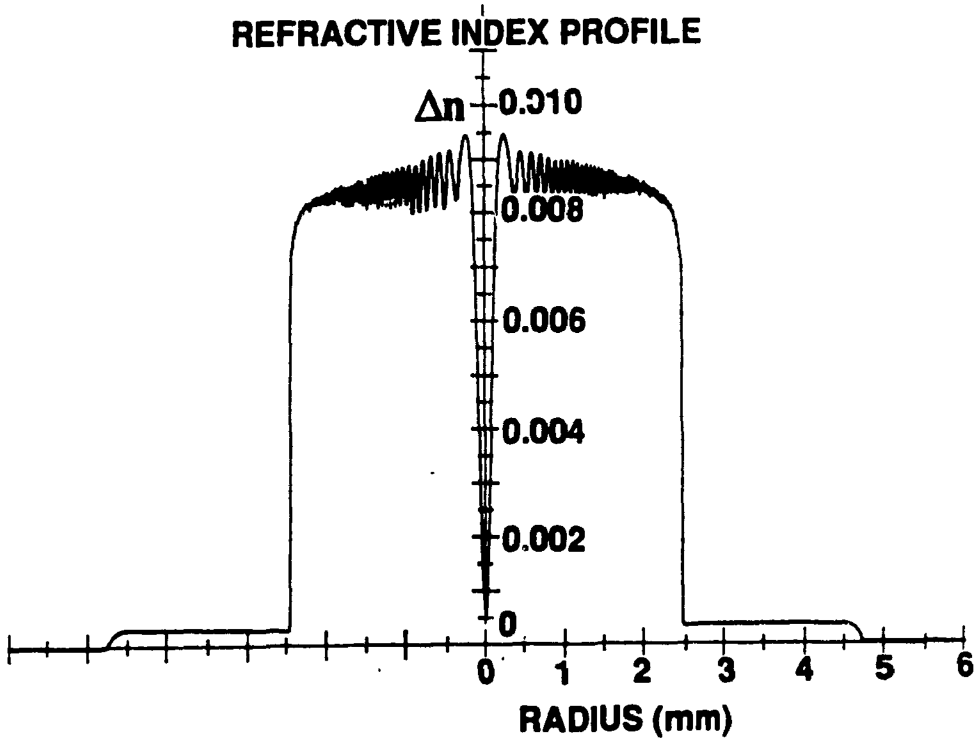

Figure 2.6 *Optical refractive index profile of 8% GeO_2 doped step index glass rod.*

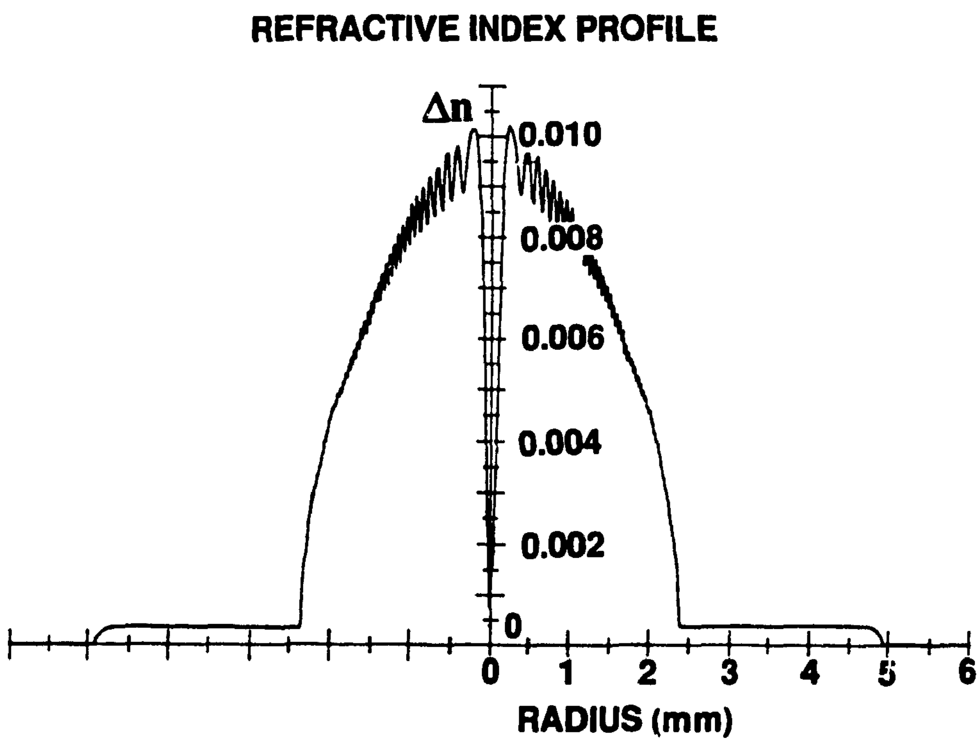

Figure 2.7 *Optical refractive index profile of 8% GeO_2 doped GRIN glass rod.*

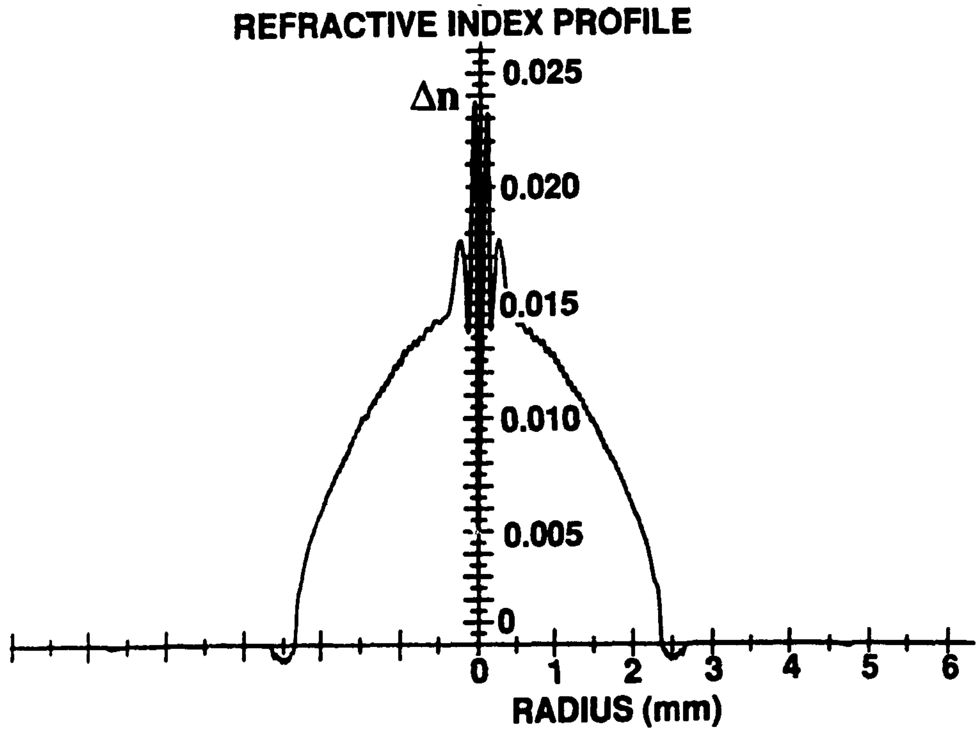

Figure 2.8 *Optical refractive index profile of 17% GeO_2 doped GRIN glass rod.*

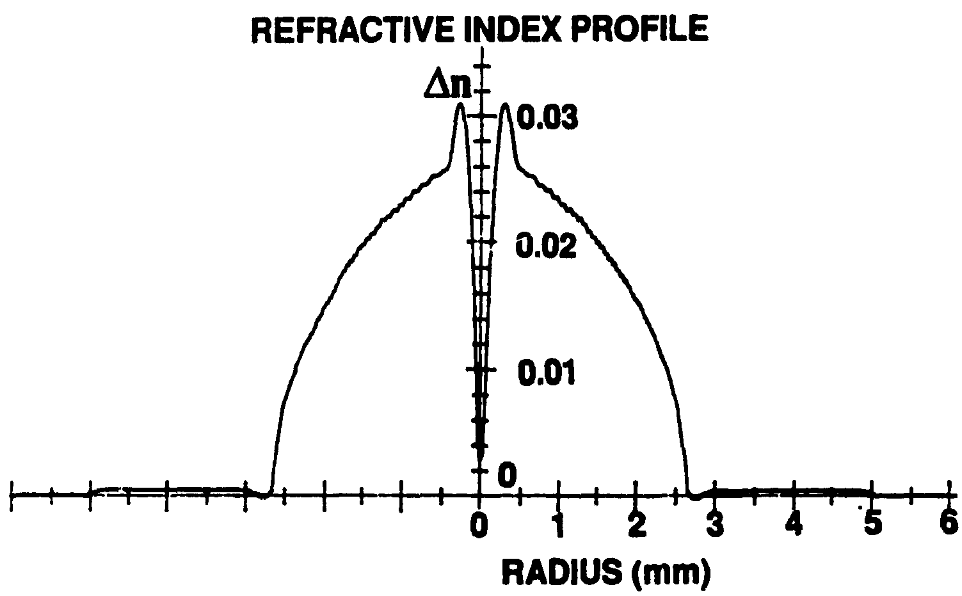

Figure 2.9 *Optical refractive index profile of 31% GeO_2 doped GRIN glass rod.*

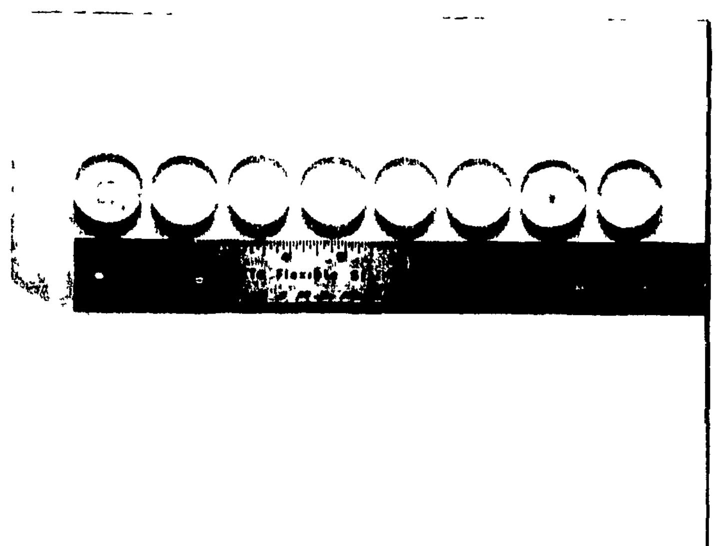

Figure 2.10 *Samples used in the measurement of the acoustic velocity profiles.*

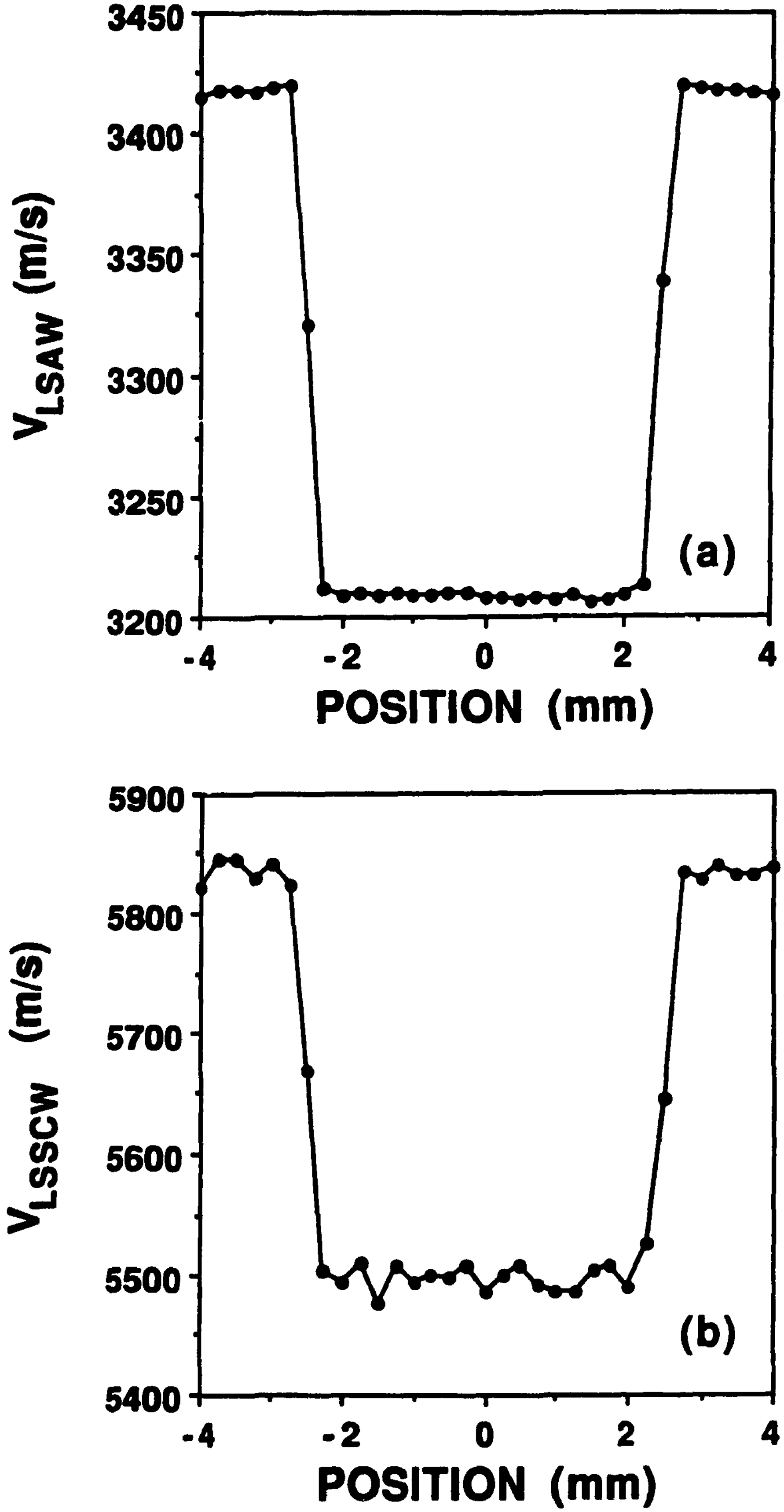

Figure 2.11 *Acoustic velocity profiles of the 8% GeO_2 doped step index glass rod, (a) v_{LSAW} and (b) v_{LSSCW}.*

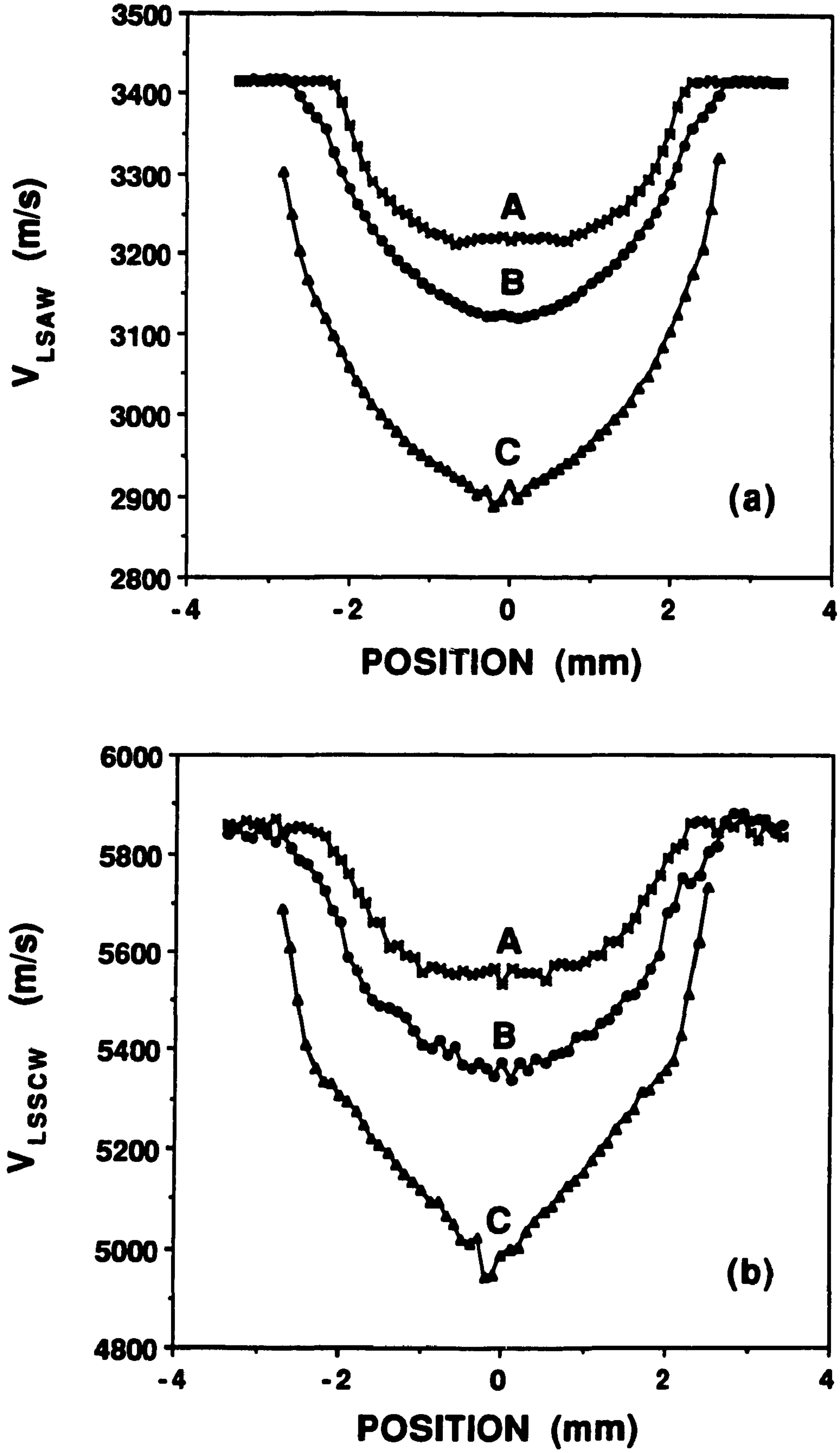

Figure 2.12 *Acoustic velocity profiles of the 8%(*), 17%(●), and 31%(▲) GeO_2 doped GRIN glass rod, (a) v_{LSAW} and (b) v_{LSSCW}.*

2.3 Theory:

2.3.1 Introduction:

When a plane wave propagates in a rod in which the refraction index follows a graded distribution where, at the center, the index is maximum, the wavefronts will gradually become sphere-like curves. It is due to the fact that a high refractive index means a low phase velocity. The waves may therefore be focussed at some position. To analyze the focussing effect in the graded index medium, it is convenient to use the ray theory to obtain the ray equation which provides two coordinate variables as functions of the third variable. In the radial graded index medium, it is useful to express r and θ as functions of z [11].

The derivation of these equations are given in section 2.3.2, while in section 2.3.3 an example with a special index distribution function is analyzed for the case where the rod is long enough for the acoustic waves to be focussed inside the rod. In section 2.3.4, a case where the length of the rod is less than a quarter pitch is analyzed. Section 2.3.5 explains a method to determine the equation of the velocity profile of our samples.

2.3.2 Derivation of the Basic Equations for the GRIN Rod:

2.3.2.1 Fermat Principle and Euler Equations:

In an inhomogeneous isotropic medium, if the acoustic velocity can be expressed in the form of $V(x,y,z)$, and if V_0 is the velocity at the reference point (x_0, y_0, z_0), the acoustic index can be defined by

$$n(x,y,z) = V_0/V(x,y,z). \tag{2.1}$$

The path of the acoustic ray starting from a point to another point in such a medium can be derived from the Fermat principle. The Fermat principle states that if C is a ray joining two points, the ray path integral

$$L = \int_{s_0}^{s} n\,ds \tag{2.2}$$

taken along C from the first point to the second point is stationary relative to its value for any other nearby curve joining the two points. Here, s is the arc length along the curve.

It is known that the corresponding four-dimensional variation problem will lead to the correct differential equations provided the integral is cast into the form

$$L = \int_{s_0}^{s} F(x, y, z, s, x', y', z') ds, \quad (2.3)$$

where it is required that F be a homogeneous function of first order with respect to x', y', z', where $x' = \frac{dx}{ds}$, $y' = \frac{dy}{ds}$ and $z' = \frac{dz}{ds}$.

Therefore,

$$F = n(x, y, z) [x'^2 + y'^2 + z'^2]^{1/2}. \quad (2.4)$$

The well-known solutions of (2.3), called the Euler equations, are

$$(\partial F / \partial x')' = \partial F / \partial x, \quad (2.5)$$

$$(\partial F / \partial y')' = \partial F / \partial y, \quad (2.6)$$

$$(\partial F / \partial z')' = \partial F / \partial z. \quad (2.7)$$

<u>2.3.2.2 Ray Equations in a Radial Graded Index Medium:</u>

2.3.2.2.1 First and Second Euler Equations in Cylindrical Coordinates:

In cylindrical coordinates, the acoustic ray path length can be expressed in the form of

$$L = \int_{z_0}^{z} F dz, \quad (2.8)$$

with

$$F = n(r) (1 + \dot{r}^2 + r^2 \dot{\theta}^2)^{1/2}, \quad (2.9)$$

where

$$\dot{r} = \frac{dr}{dz}; \quad \dot{\theta} = \frac{d\theta}{dz} \quad (2.10)$$

and we take $\frac{dz}{ds} > 0$ in the derivation.

In order to formulate the acoustic ray tracing equations of a ray starting from (r_o, θ_o, z_o), which express z and θ as a function of r, or express r and θ as a function of z, the first and second Euler equations in cylindrical coordinates can be used.

From the second Euler equation (for θ) we derive

$$n r^2 \dot{\theta} (1 + \dot{r}^2 + r^2 \dot{\theta}^2)^{-1/2} = c. \quad (2.11)$$

The constant c has the same sign as $\dot{\theta}$ and it represents the well-known skewness invariant valid for any ray in any system having cylindrical symmetry. From (2.11), we obtain

$$\dot{\theta} = \frac{c(1+\dot{r}^2)^{1/2}}{mr^2}, \tag{2.12}$$

where

$$m = \left(n^2 - \frac{c^2}{r^2}\right)^{1/2}. \tag{2.13}$$

The first Euler equation (for r) is

$$\frac{d}{ds}[n\dot{r}(1+\dot{r}^2+r^2\dot{\theta}^2)^{-1/2}] = (1+\dot{r}^2+r^2\dot{\theta}^2)^{1/2}\frac{dn}{dr} + nr\dot{\theta}^2(1+\dot{r}^2+r^2\dot{\theta}^2)^{-1/2}. \tag{2.14}$$

By substituting (2.12) into (2.14) to eliminate $\dot{\theta}$, and by using (2.13), we derive

$$\frac{d}{ds}\left[\frac{m\dot{r}}{(1+\dot{r}^2)^{1/2}}\right] = (1+\dot{r}^2)^{1/2}\frac{dn}{dr}. \tag{2.15}$$

From (2.15) we have

$$\left[\frac{m\dot{r}}{(1+\dot{r}^2)^{1/2}}\right]^2 + k = m^2 \tag{2.16}$$

or

$$\frac{m^2}{1+\dot{r}^2} = k. \tag{2.17}$$

where k is a constant of integration. This constant has a significant meaning which can be identified from the third acoustic direction cosine

$$l = nz' = ndz/ds = n/(ds/dz) = \frac{n}{(1+\dot{r}^2+r^2\dot{\theta}^2)^{1/2}} \tag{2.18}$$

if z is an increasing function of s. Then we can have

$$l^2 = \frac{n^2}{1+\dot{r}^2+r^2\dot{\theta}^2} = \frac{n^2}{1+\dot{r}^2+\frac{c^2(1+\dot{r}^2)}{m^2r^2}} = \frac{m^2}{1+\dot{r}^2} = k = l_o^2. \tag{2.19}$$

It is demonstrated that the integration constant k is the square of the third acoustical direction cosine, and it is verified again that the third direction cosine is invariant along a ray.

2.3.2.2.2 Ray Equations:

Now, let us derive the ray equations which express z and θ as the functions of r. Equation (2.19) can be rewritten as

$$\dot{r} = \sqrt{\frac{m^2}{l^2} - 1} = \frac{g}{l_o} \tag{2.20}$$

where g is defined by

$$g = \pm(m^2 - l_o^2)^{1/2}. \tag{2.21}$$

Here the + or - is chosen as r is an increasing or decreasing function of z. Now we can have

$$z - z_o = l_o \int_{r_o}^{r} \frac{dr}{g}. \tag{2.22}$$

This is the ray path equation which expresses z as a function of r, provided n, and thereby m, is a known function of r. The resulting formula can be solved, in principle, for r in terms of z, because the constant c appearing in parameter m represents the skewness invariant and it can be determined from the initial conditions.

To obtain θ as a function of z, from (2.12), and using (2.19),

$$\dot{\theta} = \frac{d\theta}{dz} = \frac{c(1+\dot{r}^2)^{1/2}}{mr^2} = \frac{c}{r^2 l_o} \tag{2.23}$$

then

$$\theta = \theta_o + \frac{c}{l_o}\int_{z_o}^{z} \frac{dz}{r^2}. \tag{2.24}$$

With r previously determined in (2.22) as a function of z, (2.24) yields θ as a function of z. Once both r and θ are known as functions of z, the ray equations are formulated.

2.3.2.2.3 Ray Direction Cosines and Skewness Invariant:

Once the above equations have been evaluated, the acoustical ray cosines of the ray at any point can be obtained, because

$$p = nx' = n\frac{dx}{ds} = n\frac{dx/dz}{ds/dz} = l\frac{dx}{dz} = l_o\frac{dx}{dz}$$

$$q = ny' = l_o\frac{dy}{dz} \tag{2.25}$$

$$l = l_o.$$

For a ray, the skewness is defined as

$$ske = xq - yp. \tag{2.26}$$

But it can be shown that

$$ske = xq - yp = x_oq_o - y_op_o = c. \tag{2.27}$$

This means that the skewness for a ray is invariant along the trace and the value of c can be determined from the start of the trace of the ray.

2.3.3 Focussing Characteristics of a Radial Parabolic Graded Index:

If the index function is

$$n = n_o(1 - Qr^2)^{1/2}, \tag{2.28}$$

we should choose r as a decreasing function of z. Then from (2.21)

$$g = -(m^2 - l_o^2)^{1/2} = -\left(n^2 - \frac{c^2}{r^2} - l_o^2\right)^{1/2}. \tag{2.29}$$

For the meridional rays starting from the plane $z = z_o$ with the acoustical ray direction normal to the starting plane $z = z_o$,

$$\cos\alpha = 0, \quad \cos\beta = 0, \quad \cos\gamma = 1. \tag{2.30}$$

Therefore, at the starting plane, for any ray

$$p_o = 0, \quad q_o = 0, \quad l_o = n(r_o). \tag{2.31}$$

Thus we can obtain the two constants

$$c = 0,$$

$$l_o = n(r_o). \tag{2.32}$$

Substituting (2.32) into (2.29), and then substituting it into (2.22), we derive

$$z - z_o = -n(r_o)\int_{r_o}^{r} \frac{dr}{\sqrt{n_o^2(1-Qr^2) - n(r_o)^2}}. \tag{2.33}$$

This equation indicates the ray trace of a given ray starting from r_o at plane $z = z_o$. From the basic integral formula of

$$\int \frac{dx}{\sqrt{a^2 - x^2}} = \sin^{-1}(x/a) + constant, \tag{2.34}$$

we have

$$r/r_o = \cos\left[\frac{n_o}{n(r_o)}\sqrt{Q}(z - z_o)\right]. \tag{2.35}$$

To obtain θ as a function of z in this example, it is necessary to check (2.23) and (2.24). Obviously, θ will not be changed for the meridional rays where $c = 0$.

Equation (2.35) is the ray trace formula for a certain ray starting from a point r_o on the plane $z = z_o$. Obviously, at the starting point $z = z_o$, $r/r_o = 1$. The distance of z from z_o when the ray crosses the z-axis, i.e., r=0, can be given by

$$\frac{n_o}{n(r_o)}\sqrt{Q}(z - z_o) = \left(J + \frac{1}{2}\right)\pi, \tag{2.36}$$

where J= 0, 1, 2, 3,... It is shown that for any ray, its trace is a sinusoidal function (r to z) and it will periodically pass through the z-axis. The "pitch distance" or periodicity length in the z-axis can be given from

$$P = \Delta z = \frac{2\pi}{\frac{n_o}{n(r_o)}\sqrt{Q}}. \tag{2.37}$$

The first "focussing point" can be obtained from the condition of J=0 in (2.36).

$$\frac{P}{4} = z - z_o = \frac{\pi}{2\frac{n_o}{n(r_o)}\sqrt{Q}}. \tag{2.38}$$

It should be noticed that in (2.37) and (2.38) the refraction index $n(r_o)$ for different rays starting at the plane $z = z_o$ is not a constant. Therefore, the "pitch length" and the "focal point" for different rays is different. We define the "caustic line length" of the "Graded Index Lens" as: for all the rays starting from the center (r=0) to the edge (r=a) of the plane z=z_o, the intersection points of the rays with the z-axis have a region on the z-axis called the "caustic line length", labeled Δf_c. It can be given by

$$\Delta f_c = \frac{\pi}{2n_o\sqrt{Q}}[n(0) - n(a)] = \frac{\pi}{2n_o\sqrt{Q}}\left[n_o - n_o(1 - Qa^2)^{1/2}\right] \cong \frac{\pi}{2}\frac{a^2}{2}\sqrt{Q}. \tag{2.39}$$

2.3.4 Focussing Characteristics Outside the GRIN Rod:

Like in optics several acoustic applications may demand that the focus of the GRIN rod be outside of the rod. In fact, in the later visualization experiments (see section 2.5) we are required to evaluate the acoustic focussing mechanisms of GRIN rod using the acoustic information outside of the GRIN rods. For an GRIN rod, if the length d is less than a quarter pitch and the focus point is outside the GRIN medium, the focussing feature will be different than the case we have discussed previously. At the second plane where $z = d$, the ray should obey Snell's law

$$n_1 \sin\sigma_1 = n_2 \sin\sigma_2, \tag{2.40}$$

where $n_1 = n(r_o, d)$ is the index of the ray starting from r_o arriving at the plane $z = d$ on the left side. The incident sine can be expressed by

$$\sin\sigma = -\frac{dr}{ds} = -\frac{dr}{dz}\frac{dz}{ds}. \tag{2.41}$$

It can obtained that

$$\sin\sigma = \frac{n_o\sqrt{Q}r_o}{n(r_o,d)}\sin\left[\frac{n_o\sqrt{Q}d}{n(r_o,0)}\right], \tag{2.42}$$

where $n(r_o, 0)$ and $n(r_o, d)$ are the indices at the starting and exit point. These values are expressed in the following equations

$$n(r_o,d) = n_o[1 - Qr(d)^2]^{1/2}, \tag{2.43}$$

$$n(r_o,0) = n_o[1 - Qr_o^2]^{1/2}, \tag{2.44}$$

$$r(d) = r_o\cos\left[\frac{n_o\sqrt{Q}d}{n(r_o,0)}\right], \tag{2.45}$$

where $r(d)$ is the distance from z-axis at the exit plane ($z=d$) for the ray starting from position $(r_o, 0)$.

Consider the left hand side of (2.40). It is a simple geometric relation that

$$\tan\sigma_2 = \frac{r(d)}{f_l} \tag{2.46}$$

and

$$\sin\sigma_2 = \frac{r(d)}{\sqrt{f_l^2 + r^2(d)}}. \tag{2.47}$$

Substituting (2.42) and (2.47) into (2.40), we can obtain

$$f_l = \frac{r(d)}{n_o\sqrt{Q}r_o}[n_2^2 - n_o^2Qr_o^2\sin^2\alpha]^{1/2}/\sin\alpha, \tag{2.48}$$

where

$$\alpha = \frac{n_o\sqrt{Q}d}{n(r_o,0)} = \sqrt{Q}d[1 - Qr_o^2]^{-1/2} \tag{2.49}$$

$$r(d) = r_o\cos\alpha. \tag{2.50}$$

From (2.48) to (2.50), f_l, the distance of the focussing point to the exit plane, can be calculated.

For the most simplified situation where the second term in α is ignored, i.e.,

$$Qr_o^2 \ll 1, \tag{2.51}$$

we can obtain

$$f_l = \left(\frac{1}{n_o\sqrt{Q}}\right)\frac{\cos(\sqrt{Q}\,d)}{\sin(\sqrt{Q}\,d)}n_2. \tag{2.52}$$

2.3.5 Method to Determine the Equation of the Velocity Profile:

We wish to fit the data to the following equation:

$$\frac{1}{V} = \frac{1}{V_o}\left(1 - \frac{Q_a}{2}r^m\right), \tag{2.53}$$

or

$$\frac{1}{V_o} - \frac{1}{V} = \frac{Q_a}{2V_o}r^m. \tag{2.54}$$

By taking the natural logarithm on both sides of (2.54), we have

$$\ln\left(\frac{1}{V_o} - \frac{1}{V}\right) = m\ln r + \ln\left(\frac{Q_a}{2V_o}\right). \tag{2.55}$$

Therefore, by plotting $\ln\left(\frac{1}{V_o} - \frac{1}{V}\right)$ versus $\ln r$, we should get a straight line with a slope m and a y-intercept $\ln\left(\frac{Q_a}{2V_o}\right)$.

In our case, we had data which contained positive and negative values for r. We simply took the absolute value of r to plot the graphs. Figure 2.13 is used to find m and Q_a for v_{LSAW} of the 17% GeO_2 doped GRIN rod. Table 2.1 shows these values along with the first quarter of the pitch (focal distance) for the six different GRIN rod velocity profiles illustrated in Fig.2.12.

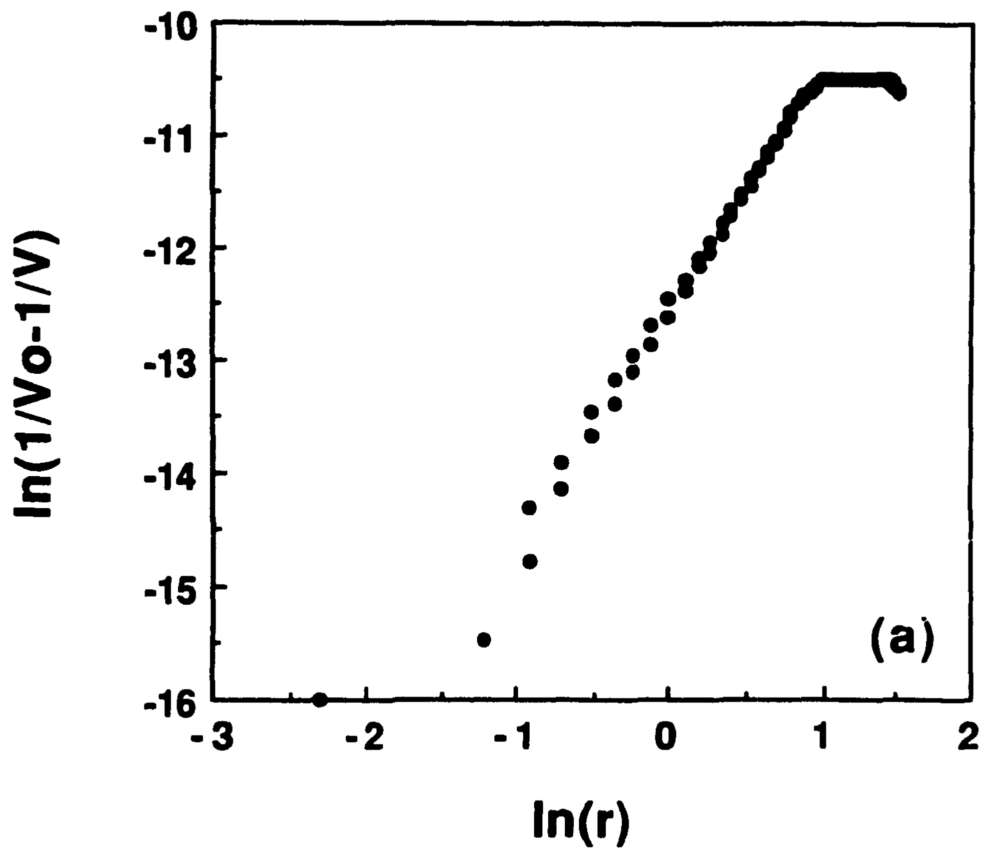

Figure 2.13 $\ln\left(\frac{1}{V_o}-\frac{1}{V}\right)$ *versus* $\ln r$ *for* v_{LSAW} *of the 17% GeO_2 doped GRIN rod.*

Sample	Velocity	*m*	Q_o(mm^{-m})	*P/4*(mm)
8%	v_{LSAW}	3.05	0.0072	18.5
	v_{LSSCW}	2.37	0.0176	11.8
17%	v_{LSAW}	2.13	0.0232	10.3
	v_{LSSCW}	2.62	0.0198	11.2
31%	v_{LSAW}	2.09	0.0238	10.2
	v_{LSSCW}	1.17	0.0554	6.7

Table 2.1 *Velocity profile constants and focal distance (P/4) of the GRIN rods such that the velocities follow the relationship* $\frac{1}{V}=\frac{1}{V_o}\left(1-\frac{Q_o}{2}r^m\right)$.

2.4 Methods of Visualizing an Acoustic Field:

Much work has been done dealing with visualization techniques for over a century. Two main approaches of visualizing an acoustic field are the Schlieren method and the photoelastic methods which have been reviewed in [38].

The Schlieren method depends on detecting the deviation of light caused by the refractive index perturbations induced by ultrasonic waves. The photoelastic method, on the other hand reveals the stresses in an ultrasonic wave using crossed Polaroids to detect the stress induced birefringence of the medium. Since we are interested in the intensity distribution of the acoustic field, we have decided to use the Schlieren technique.

The basic arrangement of the Schlieren system is shown in Fig.2.14. A parallel beam of light traverses an acoustic field. At zero acoustic intensity all of the light will be focussed by the lens at a single point blocked by a spatial filter at the Fourier plane, and there will be a dark screen at the image plane. However, a continuous wave ultrasound will act as a phase diffraction grating and will form a series of diffraction orders. By filtering out the 0th order, we can reveal the diffracted order and the intensity of the acoustic field will appear as a bright image in a dark field. However, the individual wave fronts will not be resolved. It is noted that a collimated acoustic beam will appear as a diffracted spot at the Fourier plane, while a focussing acoustic beam will appear as an arc around the 0th order.

2.5 Results and Discussion:

2.5.1 Experimental Setup:

We installed an experimental set-up as shown in Fig.2.14. Figures 2.15a and 2.15b are photographs of the experimental system. The optical probe beam was expanded to a diameter of 50mm. The focal length of the focussing lens was 75cm. In the beginning of the experiment we found out that due to the cylindrical shape of the rod and fine structures of the index profile which scatters the probe beam, it was very difficult to observe the focussing behavior of acoustic waves propagating inside the GRIN rod. Therefore, acoustic waves exiting out of the GRIN rod into a water bath were used to evaluate the necessary focussing information instead. The advantage of water is its uniformity, transparence, high photoelastic coefficient and reasonably low acoustic attenuation. The disadvantage is the acoustic reflection and refraction present at the GRIN rod-water interface. Furthermore, because liquid does not support shear acoustic waves, only experiments involving longitudinal acoustic waves are presented in this thesis.

In order to evaluate the performance of the experimental system, a non-focussed ultrasonic transducer directly contacting a bath of water was used initially. We observed a uniform light beam at the Fourier plane and a uniform acoustic field at the image plane. At the image plane a two dimensional CCD camera connected to a video recorder as shown in Fig.2.14 was used as the image recorder. We then tried a focussing ultrasonic transducer also directly contacting the water bath and an arc light beam at the Fourier plane along with a focussing acoustic field at the image plane was observed.

In addition to the above checking procedures, a uniform 10mm diameter 6mm long Pyrex rod was also used as the sample. It was bonded to a 50MHz planar (non-focussing) ultrasonic transducer. Since nearly all of our GRIN rods for the experiments were fabricated with a ~5mm diameter core which has a graded velocity distribution as shown in Fig.2.12, a planar acoustic wave front can be assumed to be launched into the test sample if a high frequency ultrasonic transducer is used. It means that there should be many acoustic wavelengths across the 5mm diameter. Due to the consideration of the available ultrasonic transducers and instruments, and an acceptable acoustic attenuation in the measurement system, the 50MHz transducer was chosen. The 50MHz transducer used for the measurements had a diameter of 6.35mm. Figure 2.16 indicates that the 50MHz ultrasonic transducer indeed produces a uniform ultrasonic beam through the uniform cylindrical Pyrex rod into the water bath. It is noted that at 50MHz the longitudinal acoustic wavelength in the GRIN rods shown in Fig.2.12 is around 120μm.

2.5.2 Acoustic GRIN Rods:

2.5.2.1 Same GRIN Profile, Different Lengths:

The 17% doped GeO_2 GRIN rod as shown in Figs.2.1 and 2.12 was cut at lengths of 6mm, 9mm, 12mm, 15mm and 18mm. Based on the theory presented earlier, we estimated the focal length, or the first quarter of the focal pitch, of this GRIN rod to be 11.2mm. Figure 2.17 is a schematic of the sinusoidal behavior of the acoustic rays in the rod and the positions at which the rod was cut in order to observe the acoustic beams exiting from the rod into the water. The 6mm sample gave us a very slowly converging acoustic beam as shown in Fig.2.18. The 9mm one showed a definite converging of the beam which was thinner than the 6mm one, but the focal region was very far from the transducer as shown in Fig.2.19. Due to the high acoustic attenuation the focus could not be observed. We did observe the focussing and even the diverging regions as indicated in Fig.2.20 with the 12mm sample due to the short acoustic propagation distance in the water. The focus was near the edge of the lens and the diameter of the beam was much smaller than in the two previous cases. Figure 2.21 demonstrates that for the 15mm sample, the acoustic beam was diverging, yet still quite narrow. For the 18mm sample, the acoustic beam had widened and it was almost collimated as illustrated in Fig.2.22. From Figs.2.18 to 2.22 we can conclude that Fig.2.17 is a very good representation of the acoustic ray behaviors inside the GRIN rod. The difference between the estimated focal length of 11.2mm and the observed focal length of 13mm is primarily due to the fact that the velocity profile has a center dip and is not parabolic (m=2.62) as shown in Table 2.1.

It is noted that due to the abrupt velocity change at the rod center, the acoustic wave energy is not concentrated at the rod center implying that the focussing beams are not formed by a solid cone but rather by a hollow one. Therefore in Figs.2.18 to 2.22 we see a stronger beam intensity away from the center. In addition, all the Schlieren visualization images presented in this thesis were photographs of the screen of the video recorder shown in Figs.2.14 and 2.15.

2.5.2.2 Same Length, Different GRIN Profiles:

In order to investigate the effects of different GRIN profiles as shown in Fig.2.12 on focussing behaviors, rods with nearly the same length but with different profiles were then used as samples. Figure 2.23 shows the acoustic beam intensity exiting out of a 5.5mm long 31% doped GeO_2 GRIN rod. Comparing Fig.2.23 with Fig.2.18 obtained with a 6mm 17% doped GeO_2 rod, we can see that the focal length decreases with a steeper GRIN velocity profile or an increasing GeO_2 dopant concentration, as expected. A 12mm 8% GeO_2 doped GRIN rod was also used for the measurement and the result is given in Fig.2.24. We can notice that the focal length is longer for the 8% GeO_2 doped rod than the 12mm 17% GeO_2 doped rod by comparing Fig.2.24 with Fig.2.20. It is interesting to note that we also tried a step index rod 12mm long and with an 8% GeO_2 dopant concentration as shown in Fig.2.11 and obtained a collimated beam which is shown in Fig.2.25.

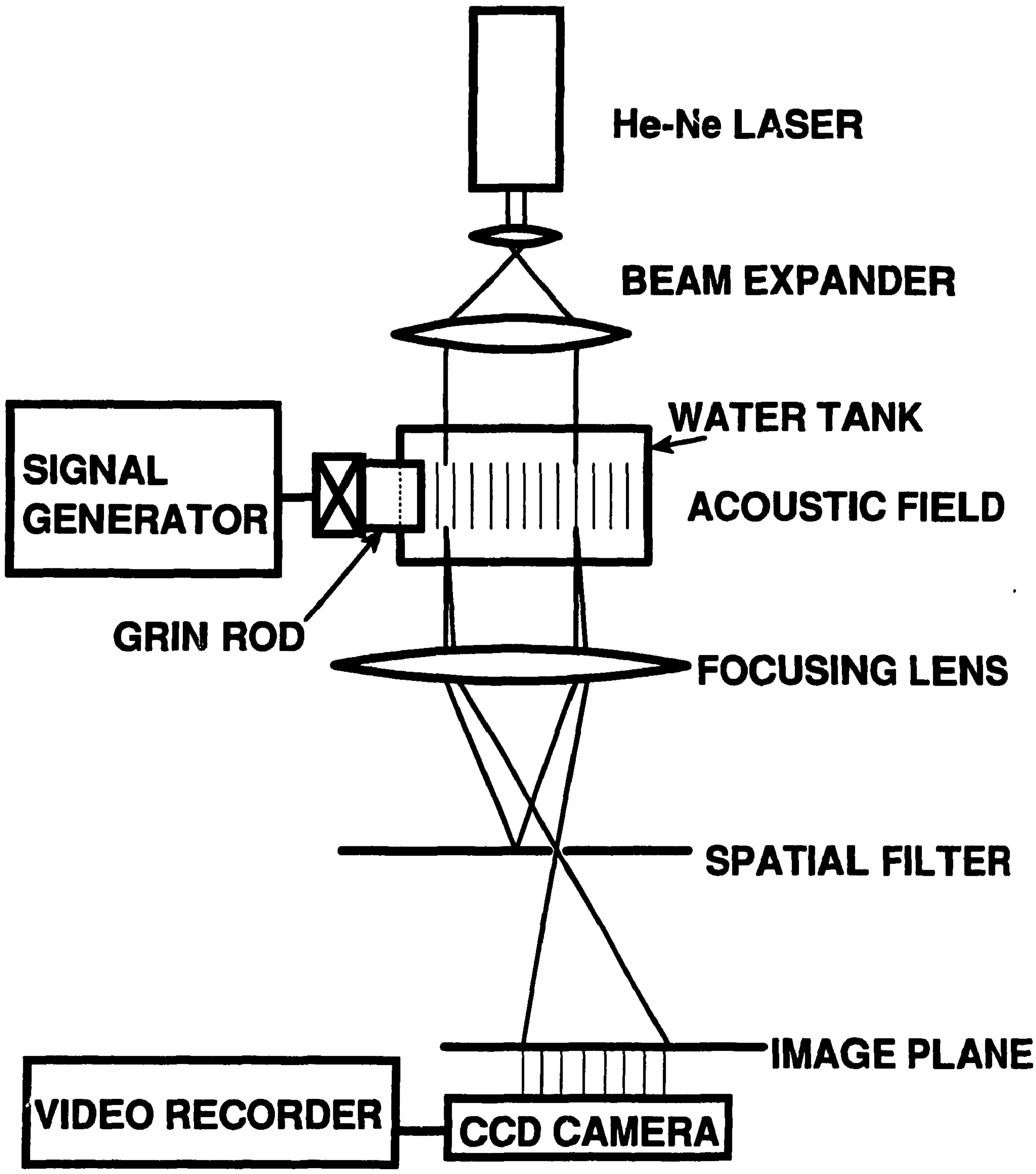

Figure 2.14 *Schematic of a Schlieren visualization system.*

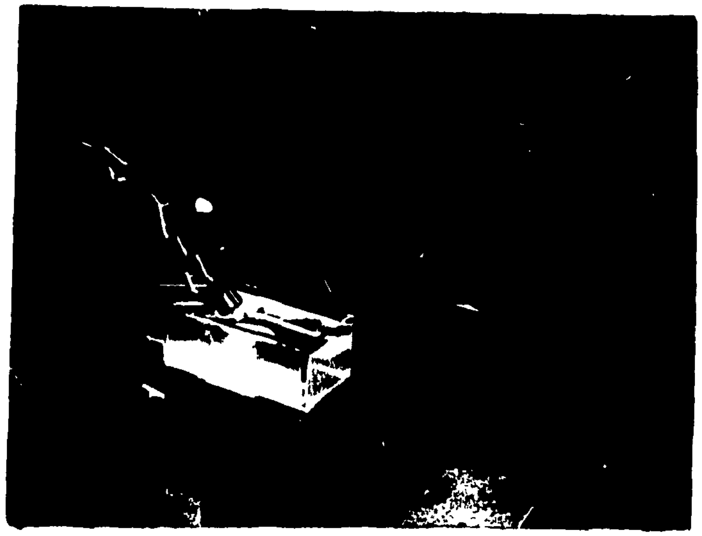

(a)

(b)

Figure 2.15 *Photographs of the experimental set-up for the visualization of ultrasound, (a) laser and transducer, (b) frequency generator, CCD camera and monitor.*

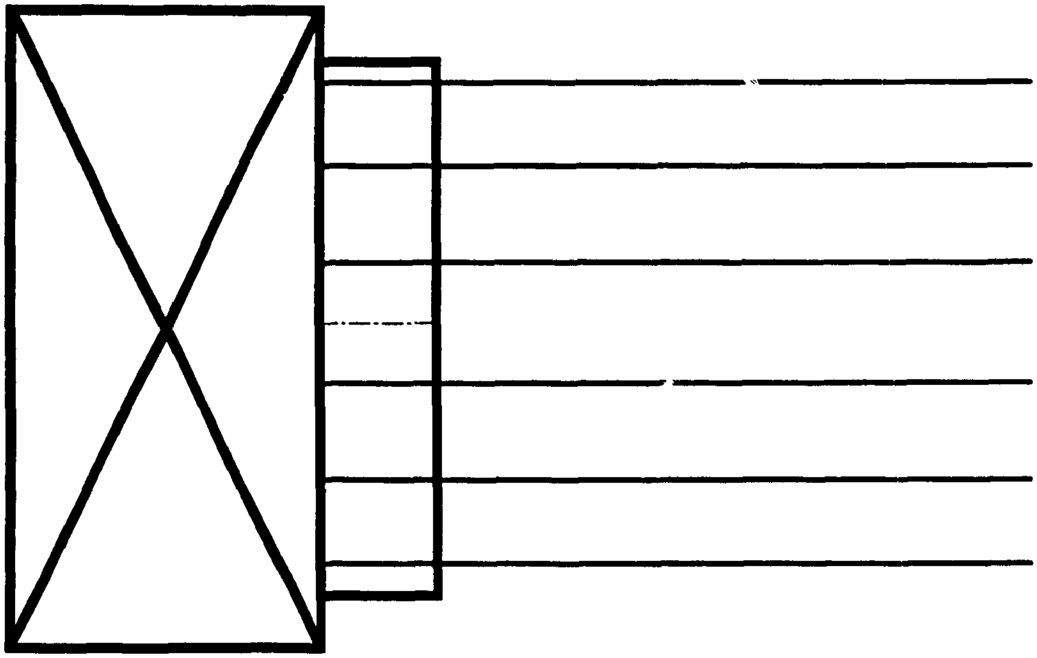

6mm UNIFORM PYREX ROD

Figure 2.16 *Image of an acoustic beam coming out of a 6mm long Pyrex rod into the water. Arrow indicates the rod-water interface.*

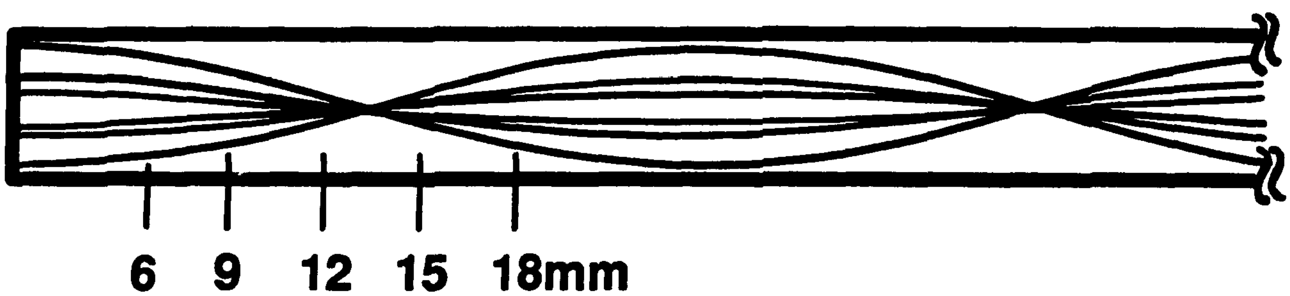

Figure 2.17 *Acoustic rays in an acoustic GRIN rod. Arrows show the rod-water interface plane for the Schlieren visualization measurements.*

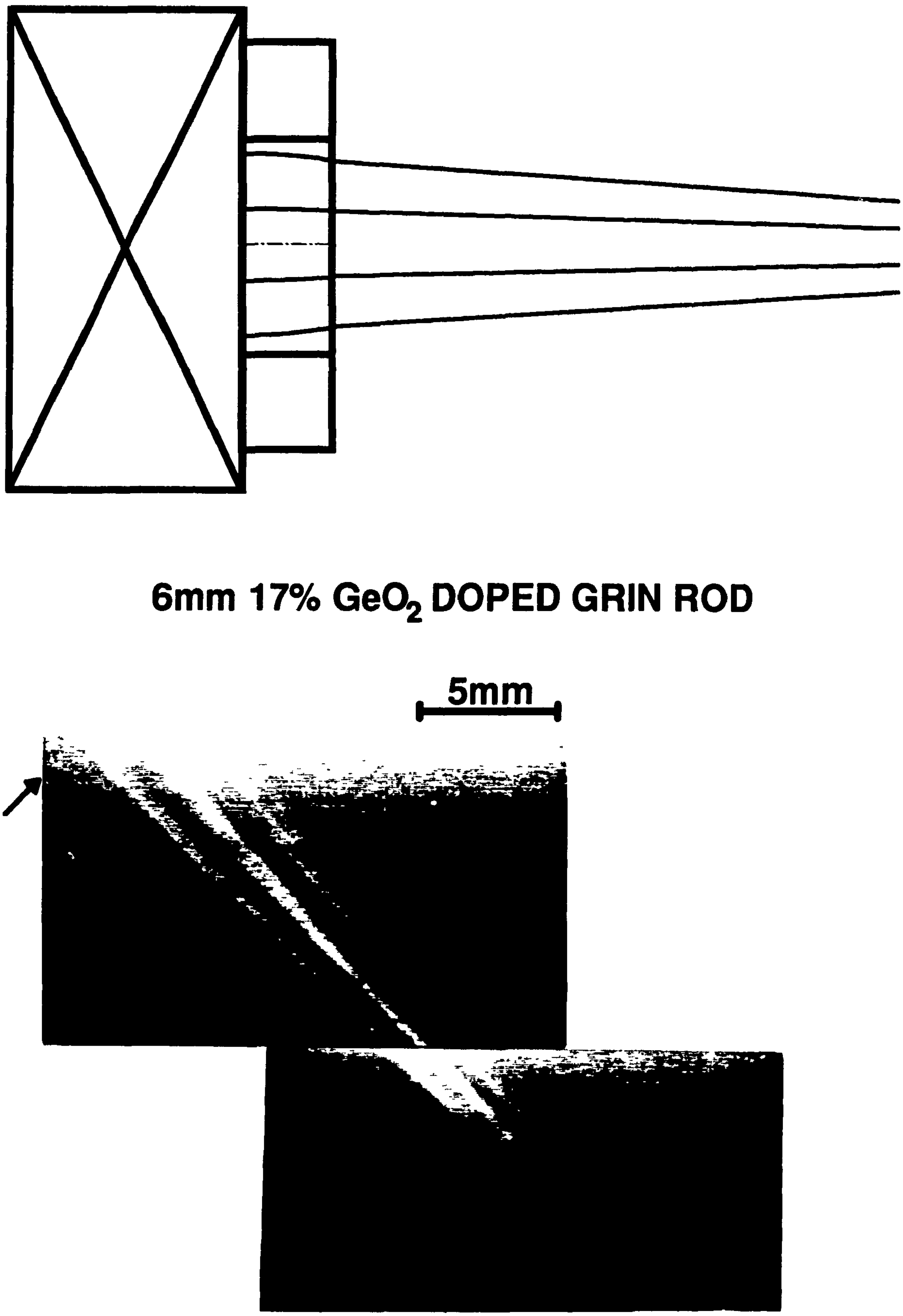

Figure 2.18 *Image of acoustic waves coming out of a 6mm long 17% GeO_2 doped GRIN rod. Arrow indicates the rod-water interface.*

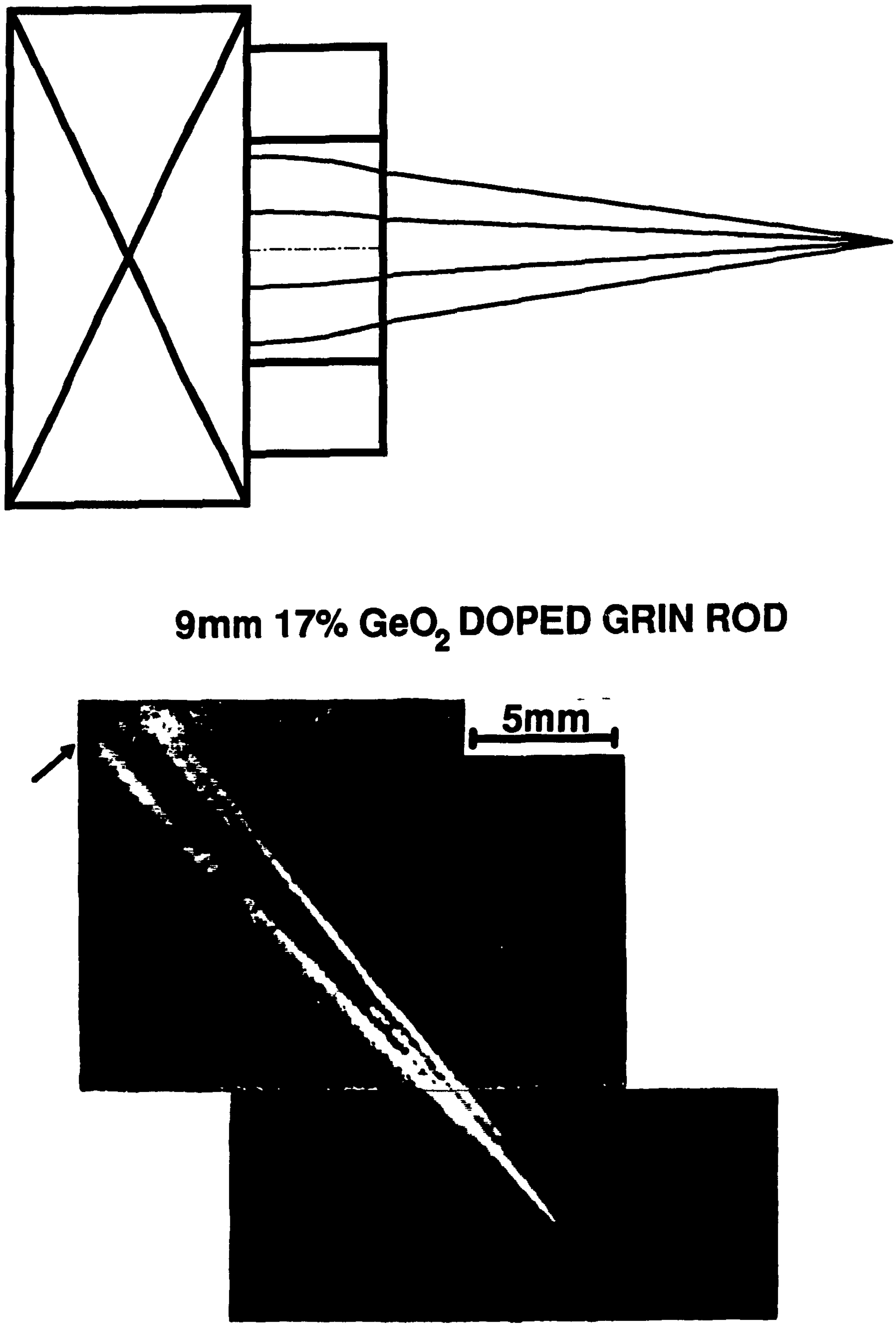

Figure 2.19 *Image of acoustic waves coming out of a 9mm long 17% GeO_2 doped GRIN rod. Arrow indicates the rod-water interface.*

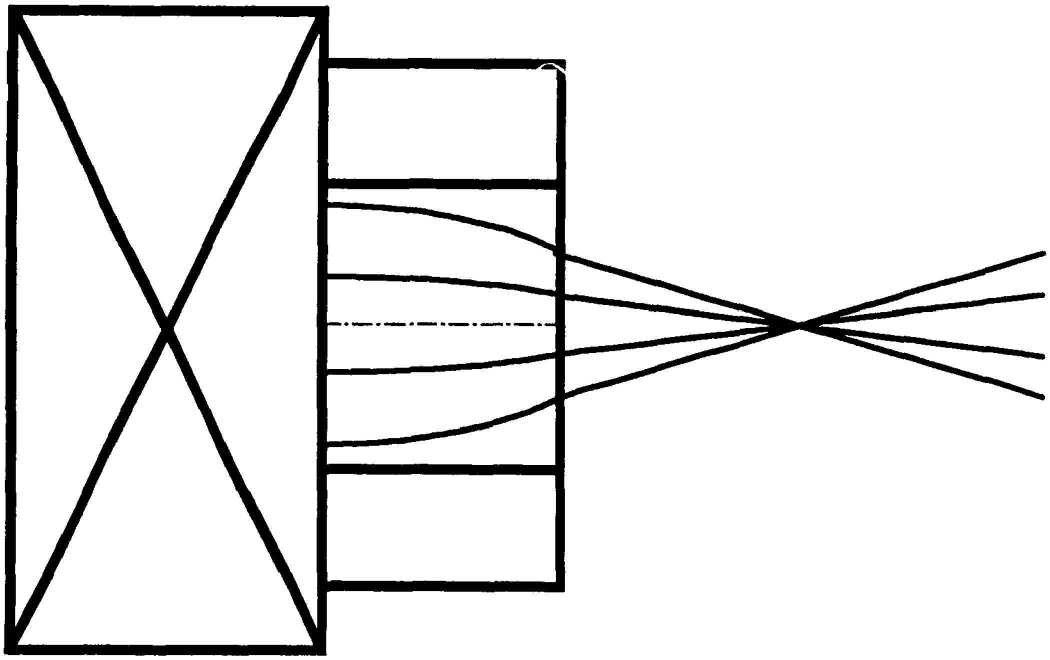

12mm 17% GeO_2 DOPED GRIN ROD

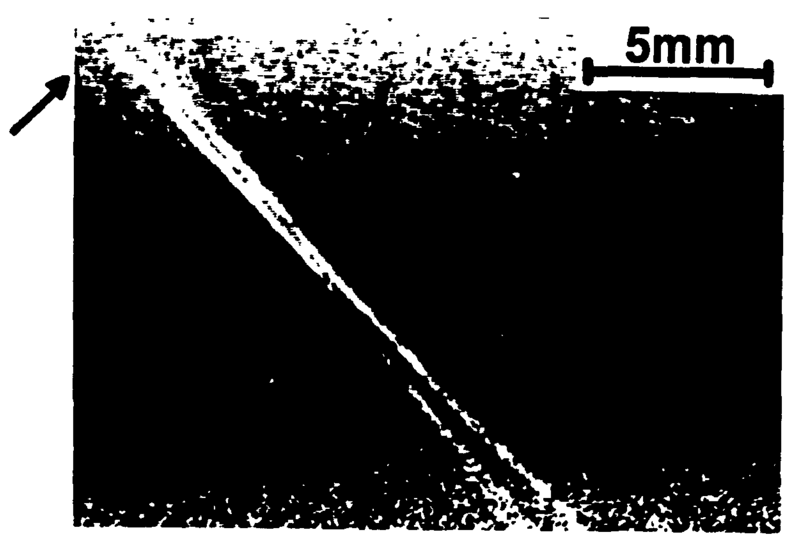

Figure 2.20 *Image of acoustic waves coming out of a 12mm long 17% GeO_2 doped GRIN rod. Arrow indicates the rod-water interface.*

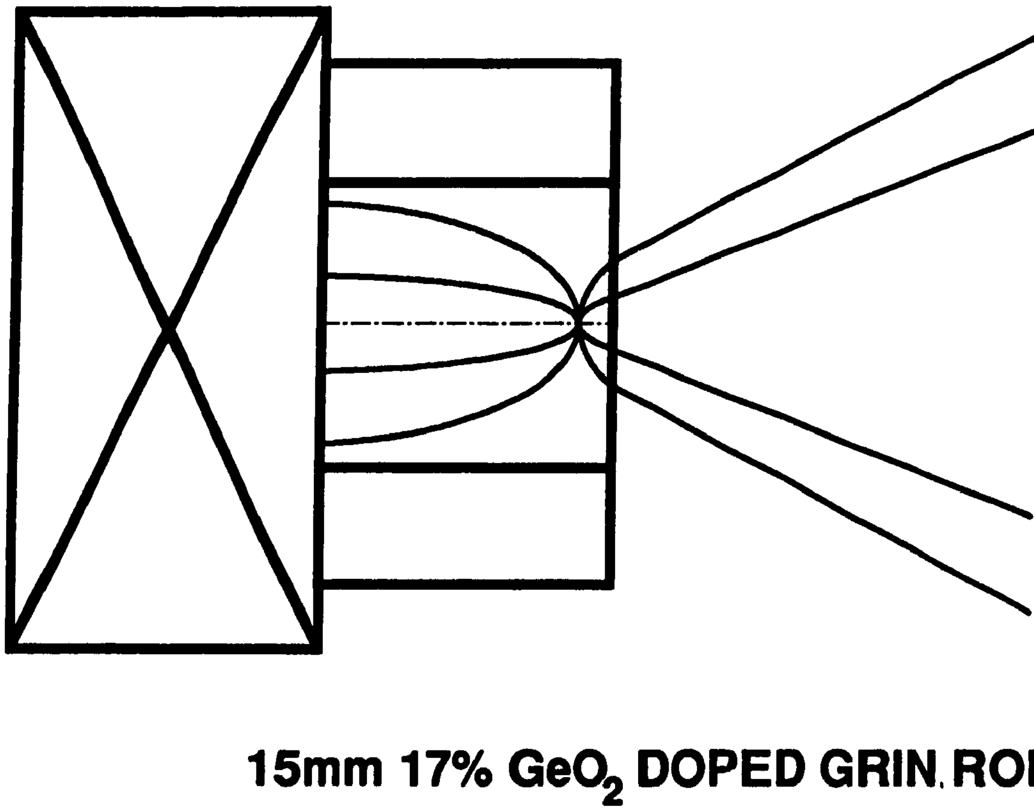

Figure 2.21 *Image of acoustic waves coming out of a 15mm long 17% GeO_2 doped GRIN rod. Arrow indicates the rod-water interface.*

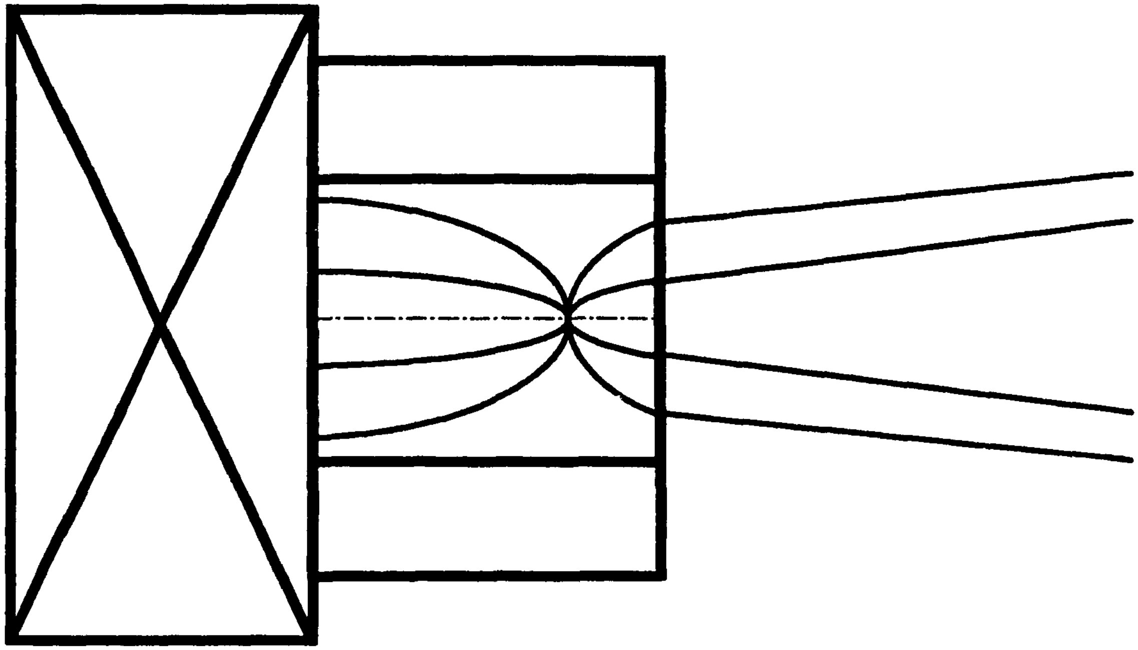

18mm 17%GeO_2 DOPED GRIN ROD

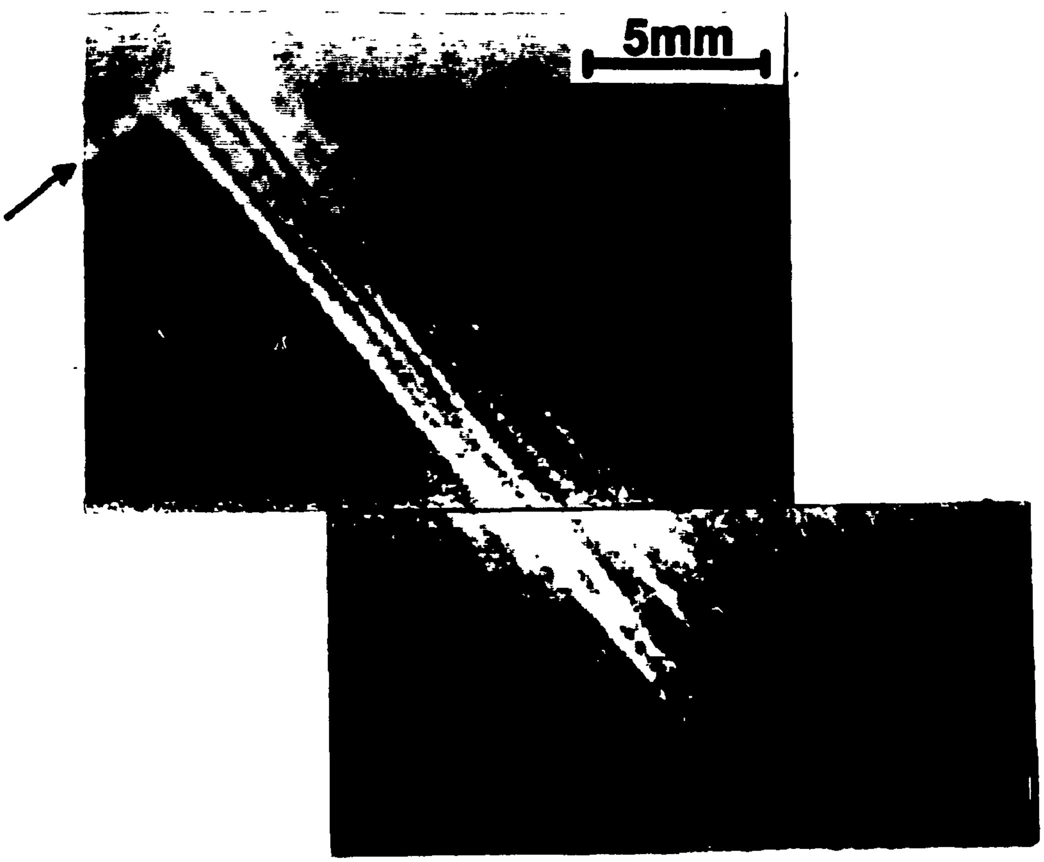

Figure 2.22 *Image of acoustic waves coming out of a 18mm long 17% GeO_2 doped GRIN rod. Arrow indicates the rod-water interface.*

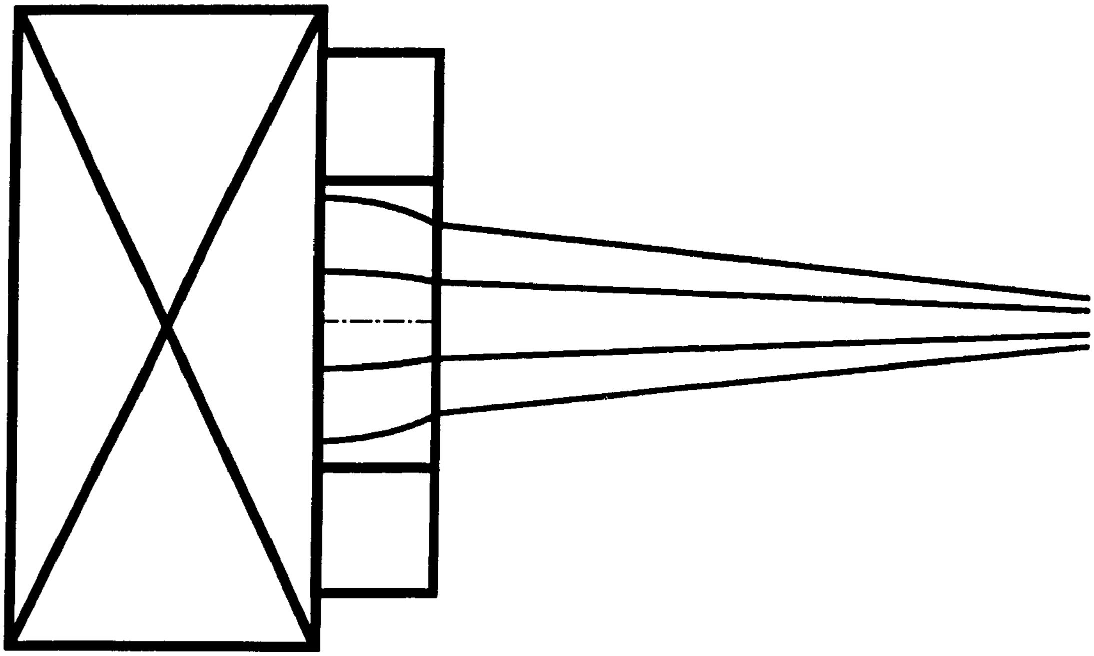

5.5mm 31% GeO_2 DOPED GRIN ROD

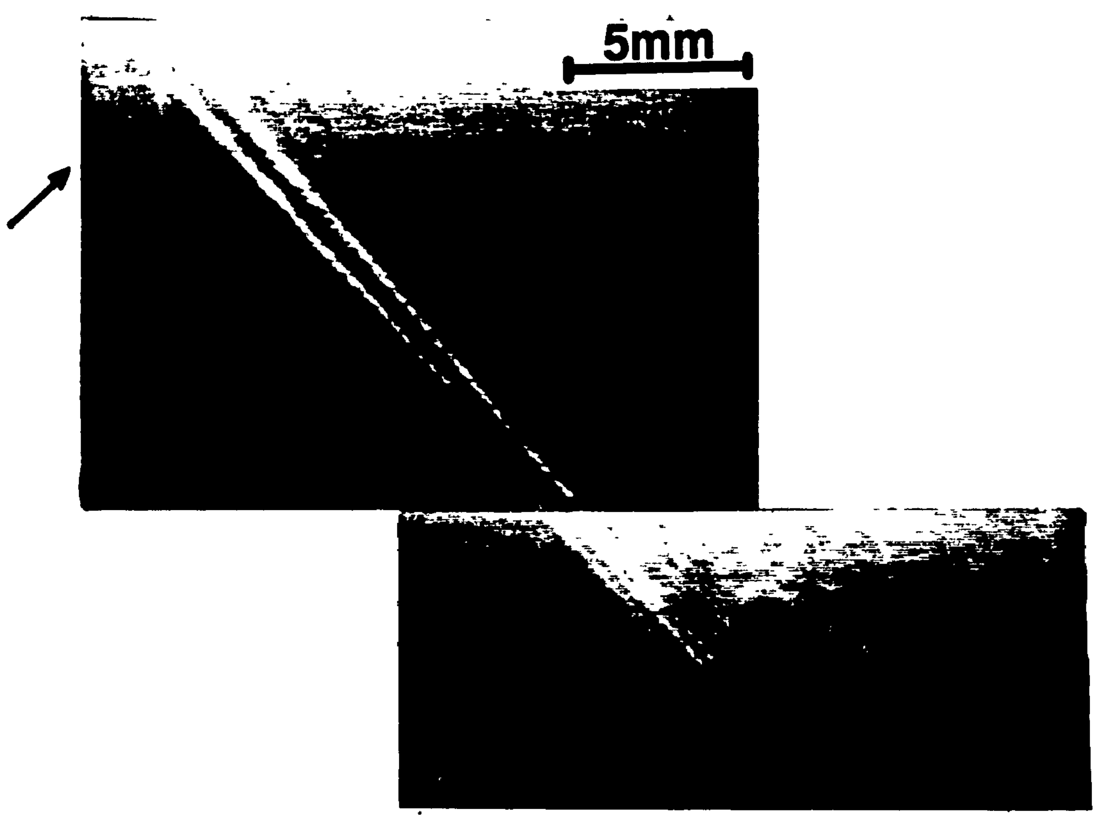

Figure 2.23 *Image of acoustic waves coming out of a 5.5mm long 31% GeO_2 doped GRIN rod. Arrow indicates the rod-water interface.*

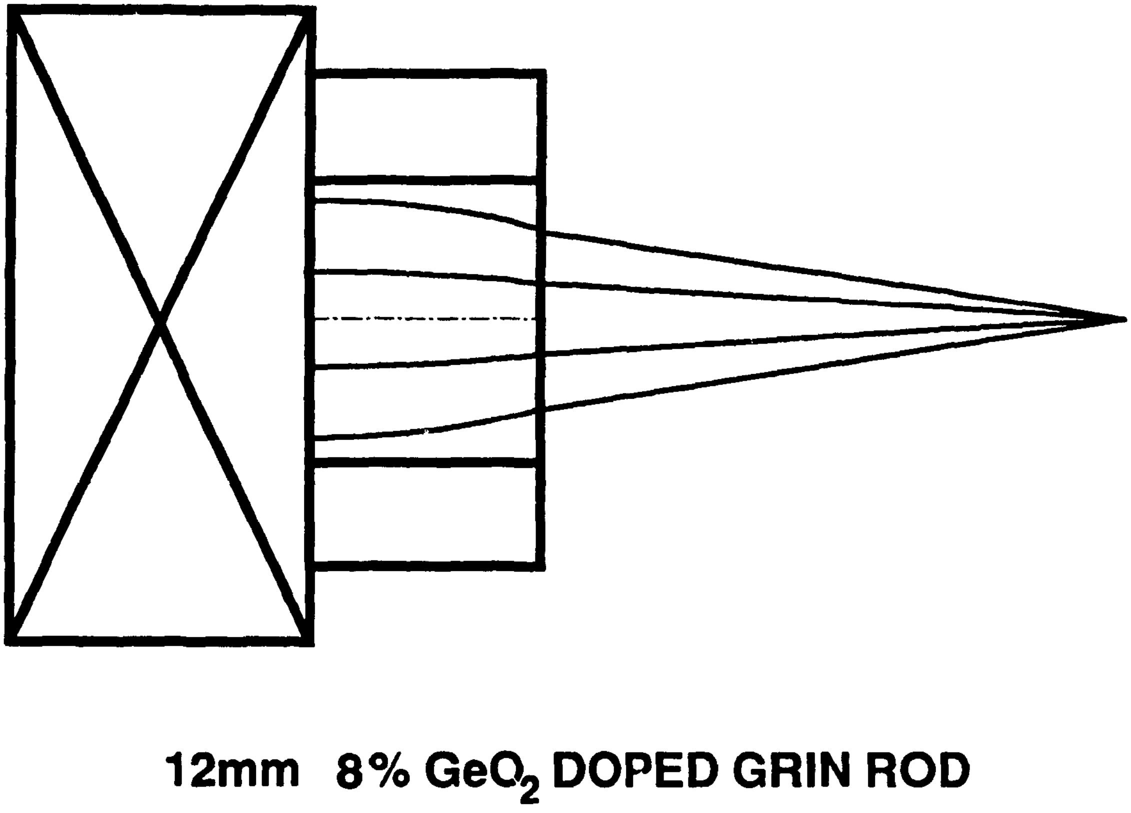

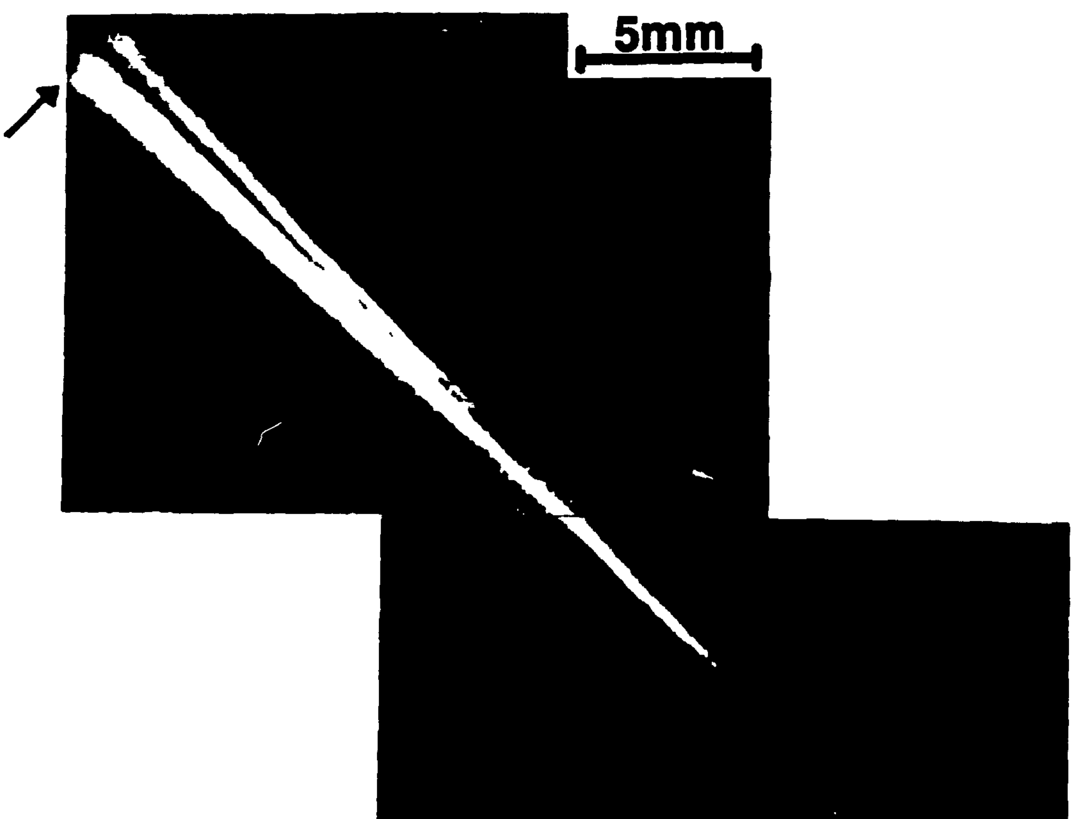

Figure 2.24 *Image of acoustic waves coming out of a 12mm long 8% GeO_2 doped GRIN rod. Arrow indicates the rod-water interface.*

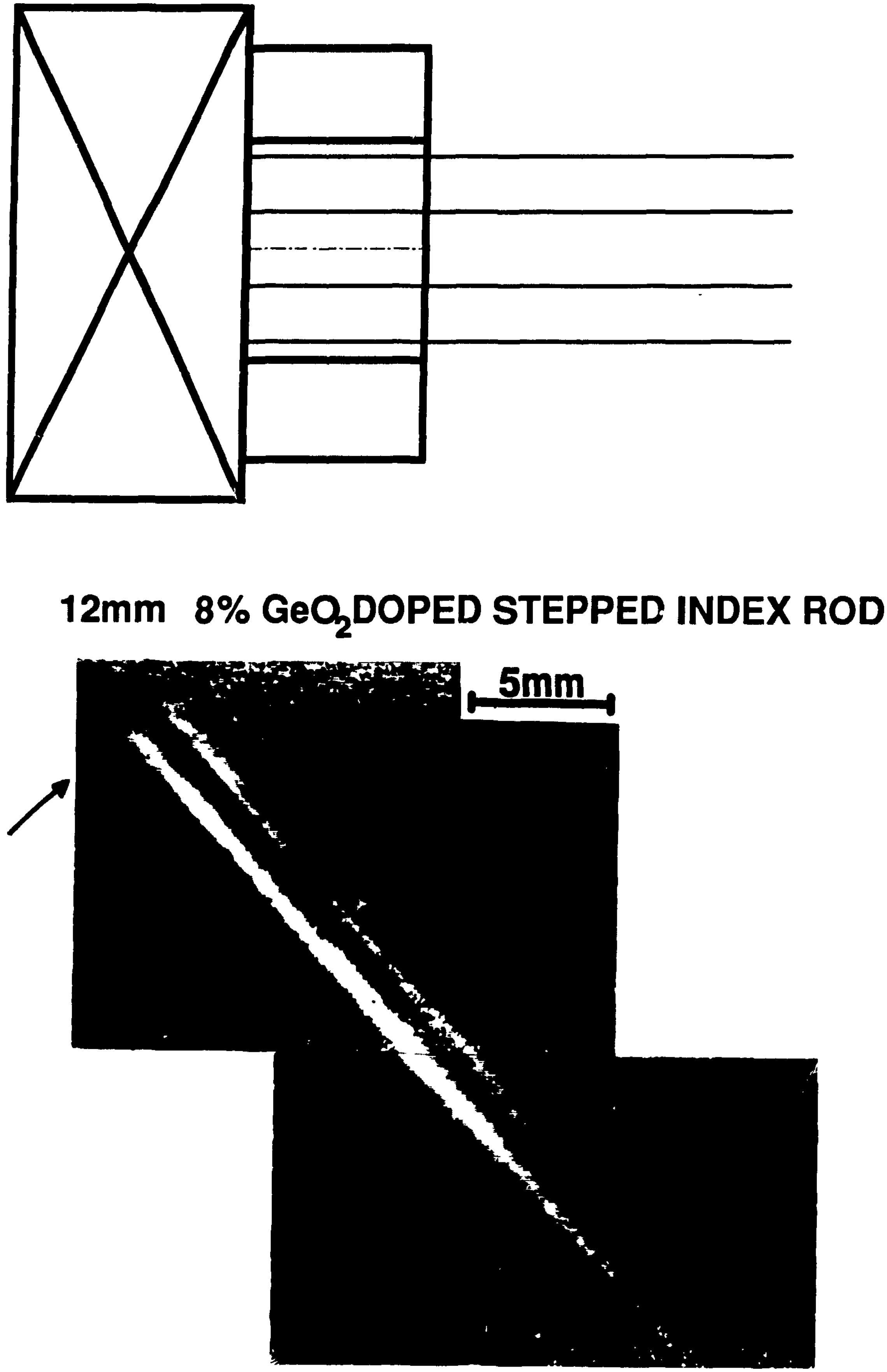

Figure 2.25 *Image of acoustic waves coming out of a 12mm long 8% GeO_2 doped step index rod. Arrow indicates the rod-water interface.*

2.5.2.3 Same GRIN Sample, Different Acoustic Frequencies:

Our next study was to change the acoustic frequency and observe the effect. The aim was to determine at which frequency the ray acoustic approach can be reasonably acceptable to represent the acoustic wave propagation inside the core of the cladded GRIN rod. We used a 9mm 17% GeO_2 doped GRIN rod. It should be reminded that this rod has a ~5mm diameter core and ~2.4mm thick cladding. At 10MHz, the beam exiting from the rod did not seem to focus but it was formed of three beams as shown in Fig.2.26. Figure 2.27 shows the results obtained at 20MHz and the focus is slightly recognizable. At 30MHz we could clearly see the focal region. The pattern of beams at 30MHz as demonstrated in Fig.2.28 is a typical focussing pattern where three beams become two and back to three beams after the focus. This suggests that the ray acoustic approach is resonably valid for acoustic frequencies over 30MHz which means that the GRIN rod has an aperture of more than 25 wavelengths. Figures 2.26, 2.27, 2.28 and 2.19 also indicate that the focal distance increases slightly with frequency.

2.5.3 Long Buffer Rods:

Then the system was used to visualize an acoustic beam exiting from long buffer rods. Due to the consideration of the acoustic attenuation in long rods the operating frequency was chosen to be 10MHz. The aim was to observe the acoustic guiding effect due to the presence of the cladding. The first rod tested was a 29cm 8% GeO_2 doped step index rod and at 10MHz the field was basically collimated and concentrated in the core as shown in Fig.2.29. Then we tried a 33cm 8% GeO_2 doped GRIN rod. At 10MHz, the field shown in Fig.2.30 was narrower than the previous sample. No observable change could be seen when we cut 6mm off the end of the rod, twice. This indicates that at 10MHz, the acoustic waves are guided in the core and that the cladding has an effect. In both these samples, the signal exiting from the rods was quite strong. The details of the guiding effect in such long rods can be found in [14].

2.5.4 GRIN Optics:

Another step was to study the optical focussing behaviors of the GRIN rod. We may then be able to correlate the acoustics and the optics of the rod. The optics may be more easily used to explain certain questions about the acoustic measurement results and in particular about the center dip in the optical refractive index profile due to the MCVD fabrication method. We launched a collimated light beam into the 12mm 17% GeO_2 doped

GRIN rod and recorded the beam coming out from the rod at three different positions. The images are given in Fig.2.31. We can see that the beam is not uniform, being formed of many rings. This may be due to the oscillations in the refractive index profile. There exists a brighter ring indicating perhaps the fact that the light is not guided right in the center of the core due to the presence of the center dip. This observation agrees with our acoustic measurements reported in the section 2.5.2.1.

2.5.5 Commercial Products:

Optical graded index lenses are available commercially. Melles-Griot (Irvine, California) sells for example a GRIN lens to be used at a wavelength of 0.633µm with an index profile which follows the relationship

$$n(r) = n_o\left(1 - \frac{A}{2}r^2\right)$$

with

$$n_o = 1.564$$
$$\sqrt{A} = 0.247$$
$$d = 2r = 2mm$$

We also obtained a GRIN lens directly from Nippon Sheet Glass designed for a wavelength of 0.83µm with an identical profile except that

$$n_o = 1.5986$$
$$\sqrt{A} = 0.202$$
$$d = 2r = 3mm$$

These GRIN lenses, which do not have a center dip in their refractive index profiles, are fabricated by the exchange of Tl^+ or Cs^+ ions for K^+ or Na^+ ions in a silicate glass. They are widely used in photocopier and facsimile arrays, medical endoscopes, video or compact disk systems, and a wide variety of devices for splitting, and coupling light in optical fibre telecommunications applications [32].

Figures 2.32 and 2.33 show the acoustic velocity profiles of these two GRIN lenses. Again, it is interesting to compare the optical and acoustical percentage change of these lenses. However, contrary to the MCVD GeO_2 and P_2O_5 doped rods, the refractive index change and the variation in the acoustic velocity is very comparable, both in shape and in relative value. Take, for example, the Melles-Griot lens which has a maximum index variation of 2%, a 1.5% longitudinal velocity change and a 2.8% shear velocity change.

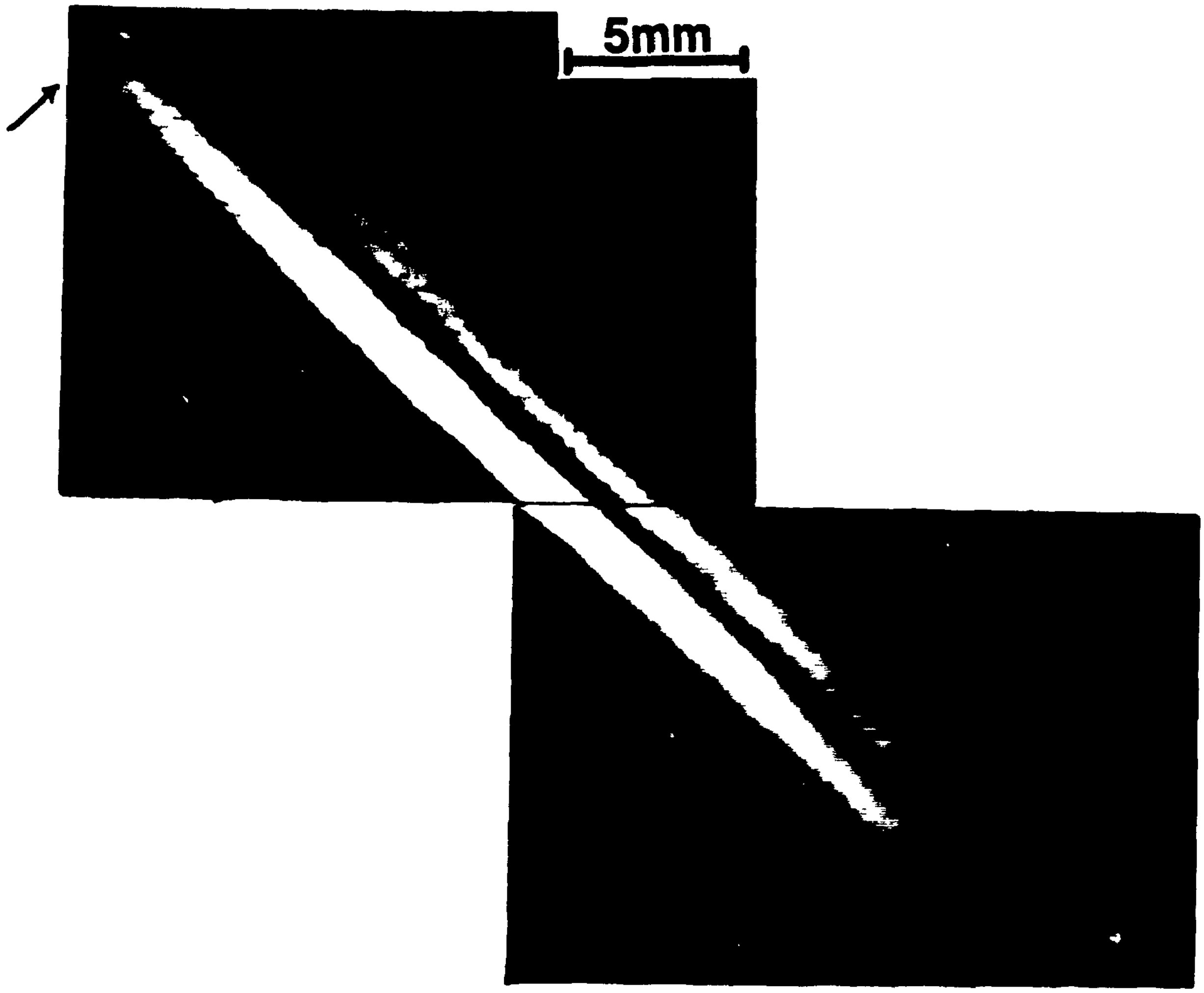

Figure 2.26 *Image of 10MHz acoustic waves coming out of a 9mm long 17% GeO_2 doped GRIN rod. Arrow indicates the rod-water interface.*

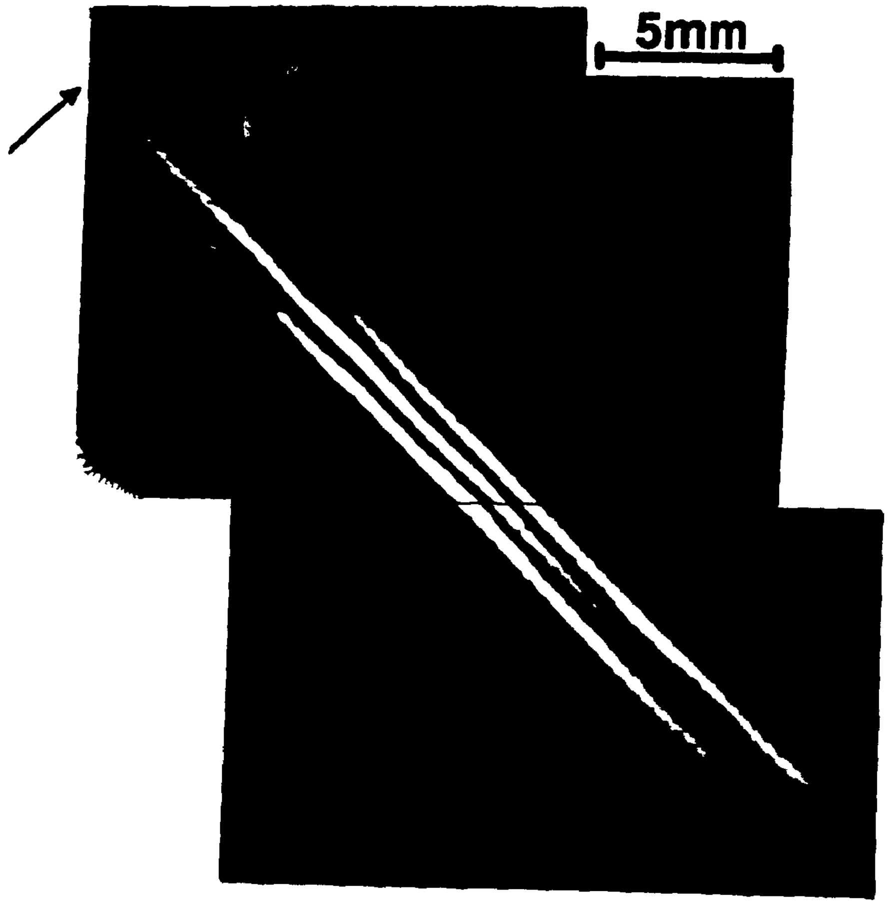

Figure 2.27 *Image of 20MHz acoustic waves coming out of a 9mm long 17% GeO_2 doped GRIN rod. Arrow indicates the rod-water interface.*

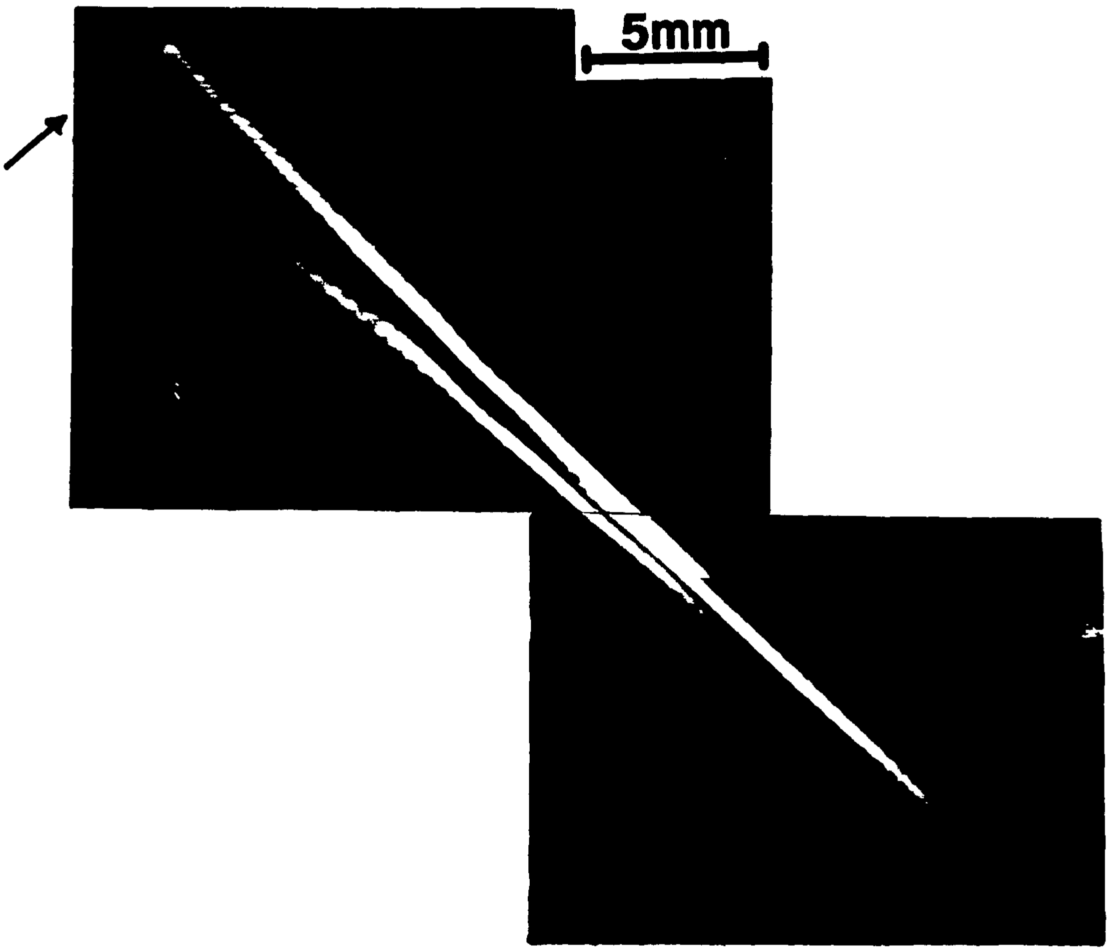

Figure 2.28 *Image of 30MHz acoustic waves coming out of a 9mm long 17% GeO_2 doped GRIN rod. Arrow indicates the rod-water interface.*

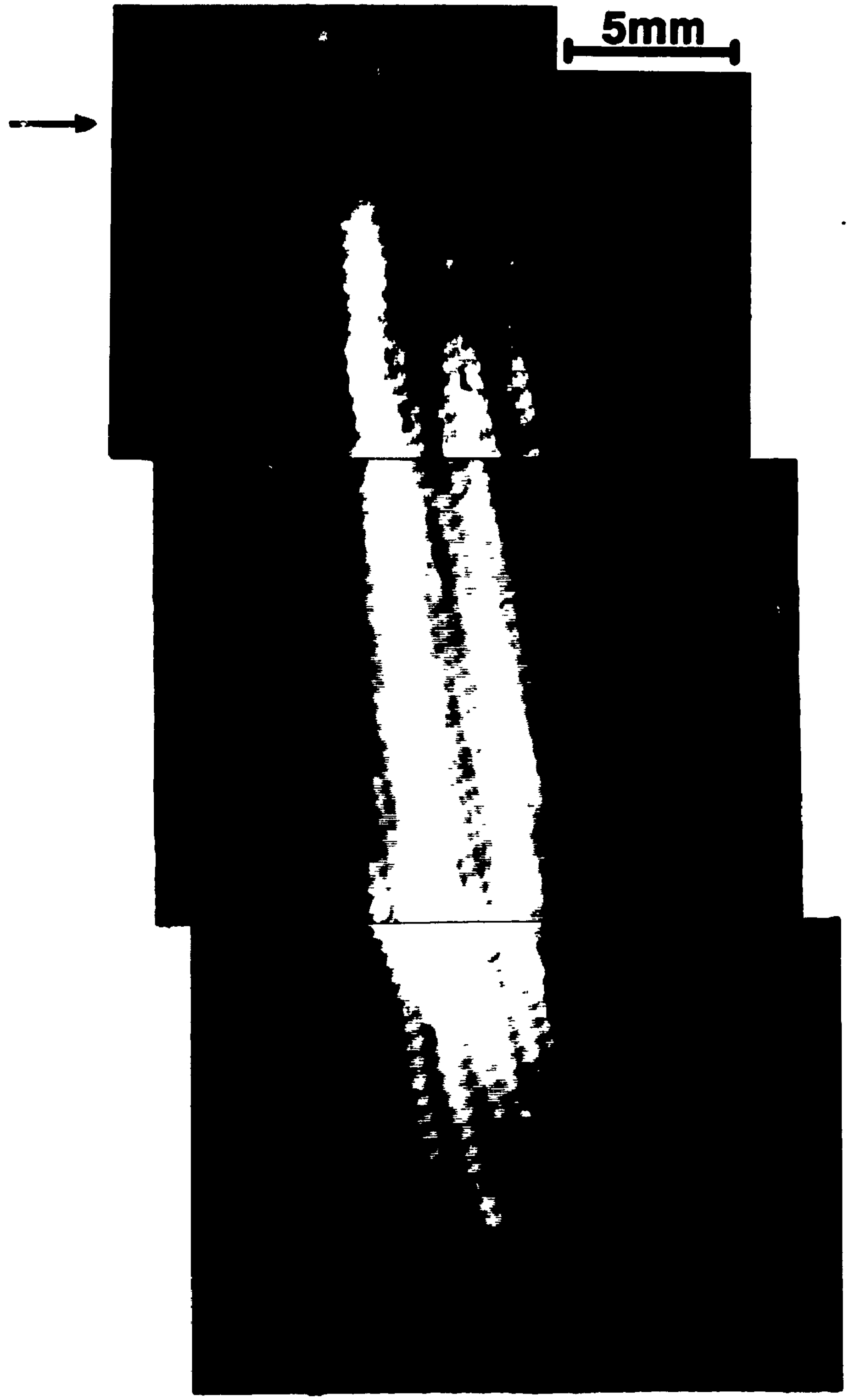

Figure 2.29 *Image of acoustic waves coming out of a 29cm long 8% GeO_2 doped step index rod. Arrow indicates the rod-water interface.*

Figure 2.30 *Image of acoustic waves coming out of a 33cm long 8% GeO_2 doped GRIN rod. Arrow indicates the rod-water interface.*

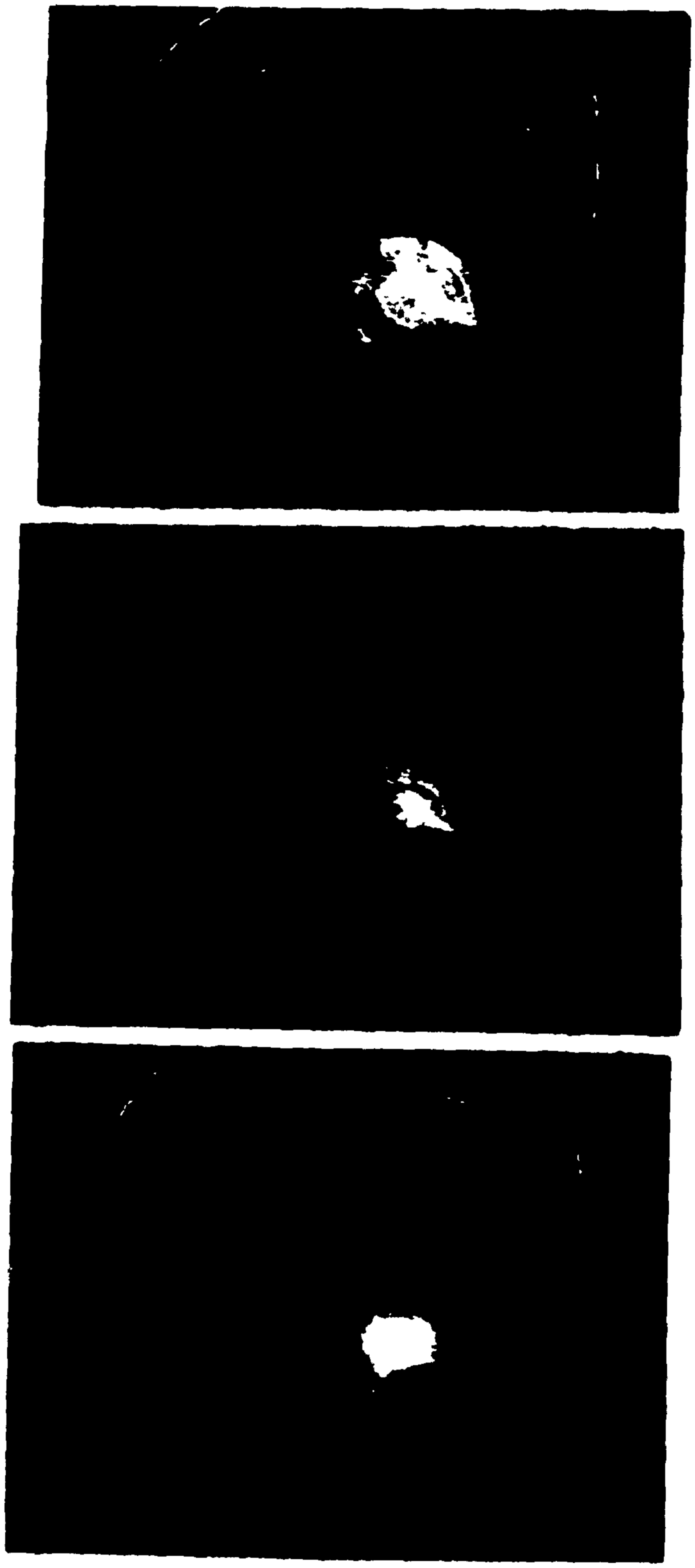

(a)

(b)

(c)

Figure 2.31 *Photographs at three different positions of laser light being sent through a 12mm long 17% GeO_2 doped GRIN rod, (a), (b) before the focus and (c) at the focus.*

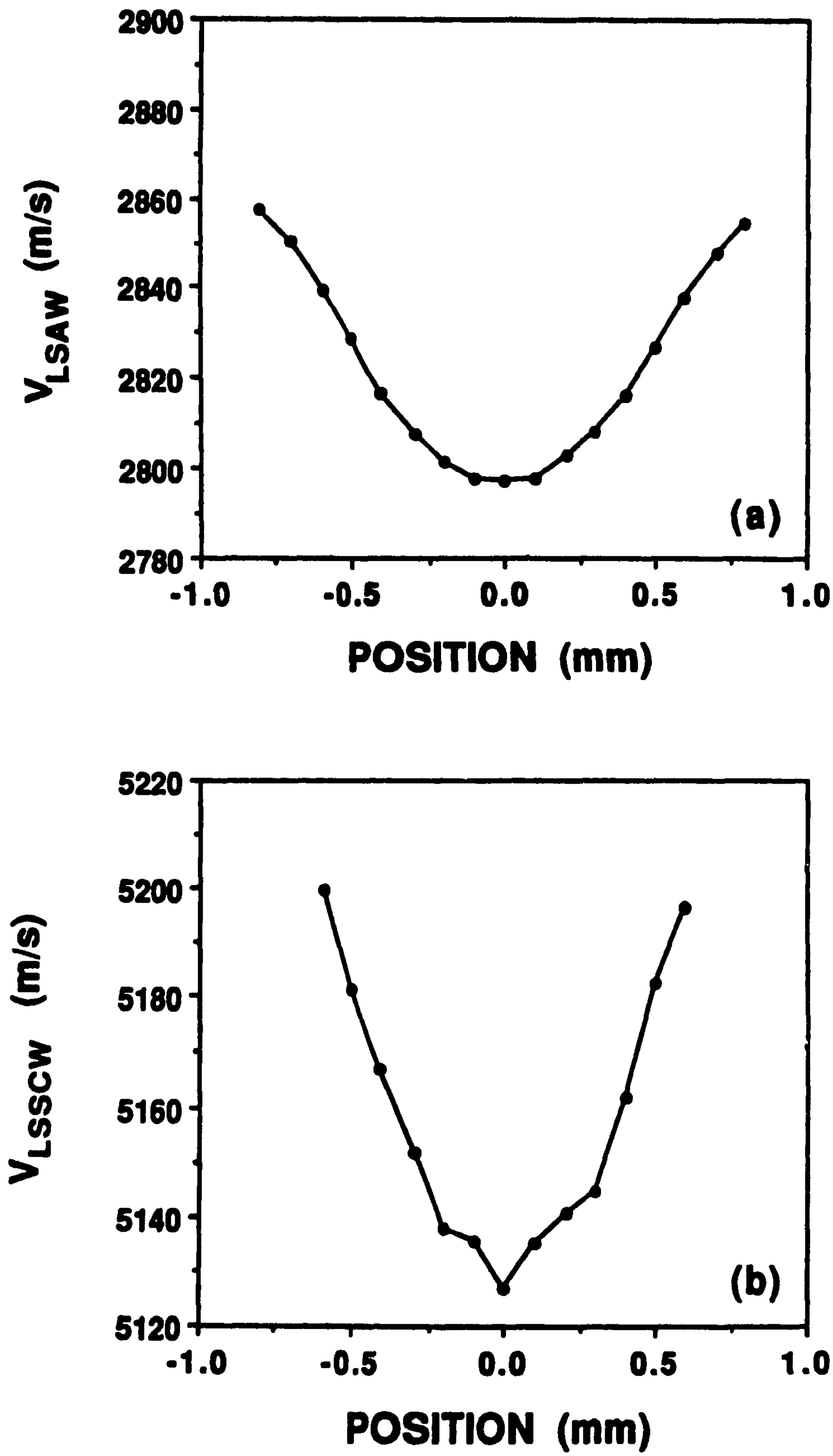

Figure 2.32 *Acoustic velocity profiles of Melles-Griot GRIN glass rod, (a)* v_{LSAW} *and (b)* v_{LSSCW}.

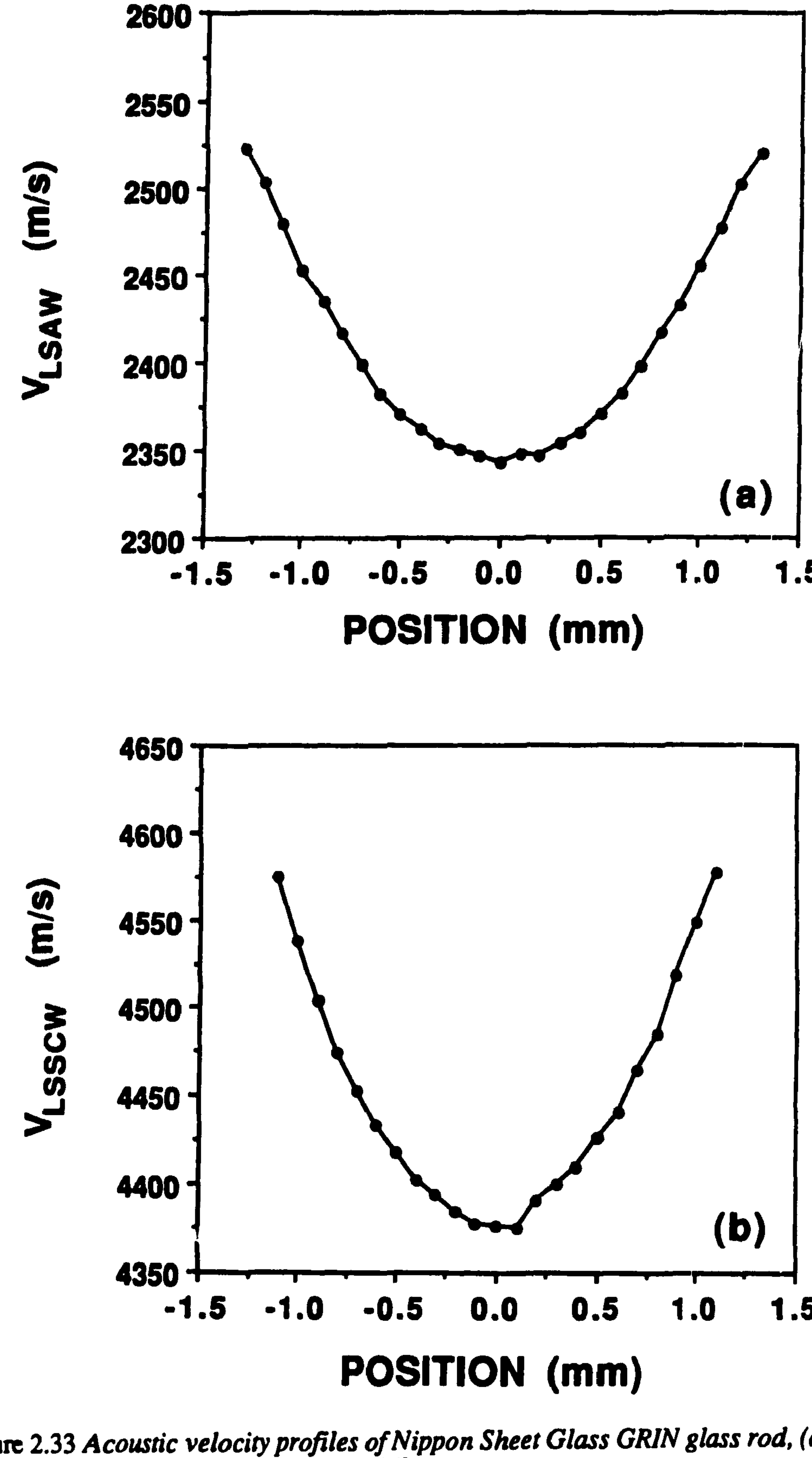

Figure 2.33 *Acoustic velocity profiles of Nippon Sheet Glass GRIN glass rod, (a)* v_{LSAW} *and (b)* v_{LSSCW}.

2.6 Potential Applications:

An interesting application of these acoustically focussing rods is a long low-noise buffer rod. When an ultrasonic transducer cannot be immersed directly into an environment under adverse conditions such as high temperature and pressure, a buffer rod is used to isolate the transducer from this environment. However, if a uniform cylindrical rod is bonded to the transducer, trailing echoes [39] will appear in a pulse-echo measurement due to the wave diffraction and the finite rod diameter. If, on the other hand, the rod guides acoustic energy in such a way that the beam does not come in contact with the walls, the trailing echoes can be eliminated or at least greatly reduced [40].

As a lens, a short piece of rod could be used, for example, to compensate the wave diffraction in the short buffer rod used in a scanning acoustic microscope. Presently, the mechanical grinding of the buffer rod ensures the proper focussing of the acoustic beam onto the sample. As mentioned in chapter 1, a planar structure can offer certain advantages. Furthermore, in addition to GRIN profiles presented in this chapter, other rods with specifically designed acoustic velocity profiles may be used in conjunction with all other types of lenses mentioned in chapter 1. For instance, an acoustic Fresnel zone plate can be achieved with ease by an acoustic velocity profile satisfying "Fresnel zone" requirements to be given in chapter 4. Furthermore, multilayer index profiles have been demonstrated in [35].

2.7 Summary:

In this chapter, focussing mechanisms of rods with graded acoustic velocity profiles have been presented. We have shown conclusively that longitudinal acoustic rays travelling in the rod will approximately follow a sinusoidal path as shown in Fig.2.17 if the velocity profile is close to parabolic. The rod can be used as a lens which focusses the acoustic energy. Again, due to the experimental limitations, only experiments involving longitudinal acoustic waves are demonstrated, although we believe that inside a GRIN rod, shear acoustic waves exhibit similar focussing mechanisms. The rods used here were fabricated like ordinary silica optical fibre preforms, but opaque materials such as metals and ceramics could be used.

Chapter 3: Ultrasonic Cylindrical Lens

3.1 Introduction:

As mentioned in chapter 1, cylindrical lenses are needed for in-line fibre optic signal processing devices. The geometry proposed for our cylindrical lens study is mainly a metallic film coated optical fibre which is coated with a piezoelectric thin film of lead zirconate titanate (PZT). On top of this PZT film there exists another thin metallic layer. The metallic film directly coated on the optical fibre serves as the inner electrode of the ultrasonic transducer while the outer electrode is the metallic film deposited on the PZT as shown in Fig.3.1a. These two electrodes are also used to perform the electrical poling radially for the PZT film to become piezoelectric [24], [26]. The thin piezoelectric PZT films coated on optical fibres may also be used as miniature ultrasonic transducers and electronically controllable deflectors if proper electrode patterns to be explained below are used. In order to have a good demonstration of ultrasonic focussing behaviors for PZT thin film transducers deposited on the thin cylindrical structures, PZT coated alumel wires as shown in Fig.3.1b are used as an alternative for PZT coated optical fibres. The explanation is given in section 3.3.1.

The PZT coated optical fibres or wires have been studied before [24]-[26]. Ultrasonic and deflection measurements were reported. In this chapter, further developments in this research are carried out, in particular, a novel laser ablation technique to fabricate complex patterns of electrodes on top of the PZT coated fibres or wires. Section 3.2 examines the fabrication and evaluation of PZT and thin metallic films coated on optical fibres and alumel wires which are used as ultrasonic cylindrical lenses. Section 3.3 looks into the response, transmission and reception capabilities of the lens while section 3.4 details optical fibre deflection measurement. Section 3.5 describes the laser ablation patterning of an IDT on the outer electrode and section 3.6 discusses a few potential applications of this cylindrical lens configuration. Section 3.7 summarizes the chapter.

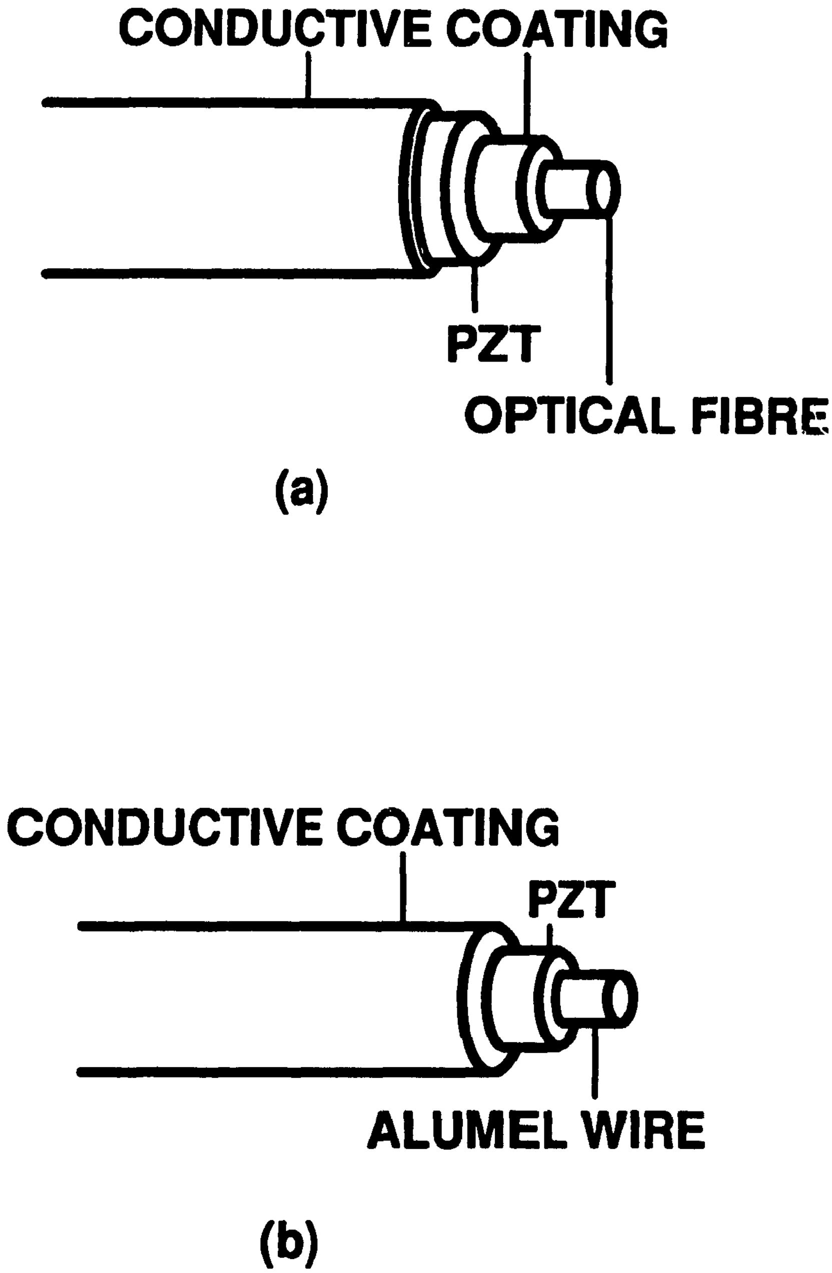

Figure 3.1 *Ultrasonic cylindrical lenses made with (a) an optical fibre and (b) an alumel wire.*

3.2 PZT and Thin Metallic Films Coated on Optical Fibres and Wires:

3.2.1 Introduction:

There exists many applications of metal films coated on optical fibres. Some of these include high temperature probes, hermetic jackets [41], polarisers [42], phase and frequency shifters [16], [17], [19], [43] and electric field sensors [44]. Thick metal coatings (15-20μm) are required for the high temperature devices while some other devices prefer thin metal films (<1μm). Optical fibre phase modulators employing piezoelectric (such as lead zirconate titanate) and metallic thin films are sometimes subjected to high temperatures during their fabrication or utilization. The thin films used must be of high quality and their quality must be maintained after the required heat treatment. In this section, the fabrication and evaluation of the PZT and thin metallic films are presented.

3.2.2 Fabrication and Evaluation:

3.2.2.1 PZT Films:

The PZT film is fabricated by Prof. M. Sayer's team at Queen's University in Kingston, Ontario [22], [23]. They use a sol-gel method. Uniform, crack-free films up to 5μm thick have been produced. This method of fabrication is especially attractive to coat fibres or wires because it only requires a dipping of the fibre or wire into the sol-gel. Wires up to 22cm long have been coated with PZT as shown in Fig.3.2.

Previous work has been done on the evaluation of the PZT films produced by Queen's University [24], [25]. These piezoelectric films used as ultrasonic thin film transducers can operate between 50 and 450MHz and have been coated on substrates such as fused quartz and metals, flat and cylindrical surfaces, and substrates with a large coating area or length. The piezoelectricity of the film is achieved by a standard electrical poling process in which the film is polarized at 175°C for 2 hours at an electric field of 3kV/mm [22].

3.2.2.2 Thin Metallic Films:

Since a thin metallic film is required to be deposited on the bare optical fibres as the inner electrode shown in Fig.3.1 for the electrical poling process, it must survive the PZT thin film fabrication process which has been reported in [22] and [26]. It means that this inner electrode must survive an operating temperature (for the annealing process) of about 550°C for a few hours.

For ultrasonic transducer and lens applications this layer is preferred to be very thin (a few μm). We collaborated with the National Optics Institute (NOI) to coat a layer of thin metallic film directly on the bare optical fibre using a coaxial method illustrated in Fig.3.3.

As the small optical fibre (<250μm diameter) is being pulled from the preform (>5mm diameter), it passes through a tungsten coil which has been wet with the desired metal, aluminum or gold in this case. The tungsten filament in a vacuum chamber is heated by applying an electric current and the metal is evaporated. The vacuum is achieved by a mechanical pump down to a pressure of approximately 10^{-3} torr. The coated fibre is then spooled. A 50cm long gold coated optical fibre and a 130cm long aluminum coated optical fibre were obtained.

The two fibres were first cleaved into several 1cm pieces. They were evaluated by an optical reflective microscope and a scanning electron microscope. We were able to estimate the thickness of the aluminum film at 0.5±0.1μm and the gold film at 0.6±0.2μm. It was found out that the gold coating thickness decreased along the length of the fibre. This was probably due to a diminishing amount of gold on the heating coil through which the fibre was pulled. However, the aluminum coating did not exhibit this tendency. A typical cross-section of both the aluminum and gold coated optical fibres are shown in Figs.3.4 and 3.6 along with their respective enlarged areas given in Figs.3.5 and 3.7.

A simple adhesion test was used to evaluate the adhesion of the metal films to the silica fibres. Adhesive tape was applied to the coated fibres and then removed. In both cases the metallic coating came off with the adhesive tape. This indicated poor adhesion.

Samples of aluminum and gold coated fibres were heated at different temperatures under different pressures to observe the quality of the films after heat treatment. This test is of interest because the inner electrode must survive the PZT thin coating process which involves heat treatment at around 550°C for a few hours [22]. The heating system used, as shown in Fig.3.8, was a furnace in which the heating chamber can be evacuated by a mechanical pump and a diffusion pump. The furnace is controlled by a computer, hence a specific heating profile can be planned. First, the samples were heated at 200°C at atmospheric pressure for three hours. No damage to either films was observed. We repeated the process at 400°C and again no damage was observed. However when we heated the samples at 600°C for three hours under atmospheric pressure both films were destroyed. Approximately 10% of the gold coating was removed and the rest was modified, probably oxidized. For the aluminum coated fibre, more than 50% of the film was removed and the rest was oxidized. Since there were damages to the films, we repeated the heating at 600°C for three hours, but this time at a pressure of 10^{-2} torr. Again, both the gold and aluminum films were damaged. However, the extent of the damage was less. The gold coated fibre only lost approximately 1% of its film. The aluminum coated fibre still lost more than 50% of its film and the oxidation was also apparent.

The uniformity of the aluminum and gold films fabricated by coaxial vacuum evaporation seems to be adequate for our purpose, however, the adhesion has not been satisfactory. There are three main factors that influence the adhesion of a film to a substrate: cleanliness of the substrate, pressure of the environment in which the evaporation takes place and the buffer material between the substrate and the film. Since the fibre was coated during the pulling from the preform, we can assume that the fibre was as clean as it can be. The estimated pressure during the evaporation was approximately 10^{-3} torr which is about two orders of magnitude higher than for a traditional vacuum evaporation. We therefore suggest using a more powerful mechanical pump or a diffusion pump to lower the pressure in order to increase the adhesion of the film. Finally, no buffer material was used between the substrate and the film to help adhesion. We suggest using a second tungsten filament earlier in the process to deposit a very thin film of titanium, nickel or chromium (50-100Å) on the fibre before depositing the aluminum or gold. However, due to the technical difficulties at NOI, the improved evaporation experiment was not carried out.

Therefore, commercially produced aluminum and gold coated multimode optical fibres were used for the coating of PZT. The thickness of the metal layer is more than 15μm. Such a metallic layer will cause additional ultrasonic attenuation at frequencies higher than 50MHz. However, they were very uniform and survived the adhesion and heat treatment test. Then, these fibres were coated with a PZT thin film as shown in Figs.3.9a and 3.9b. It is noted that for PZT coated optical fibre, the longest PZT coating length without a crack has been 20cm and the limitation comes from the length of the heating furnace. Unfortunately, to our knowledge no metallic coated single mode optical fibre is available commercially. **It has therefore been decided that phase modulation, which requires single mode optical fibre, will not be covered in this thesis.**

The outer electrode shown in Fig.3.1 does not need to go through the PZT fabrication process. Thus we used a similar coating technique shown in Fig.3.3 to deposit it on top of the PZT layer, but with a vacuum pressure of $\sim 10^{-6}$torr. The adhesion was improved.

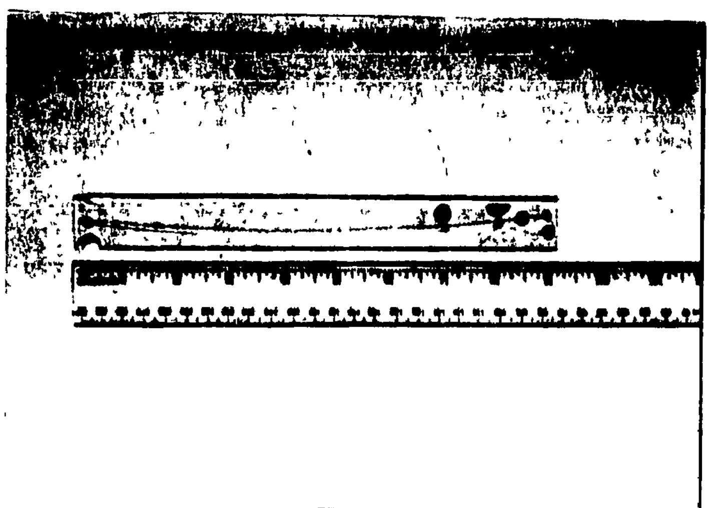

Figure 3.2 *Long PZT coated alumel wire.*

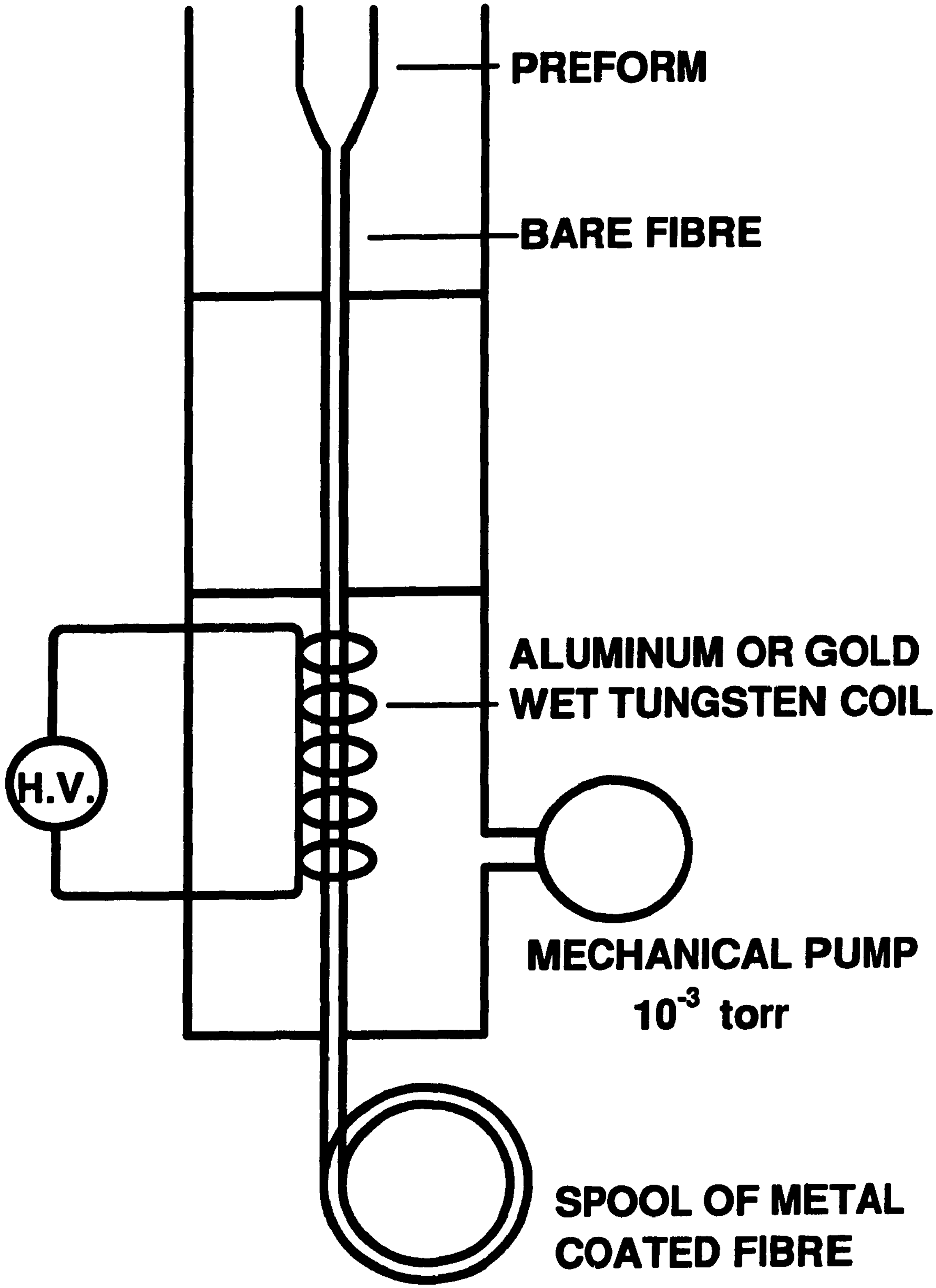

Figure 3.3 *Schematic of the fabrication process of thin metallic coatings on optical fibre.*

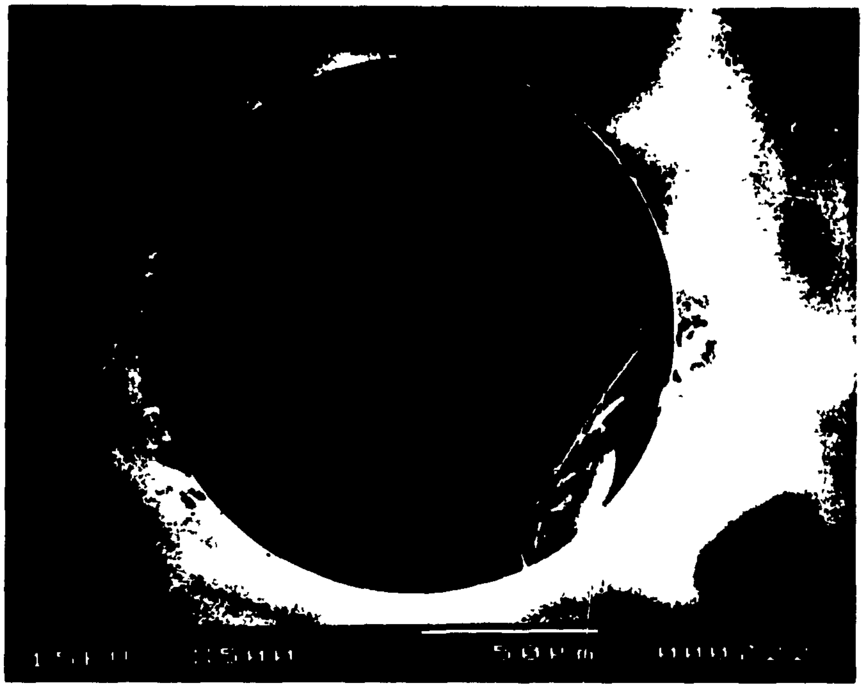

Figure 3.4 *Cross-section of an aluminum coated optical fibre.*

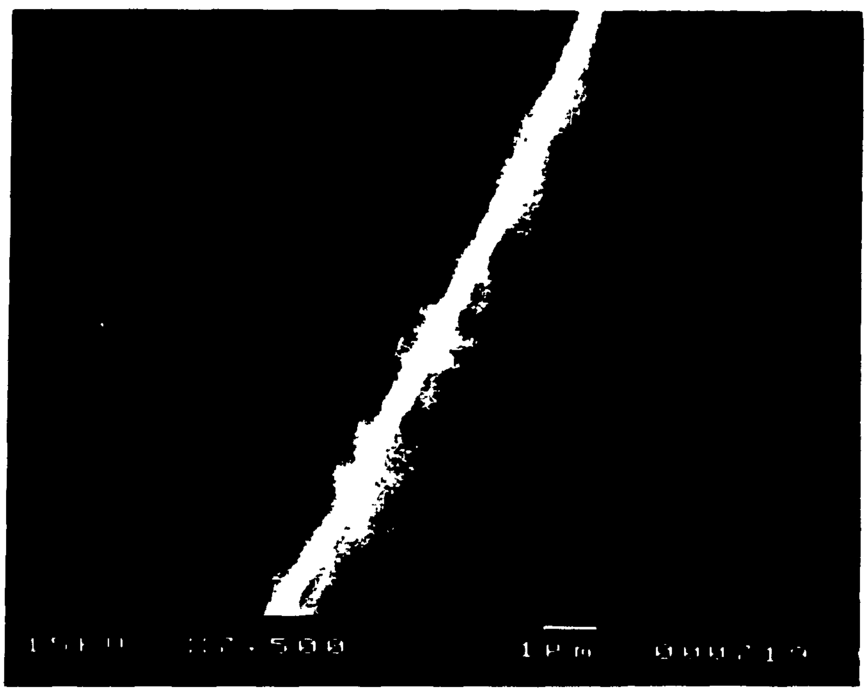

Figure 3.5 *Enlarged area of a cross-section of an aluminum coated optical fibre.*

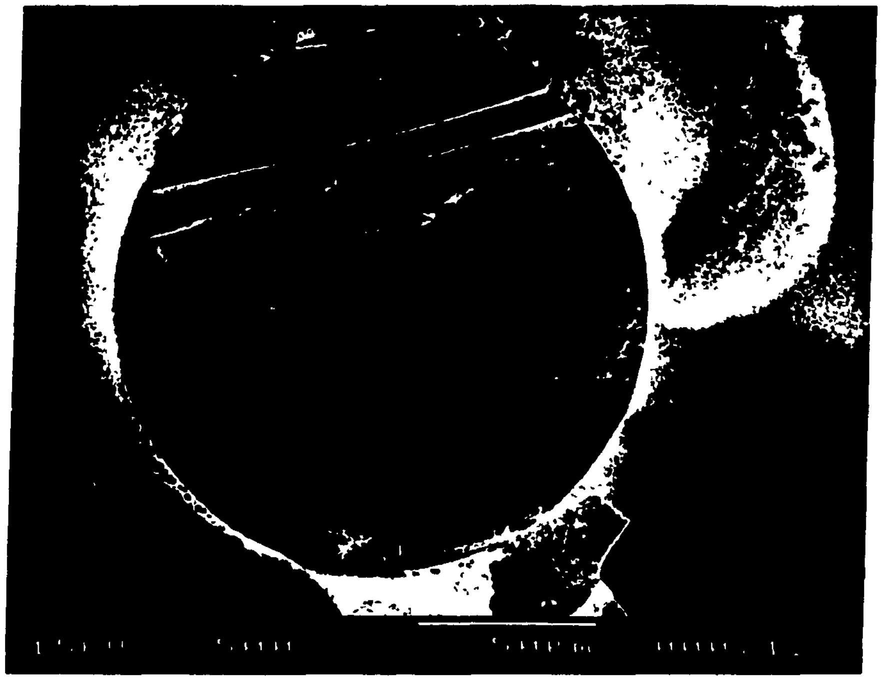

Figure 3.6 *Cross-section of a gold coated optical fibre.*

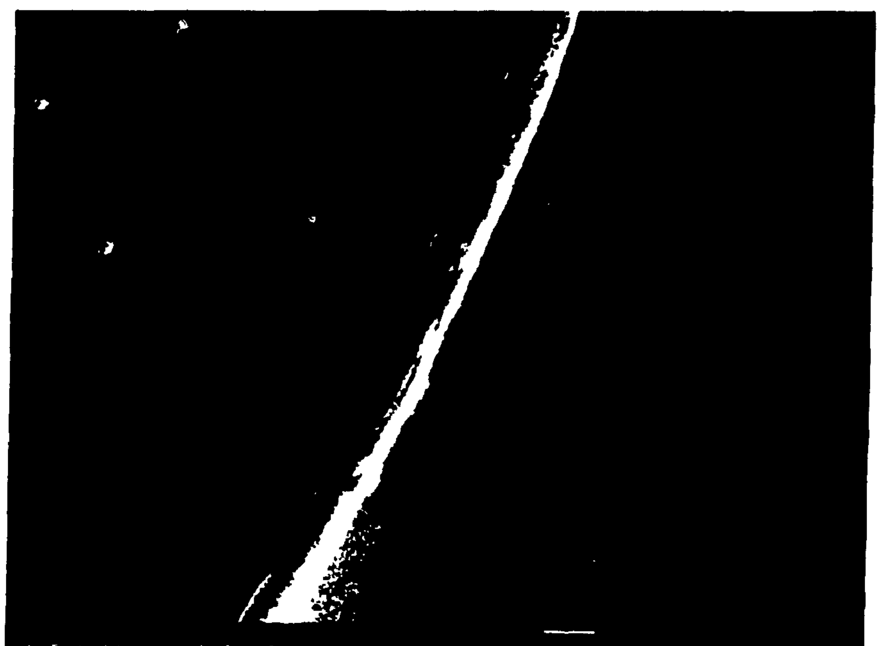

Figure 3.7 *Enlarged area of a cross-section of a gold coated optical fibre.*

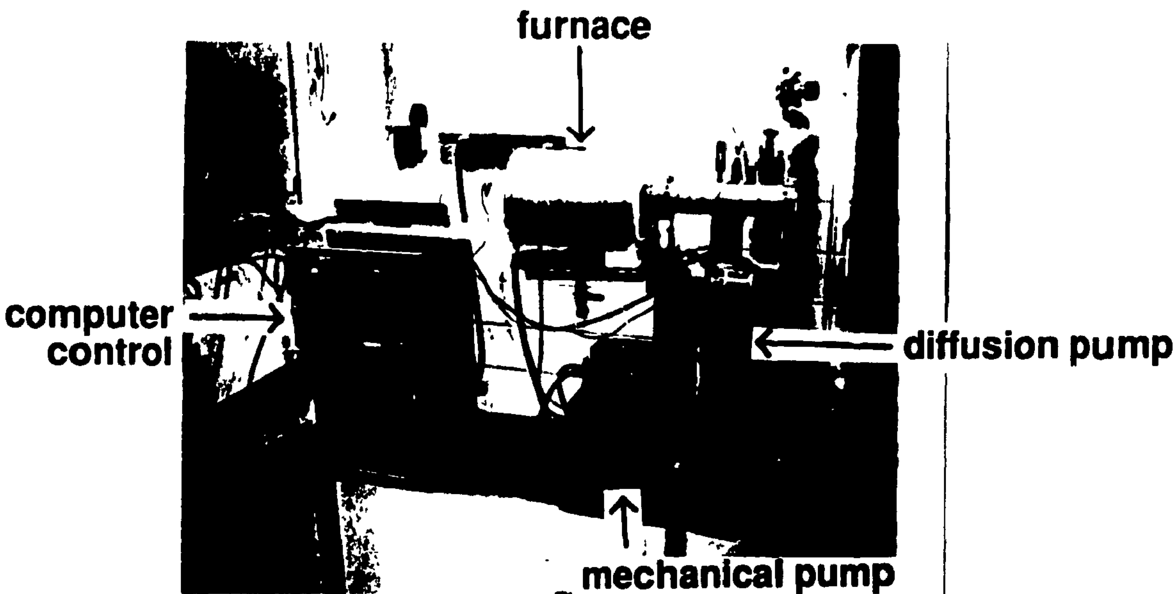

Figure 3.8 *Photograph of computer controlled heating system.*

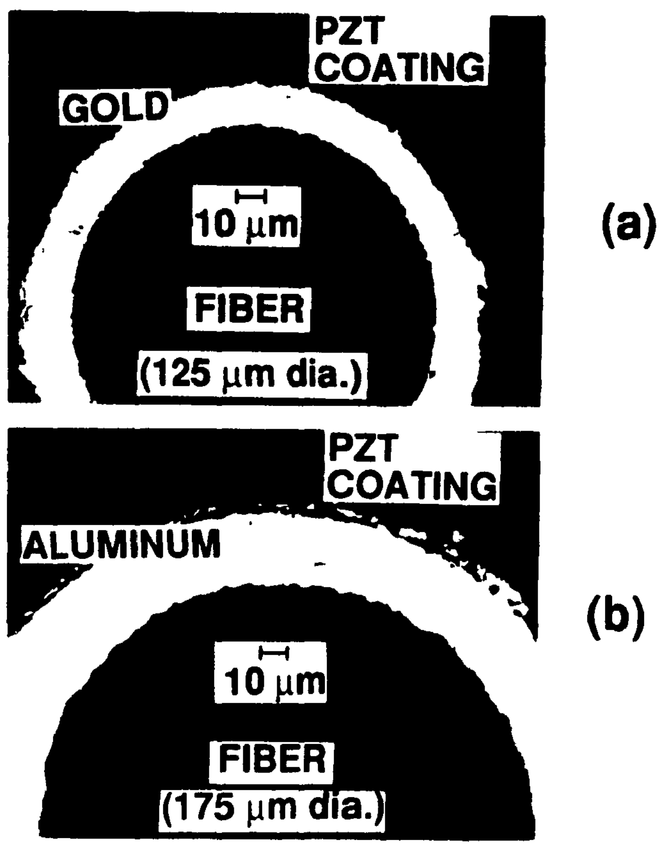

Figure 3.9 *Photographs of a cross-section of PZT coated optical fibre with (a) a gold and (b) an aluminum inner electrode*

3.3 Ultrasonic Performance:

3.3.1 Introduction:

At the present time, the diameters of commercially available metallic film coated optical fibres are small as shown in Figs.3.9a and 3.9b and the thickness of the metallic coating is larger than 15μm. In order to have a good demonstration of the ultrasonic focussing behavior of these PZT coated optical fibres using an ultrasonic pulse-echo measurement system, the system bandwidth must be close to 200MHz. Due to the limitation of our instrument which has a bandwidth of around 100MHz, PZT coated wires as given in Fig.3.1b are used as an alternative for the PZT coated fibres. Alumel wires with a diameter of 250μm diameter as shown in Fig.3.10 were coated with PZT and an outer metallic electrode. The wire itself serves as the inner electrode for the electrical poling process and ultrasonic transducer applications.

Thin piezoelectric PZT film coated optical fibres or wires can be used as cylindrical focussed ultrasonic transducers due to the fact that fibres and wires have a cylindrical geometry. The ultrasonic waves generated by the PZT will be focussed to the axis of the fibre or wire. The miniature ultrasonic transducer can be made simply with a top electrode of a small area. These miniature ultrasonic transducers could be used as a small probe in medical applications or nondestructive evaluation of materials.

3.3.2 Ultrasonic Measurements:

Figure 3.11 is a photograph of the transducers used for the experiments. Figure 3.12 shows the experimental set-up for the evaluation of ultrasonic focussing behaviors of PZT coated wires as shown in Fig.3.10. Due to the high dielectric constant (ε_r~300) of the PZT [22] and the small thickness of the thin film, the large capacitance effects on such a transducer is not negligible [25]. In order to have efficient eletro-acoustic conversion from our 50Ω electronic systems, the large capacitance of PZT thin film transducers limits the top electrode size as shown in Fig.3.12. In this section, the top electrode is about 1.5mm in length.

The first measurement performed was to verify the piezoelectricity of the device. In fact, we were measuring the response of the transducer. The transducer used as an ultrasonic transmitter as well as receiver was simply connected to a Panametrics pulser/receiver and the reflected signal was sent to an oscilloscope. The signal on the oscilloscope showed acoustic echo trains as illustrated in Figs.3.13a and 3.13b within the transducer due to the reflections caused by the large acoustic impedance mismatch at the exterior boundary with the air. The echoes are bulk acoustic wave pulses traversing across the diameter of the 250μm alumel wire, and bouncing back and forth. It is interesting to note that since the longitudinal acoustic pulse excited by the cylindrically symmetric PZT transducer goes through the center of the wire which can be regarded as the focus of the cylindrical acoustic waves, during each diagonal traversing of the wire, a 90° phase shift should exist between each successive echo [24]. Figure 3.13b clearly shows the 90° phase shift, thus confirming the ultrasonic focussing. Each adjacent echo also touches one another and this means that the 100MHz bandwidth of our pulse-echo measurement system is just good enough for the 250μm diameter alumel wire.

The second step was to use PZT coated wires as miniature ultrasonic transducers. The experimental set-up for a transmission experiment is illustrated in Fig.3.14. In the experiment, one PZT coated wire is used as the transmitter and another one is used as the receiver. A drop of kerosene which is non-conductive is used as the ultrasonic coupling medium between these two nearly identical transducers. Figures 3.15a and 3.15b show two measured signals which vary only by the distance between the two transducers. The signals received were weak but with proper signal processing from computer software, called UDASP [45], the signal-to-noise ratio (SNR) was much enhanced as shown in Figs.3.16a and 3.16b. These figures indicate that with an improved SNR, miniature ultrasonic transducers may be of use for medical applications or nondestructive evaluation of materials in areas which have only small openings for access.

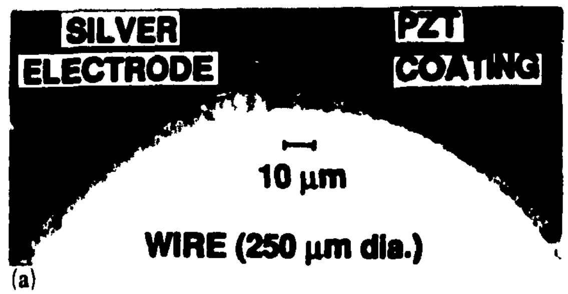

Figure 3.10 *Photograph of a cross-section of a PZT coated alumel wire.*

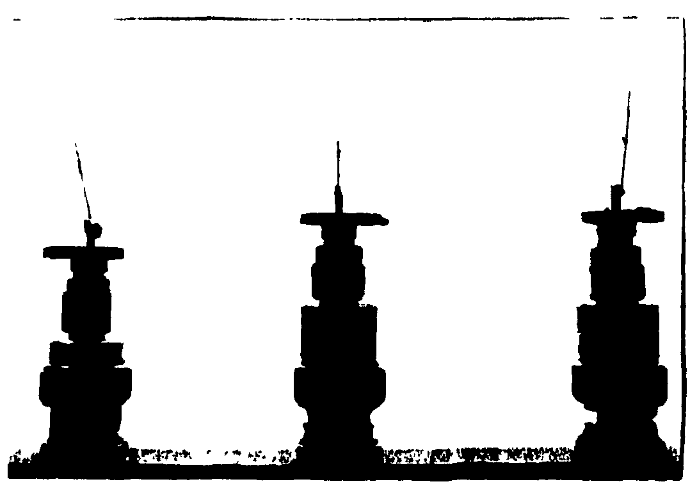

Figure 3.11 *Photograph of the cylindrical lens transducers.*

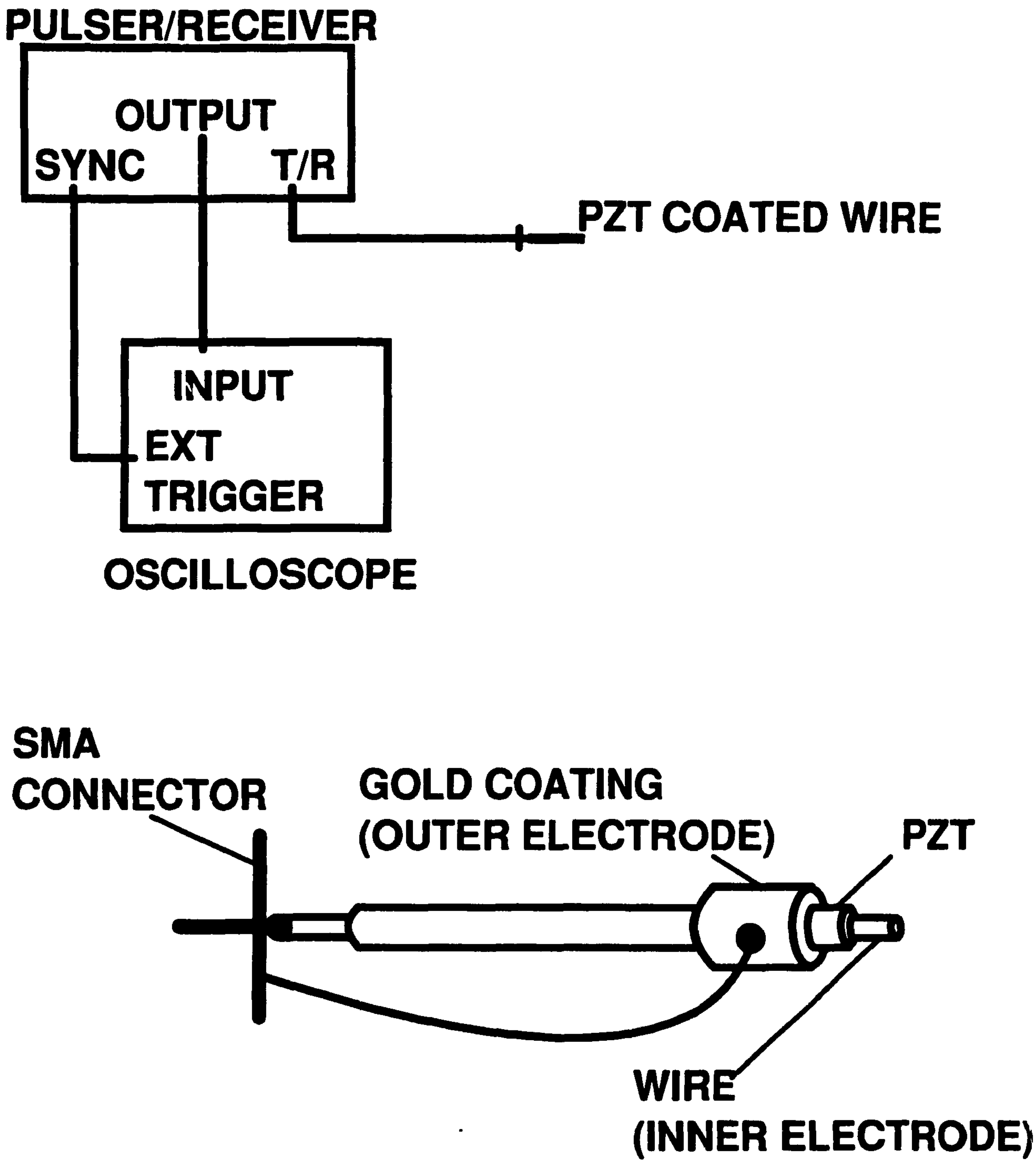

Figure 3.12 *Schematic of the experimental set-up to measure the response of a cylindrical transducer.*

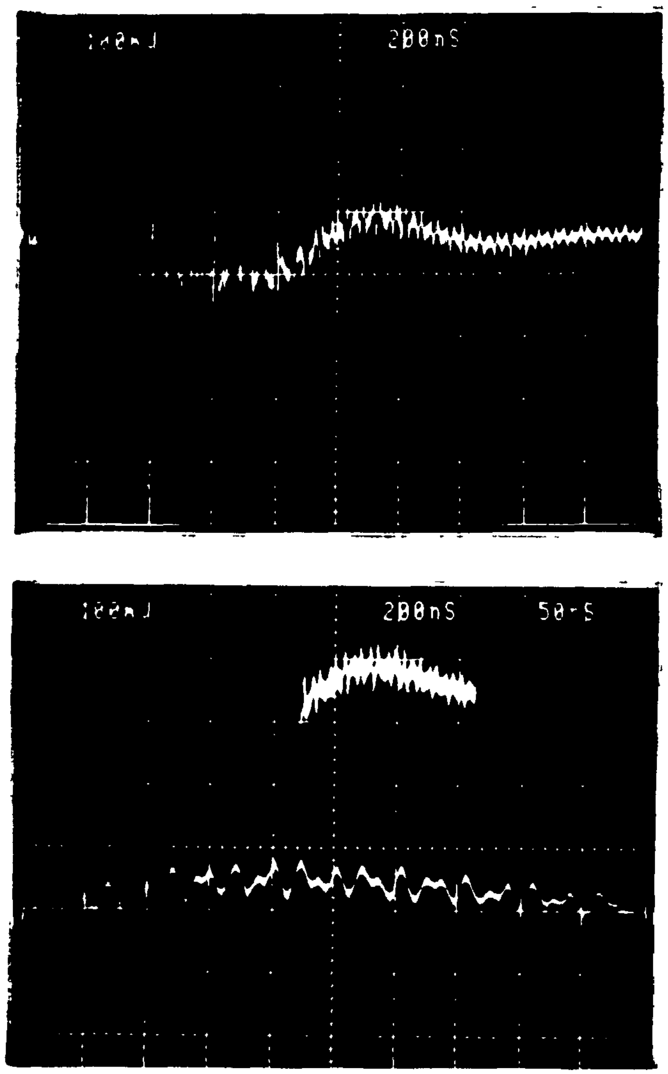

(a)

(b)

Figure 3.13 *Oscilloscope signal of cylindrical transducer, (a) longitudinal pulse-echo trains obtained with PZT coated wire operated in reflection mode and (b) ten echoes showing 90° phase shift between each successive echo.*

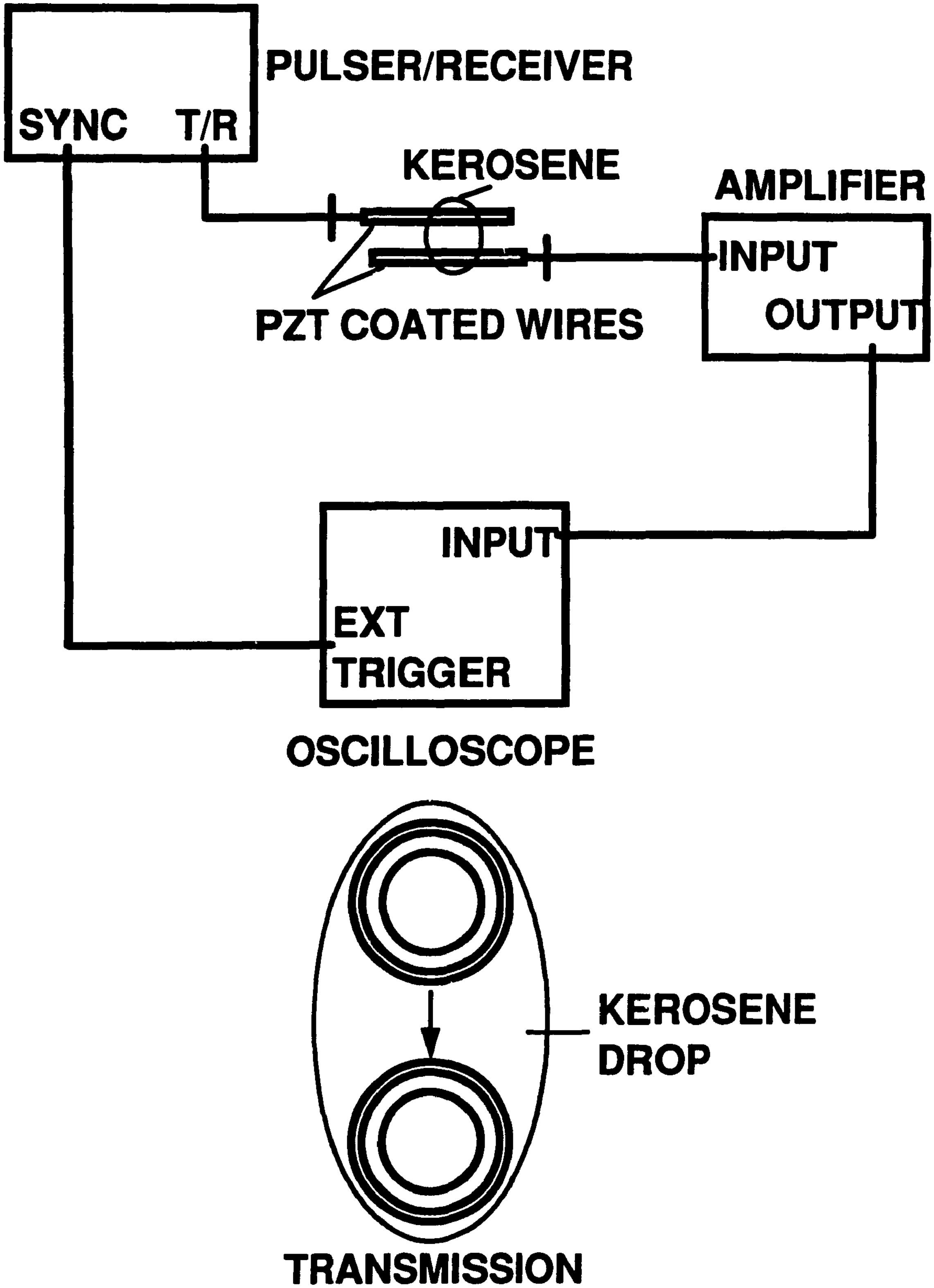

Figure 3.14 *Schematic of the experimental set-up to measure the transmission and reception capability of a cylindrical transducer.*

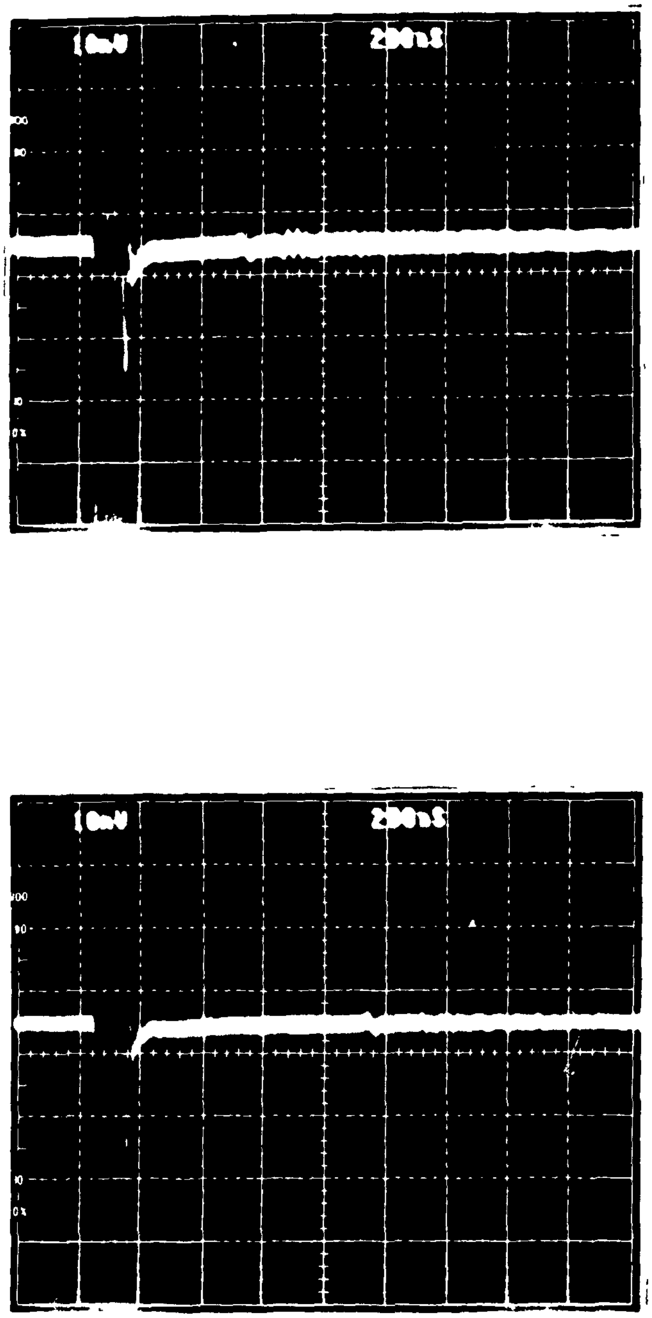

(a)

(b)

Figure 3.15 *Oscilloscope signals of transmitted pulse by a cylindrical transducer, (a) transducers are close together and (b) transducers are farther apart.*

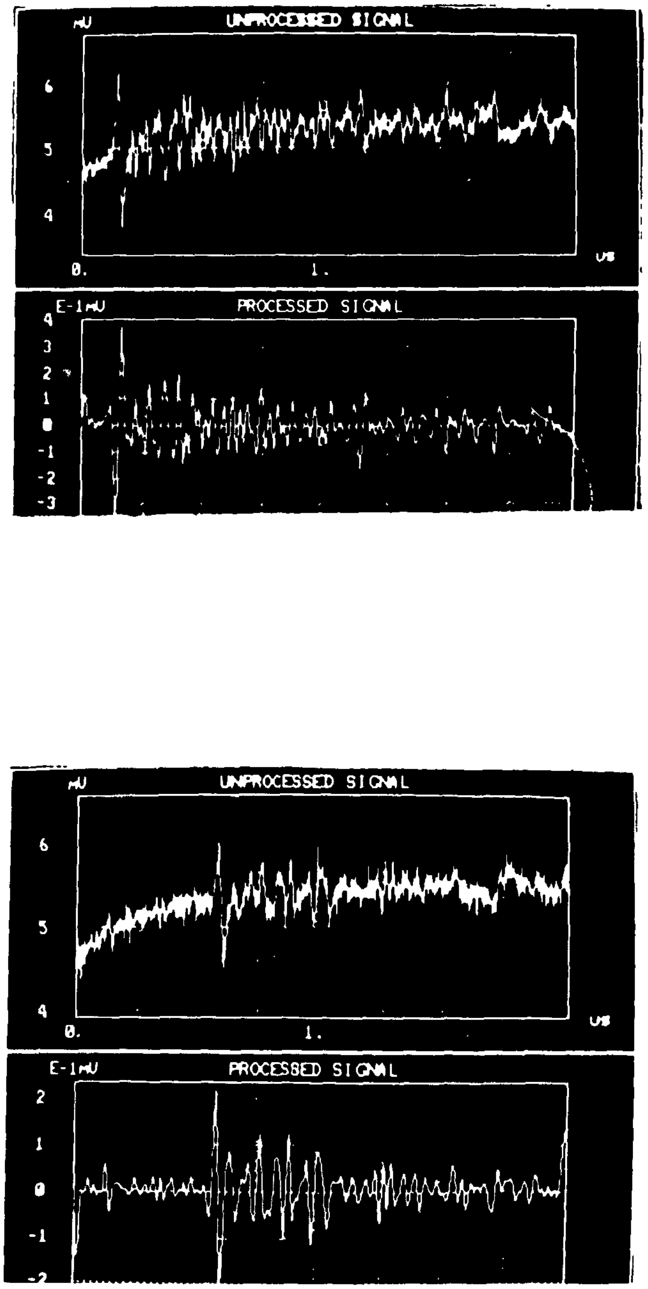

(a)

(b)

Figure 3.16 *Digitized and filtered signals of transmitted pulse by a cylindrical transducer, (a) transducers are close together and (b) transducers are farther apart.*

3.4 Deflection With PZT Coated Optical Fibres:

3.4.1 Introduction:

Since PZT is a piezoelectric material, with a proper electrode pattern on top of a PZT coated optical fibre an electronically controllable deflecting optical fibre is possible. This technology could be used to direct the tip of an optical fibre probe for imaging or laser surgery. In this section we present a method by which a PZT coated optical fibre can be deflected periodically.

3.4.2 Deflection Mechanism:

When a PZT layer coated on a fibre is not uniform, as is our case, if a voltage is applied across the radially poled PZT film, the strains produced along the fibre are not symmetric and the fibre will bend. If the length of PZT coated fibre is long enough, the bending force will be large enough to cause deflections in the order of millimeters.

3.4.3 Experimental Set-up:

A method similar to the common knife edge technique was used to measure the deflection. This technique was particularly of interest to estimate the very small deflections (<100μm). The set-up used is illustrated in Fig.3.17. Laser light was focussed on the free end of a PZT coated fibre. The light which was not blocked by the fibre was then collected by another lens to a photodetector. Hence, the vibrating fibre would cause an amplitude modulation of the light which would be observed by the photodetector. The signal was sent to an oscilloscope for quantitative measuring of the deflection. The fibre was isolated from the disturbance due to large air displacements by means of a box. The fibre used for this measurement was 10cm long.

First, a calibration curve had to be drawn to estimate the deflection. The fibre was fixed on a three-axis micrometer translational stage. The fibre was then set at the focus of the beam by collimating the light reflected by the aluminum coating. The fibre was then moved by increments of 5μm and the DC voltage on the oscilloscope was recorded. The process was repeated three times to produce the data plotted in Fig.3.18.

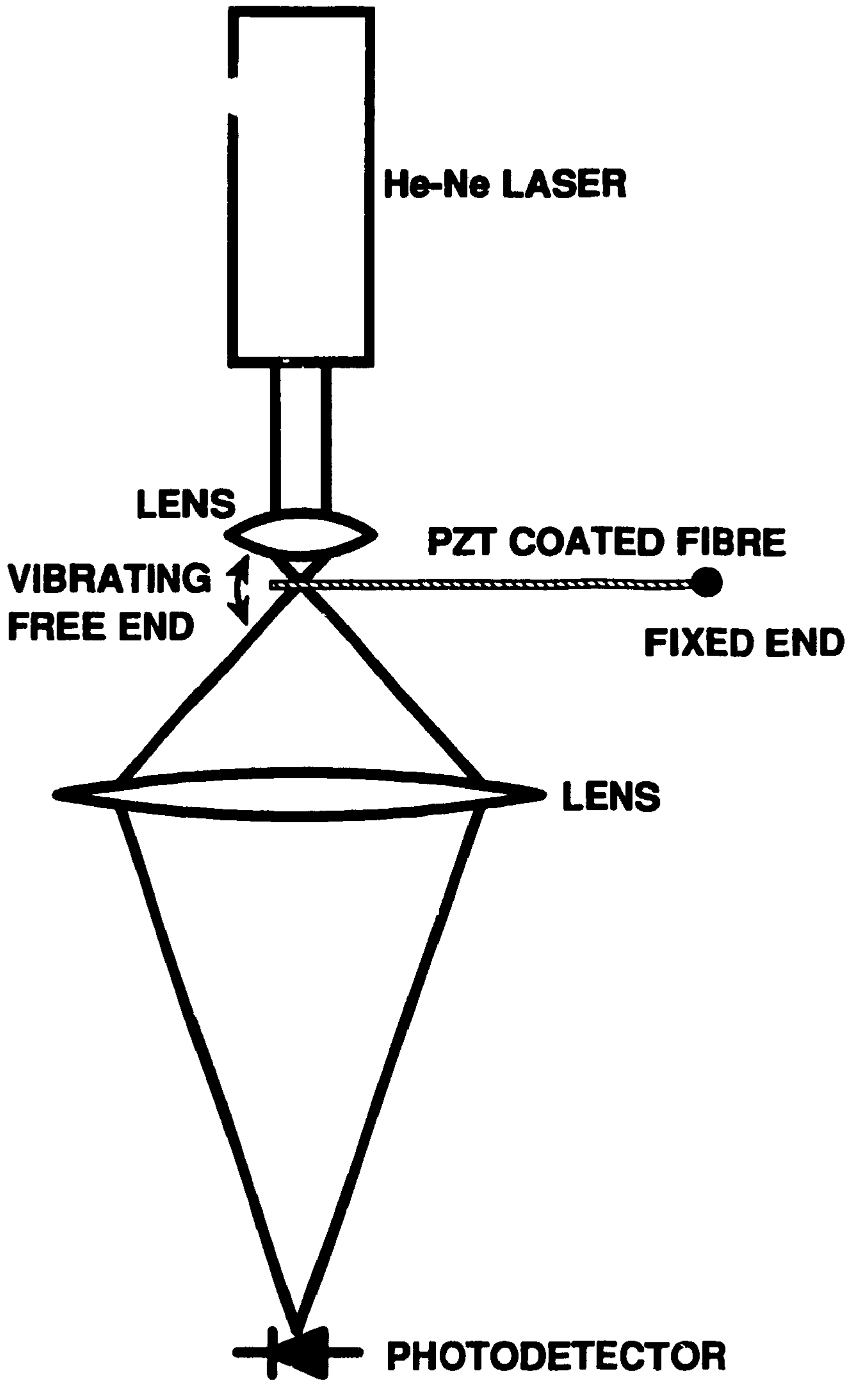

Figure 3.17 *Knife edge technique to measure the deflection of a PZT coated optical fibre.*

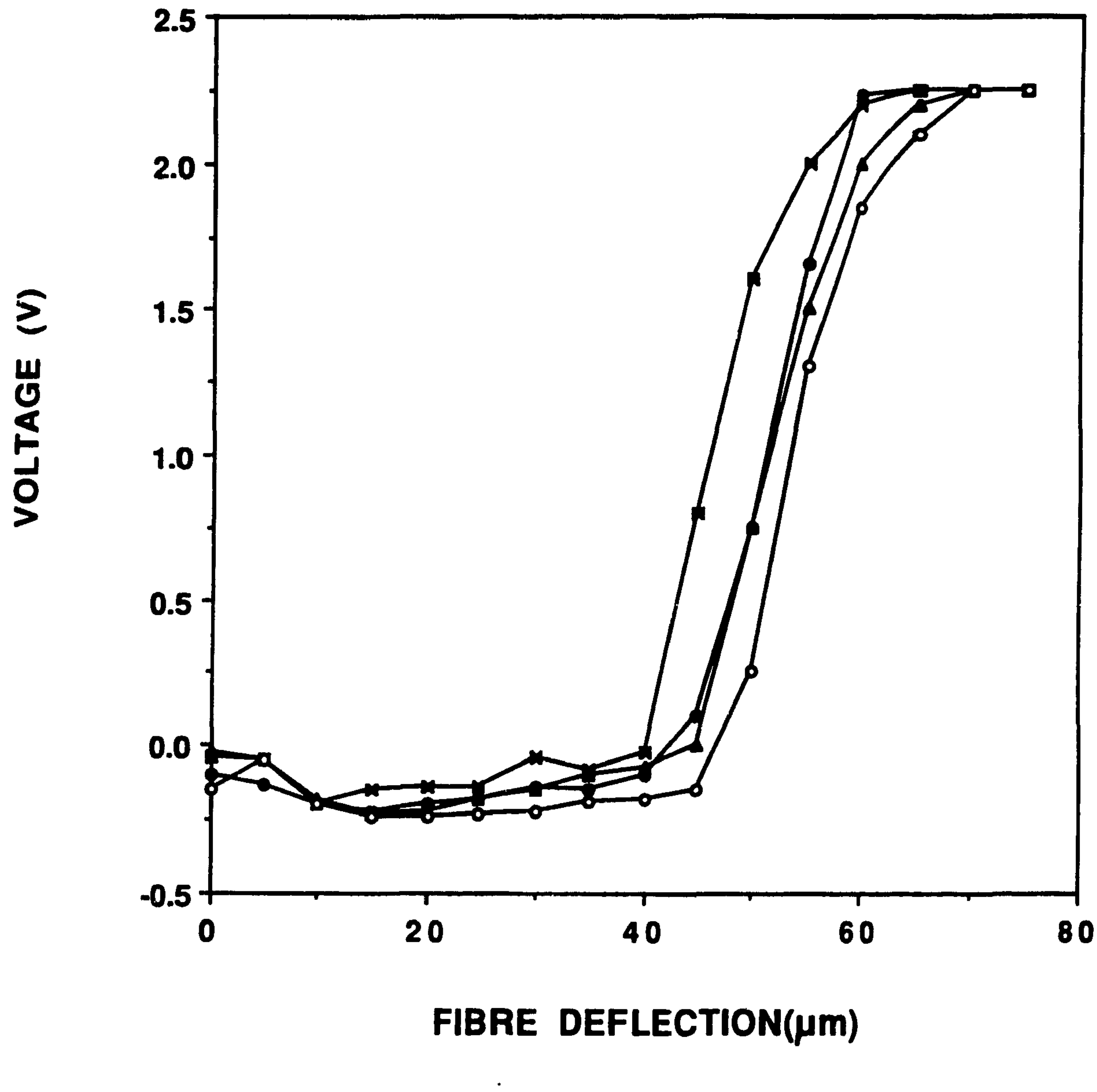

Figure 3.18 *Calibration curve to measure the deflection of a PZT coated optical fibre.*

3.4.4 Results:

The inner and outer electrodes of the PZT coated fibre were connected to an SMA connector. A sinusoidal signal with a 12V peak-to-peak voltage from a function generator was applied across these two electrodes. Figure 3.19 is a photograph of the PZT coated fibre used for the deflection. The fibre acting like a vibrating string only vibrated at discrete resonant frequencies. Figures 3.20-3.24 show the signals from the photodetector for 10.6kHz, 1.36kHz, 290Hz, 94.1Hz and 8.63Hz. The estimated deflections were 1μm, 4μm, 100μm, 150μm and >200μm respectively. The deflections increased with a decreasing frequency. However, this was true only at resonant frequencies all the way down to 4.3Hz. The deflection at this frequency was so large that the knife edge technique was not effective due to the fact that the photodetector used for this experiment was saturated. Since the deflection was in the order of a millimeter, which is visible by the naked eye, it was decided to videotape the deflection. A CCD camera recorded the event through a viewing microscope. Then the film was stopped at each frame to take a series of pictures as shown in Figs.3.25a-3.25d, which indicates a deflection of ~800μm since the total fibre diameter is ~240μm. Lower frequency signals, from 4.3Hz to DC, were applied to the fibre but no deflections were observed.

3.4.5 Discussion:

It is interesting to note that the fibre only vibrated at certain discrete resonant frequencies, even at low frequencies. We think that these resonant frequencies are determined by the mechanics of the entire system including the thickness of the PZT thin film and the fibre length. The data presented in this section is approximate, as the vibration from the room caused much uncertainty. The box used to decrease the flow of air on the fibre was not hermetic and so this aspect of the noise on the oscilloscope could be improved. Naturally, the use of a shorter fibre would decrease the noise, at the expense of a smaller deflection.

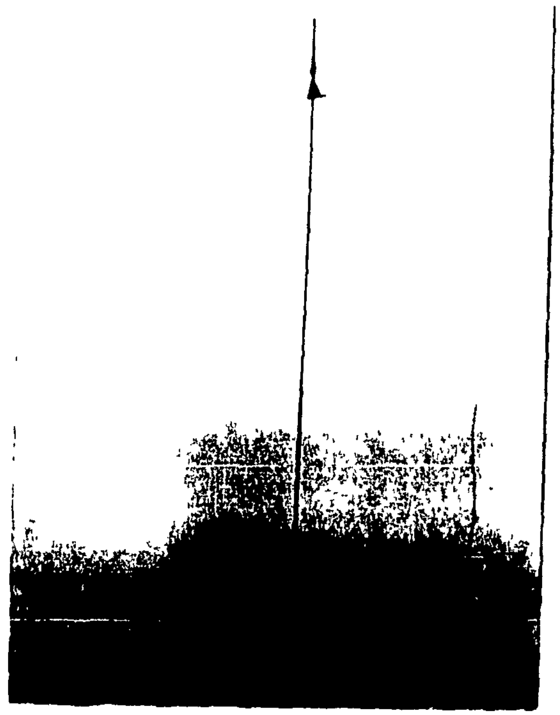

Figure 3.19 *Photograph of the PZT coated optical fibre used for the deflection experiment.*

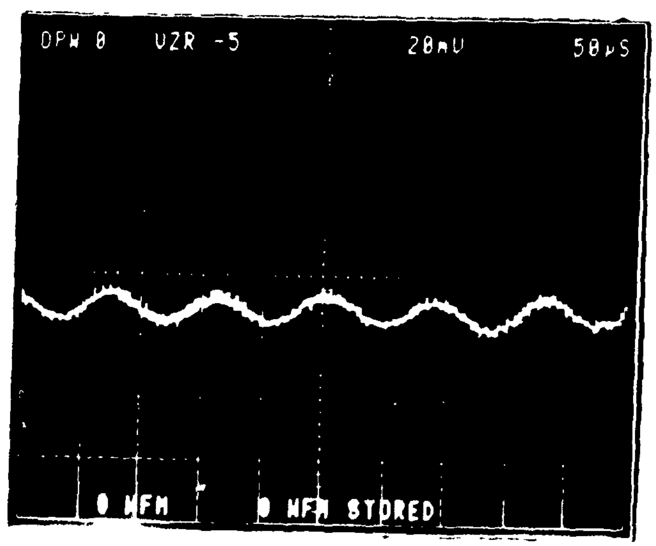

Figure 3.20 *Signal from the photodetector of a PZT coated optical fibre vibrating at 10.6kHz (deflection~1μm).*

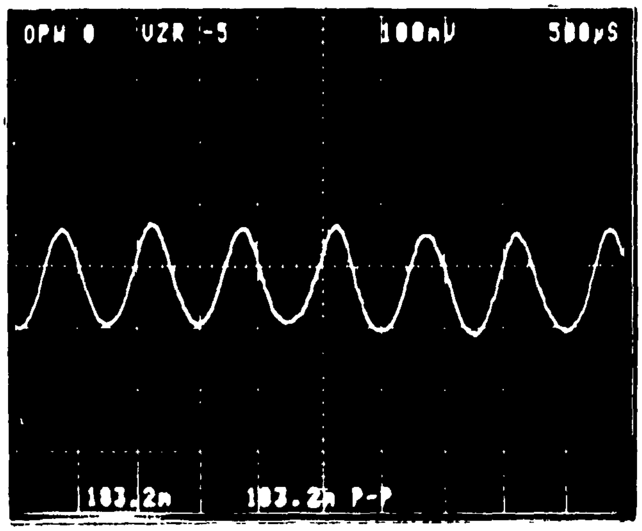

Figure 3.21 *Signal from the photodetector of a PZT coated optical fibre vibrating at 1.36kHz (deflection~4μm).*

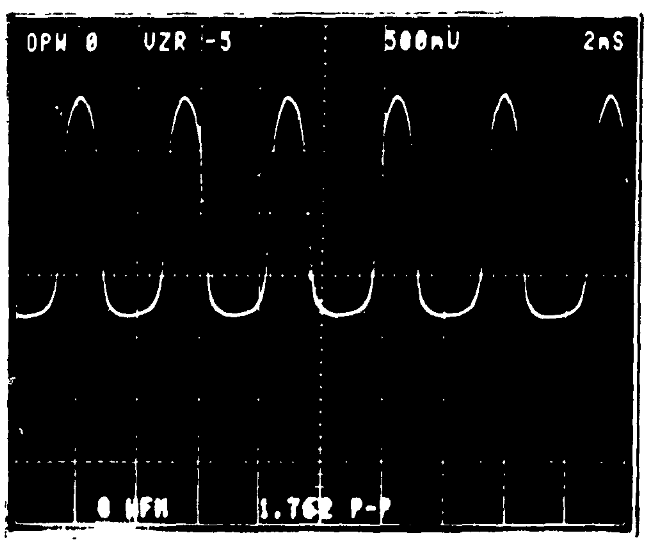

Figure 3.22 *Signal from the photodetector of a PZT coated optical fibre vibrating at 290Hz (deflection~100μm)*

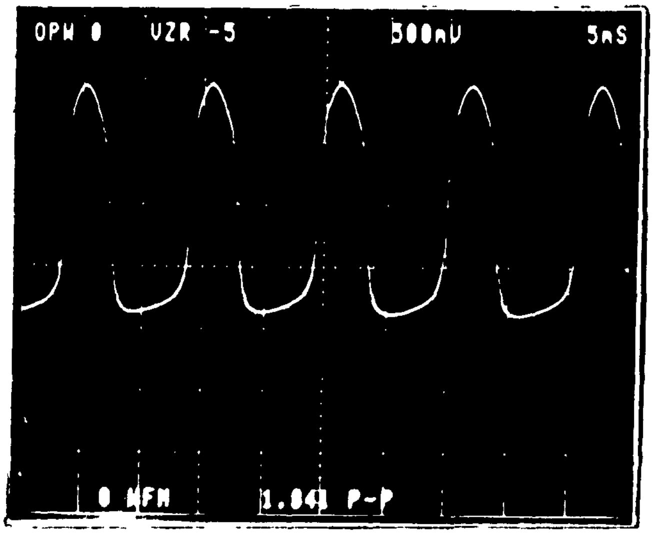

Figure 3.23 *Signal from the photodetector of a PZT coated optical fibre vibrating at 94.1Hz (deflection~150μm).*

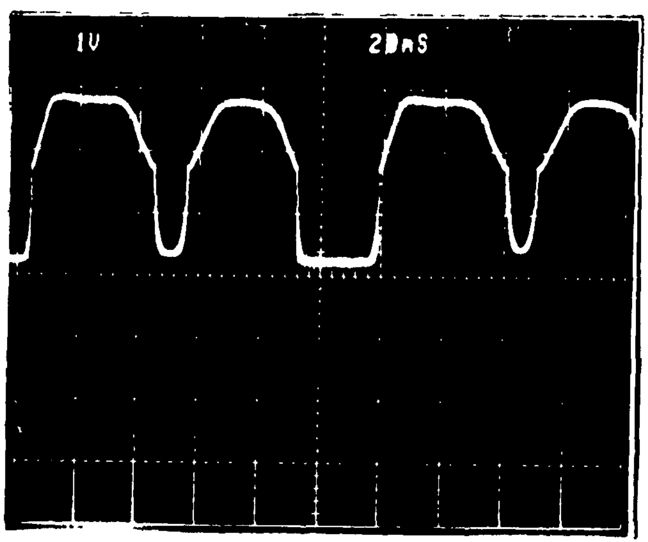

Figure 3.24 *Signal from the photodetector of a PZT coated optical fibre vibrating at 8.63Hz (deflection>200μm).*

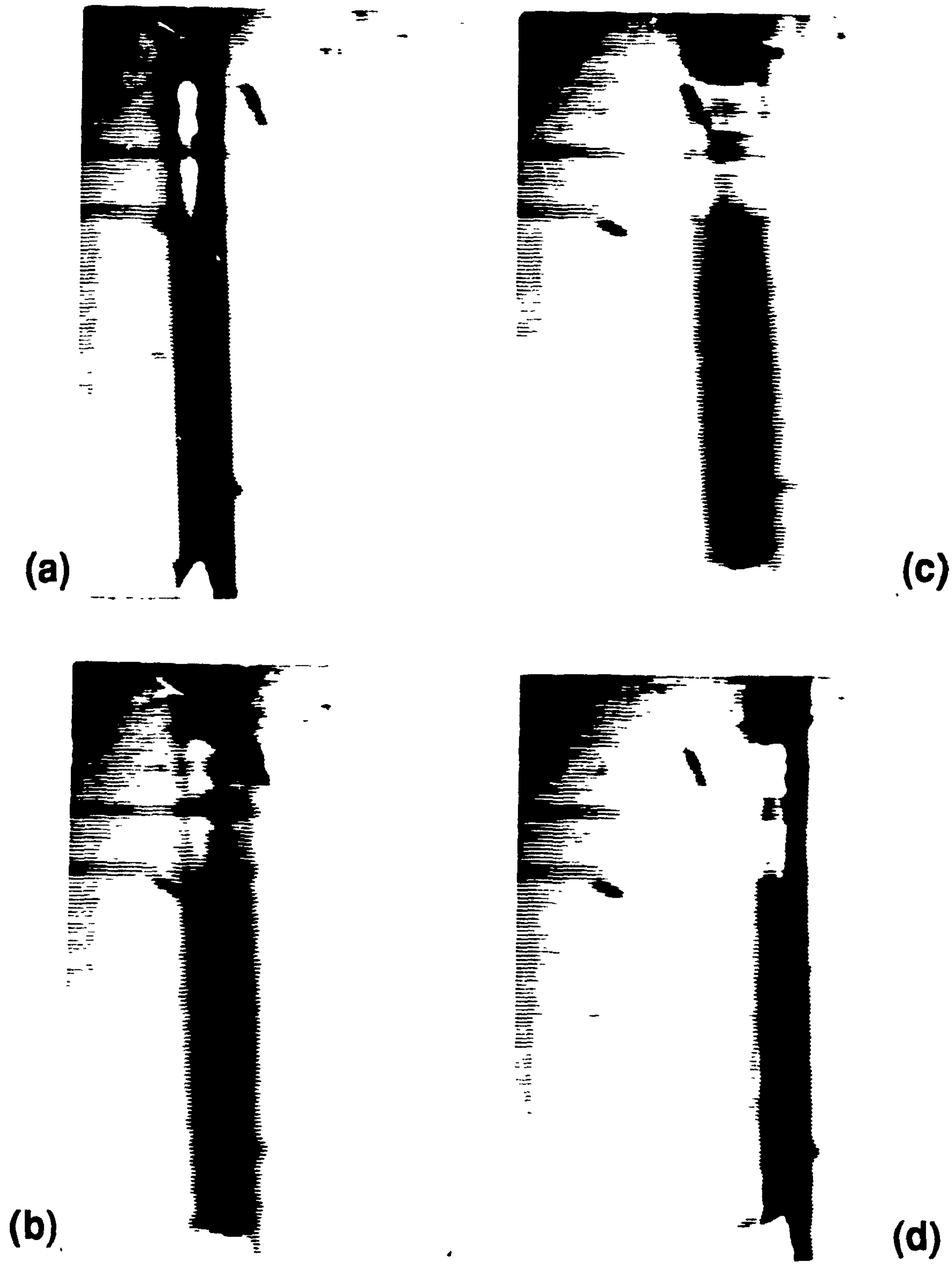

Figure 3.25 *Photographs of PZT coated optical fibre vibrating at 4.3Hz with a peak to peak deflection (from (a) to (d)) of ~800μm.*

3.5 Patterning by a Laser Ablation Technique:

3.5.1 Introduction:

It has been mentioned earlier that the piezoelectricity of the PZT thin film can be achieved by a radial poling which is to apply a voltage across the inner and outer electrodes at a proper elevated temperature [24], [26]. However, an axial poling, that is to apply a voltage across the two pairs of interdigital transducer (IDT) as shown in Figs.3.26a and 3.26b of the outer electrode is an alternative [46]. The radial poling is preferred for ultrasonic applications which require the fundamental resonant frequency of the thin piezoelectric PZT film as described in sections 3.3 and 3.4. High frequency (>100MHz) single mode optical fibre modulators can be constructed due to the fact that the focussed acoustic waves perturb the refractive index and thus change the phase of the guided light wave. The axial poling is favorable for many other applications including low frequency (<10MHz) single mode optical fibre phase modulators explained below.

The phase modulator is a vital component for fibre optic interferometric types of sensors applications. PZT coated optical fibres satisfy nearly all its basic requirements such as small size, light weight and good flexibility. An additional requirement for a good phase modulator is to be efficient. That means to use a minimum electric voltage and power to achieve a 180° phase change for the guided light inside the fibre core of a single mode optical fibre. If the spacing between the comb-like interdigital transducer fingers as shown in Fig.3.26a can be made small and the PZT coating length is long enough, high efficiency phase modulators could be made. The operation principle is that if the direction of the applied electric field aligns with the net electric dipole direction of the PZT film, the PZT coated fibre will extend. Otherwise it will contract. Either extension or contraction will change the fibre length and thus the phase of the guided light wave. Thus the length perturbation and not the focussed acoustic waves mentioned above is the source of the phase modulation here. It is noted that the net electric dipole direction is, in fact, the direction of the electric field during the poling process.

Figure 3.26b shows a geometry for a deflection application. We assume that two pairs of IDT are made in the opposite side of a PZT coated fibre and both are axially poled. If applied voltages can make one side of PZT expand and the opposite side contract, the optical fibre will be bend toward the contracted side. The bending will depend on the magnitude of the applied voltage, which means an electronically controllable deflection.

Standard photolithographic techniques to fabricate a fine IDT pattern on a cylindrical surface with a radius of curvature less than a few hundred μm presents many difficulties. It is one of the purposes of this thesis to develop a technique to fabricate such an IDT pattern on the thin optical fibres. We propose to use a laser ablation technique using a high energy pulsed Nd:YAG laser.

3.5.2 Ablation Process:

We used a Q-switched Nd:YAG laser to perform the ablation. The repetition rate was 0.5Hz. The laser energy was ~0.5J/pulse with a pulse width of about 15ns. It corresponded to a peak power of ~33MW. The molecules of the top metallic layer were heated by the absorbed laser beam energy and vaporized instantly causing them to be released from the bulk of the outer electrode.

3.5.3 Preliminary Work:

When executing laser ablation it is important to know how to control the energy density of the pulsed laser beam. The main factors are pulse width, pulse repetition rate, voltage supplied to the controller, beam current and depth of focus of the lens used in the delivery path. The laser which we had access to did not have a variable beam current nor a variable pulse width. The largest repetition rate was 0.5Hz. Therefore, we controlled the energy density by varying the voltage supplied and the depth of focus.

3.5.4 Beam Path:

The initial beam path consisted simply of mirrors to direct the beam on the target and a lens to focus the beam to a small spot, since the beam diameter coming out of the laser was approximately 1cm. We used an aluminum coated glass plate as the target. Minimizing the spot size was the first objective. With this initial set-up, the minimum spot size was approximately 90μm.

Since the spot size was much too large for our application, we decided to add a beam expander in the beam path. This would increase the angle of deflection from the focussing lens thereby reducing the spot size. Remember that spot size is defined as the area where the metal is completely ablated out. The smallest spot obtained with this set-up was 15μm diameter. To produce a line, we simply overlapped the spots. Figure 3.27 is a schematic of the final beam path used in the experimental set-up.

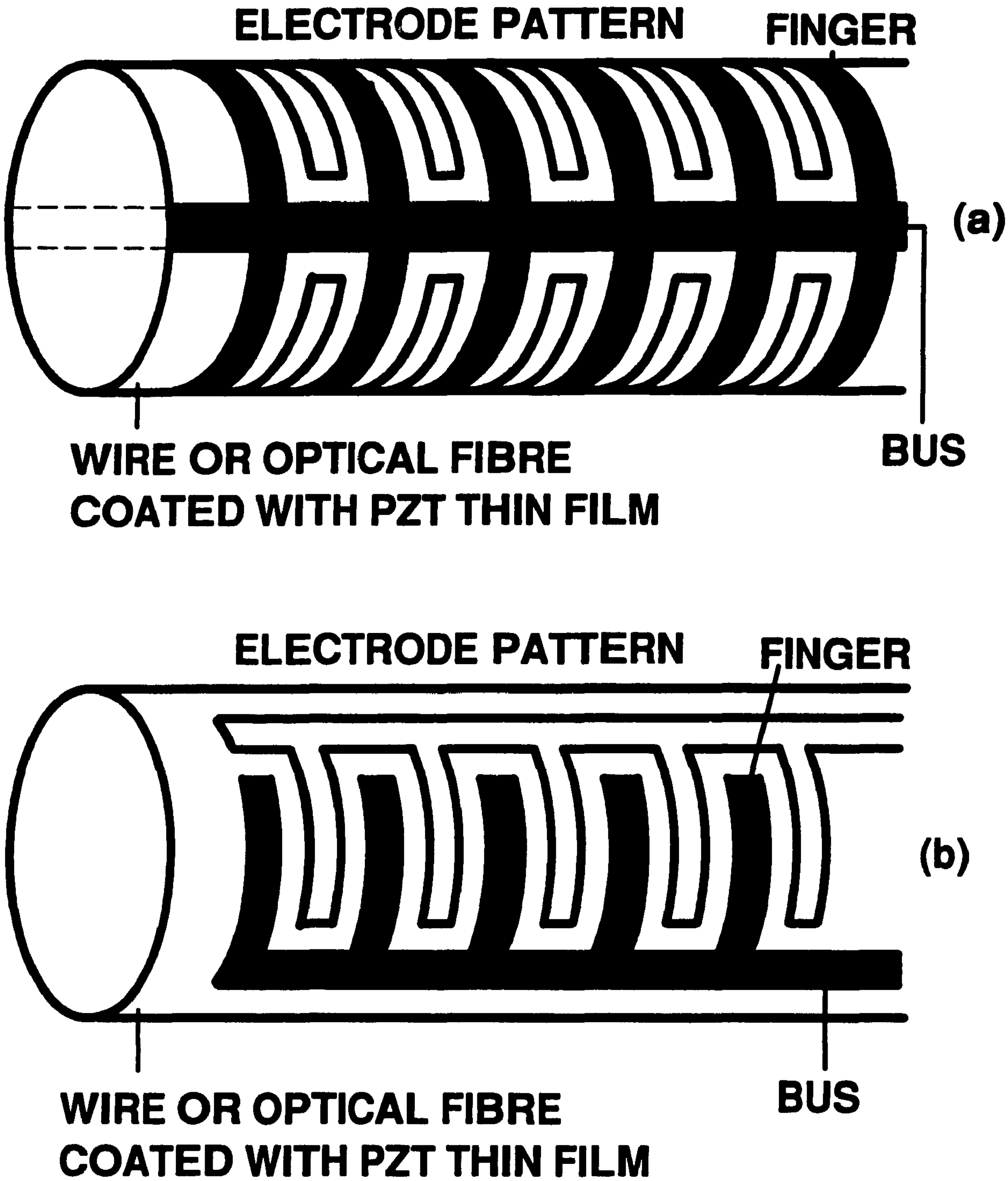

Figure 3.26 *Two interdigital transducer patterns on the outer electrode of a cylindrical lens, (a) pattern for phase modulator and (b) pattern for deflection applications.*

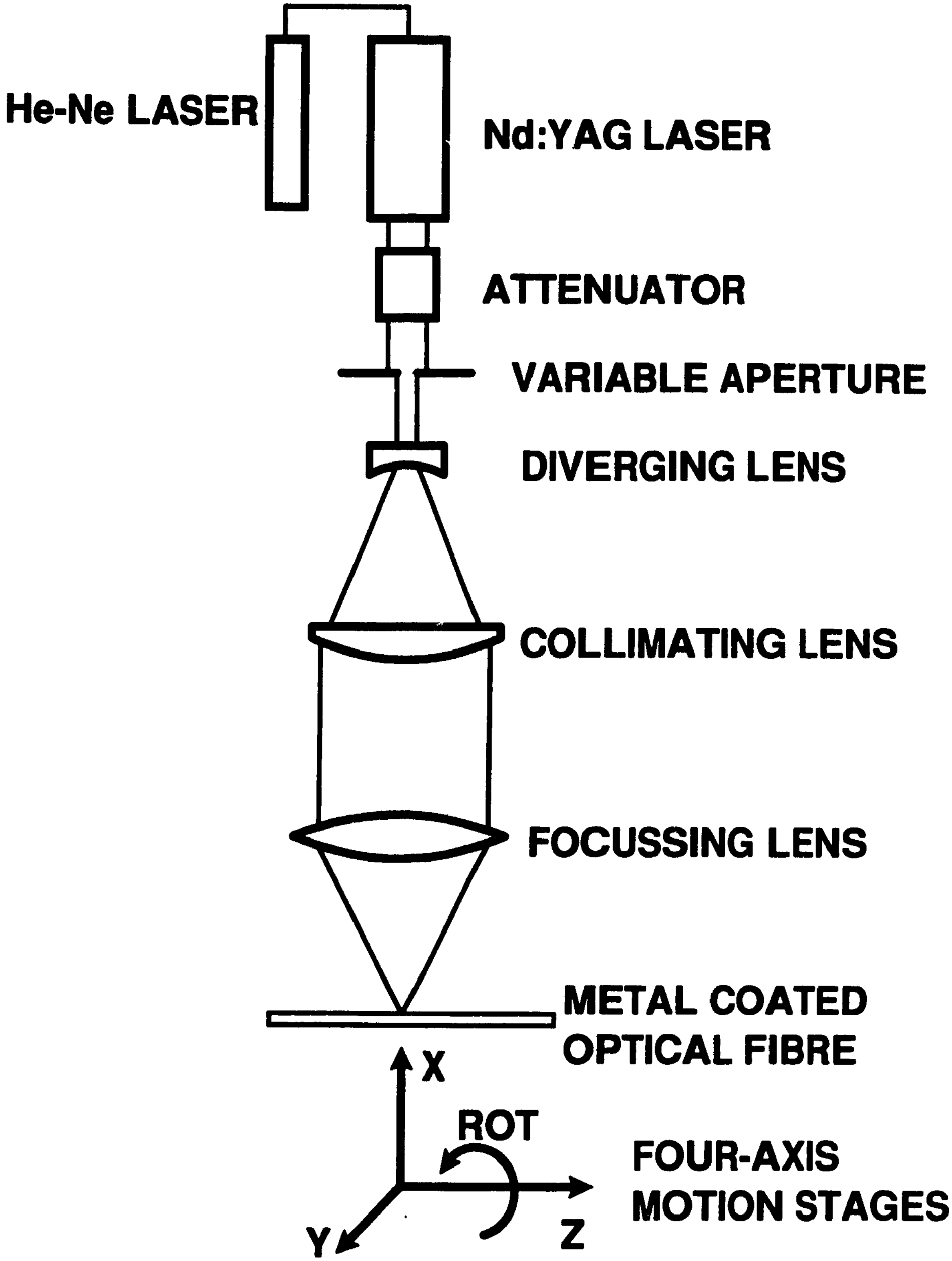

Figure 3.27 *Schematic of the beam path used in the laser ablation experiments.*

3.5.5 Motion Stages and Process Control:

The fibre holder consisted of two chucks used in fibre couplers. The two chucks were held taut and were fixed in line with the axis of a stepping motor. This stepping motor therefore controlled the rotation of the fibre. This system was fixed to a mechanical translation stage coupled to another stepping motor. Both stepping motors were controlled by an IBM PC. The chip used was the CY512 Intelligent Positioning Stepper Motor Controller. A basic program called "stepper" controlled the card This program enabled us to program the entire ablation process including the firing of the laser. Two other manual translation stages were used to position the fibre. A schematic of the motion stages and their computer control is shown in Fig.3.28. A viewing microscope was set-up at an angle to inspect the ablation as it was going on. Figure 3.29 is a photograph of the motion stages and viewing microscope.

3.5.6 Ablation Results:

We used an optical fibre coated with an aluminum outer electrode. Using the above mentioned set-up, we were able to produce an IDT with fingers which were 20μm wide and whose spacing between the fingers was 40μm. We were limited to 180° on the optical fibre because once the infra-red light has ablated the metal on one side, it travels through the glass fibre and ablates the metal on the other side, therefore producing two IDT's simultaneously. This means that the length of the fingers was limited to about 50μm. Figures 3.30a and 3.30b are photographs of the pattern on the fibre taken by a scanning electron microscope.

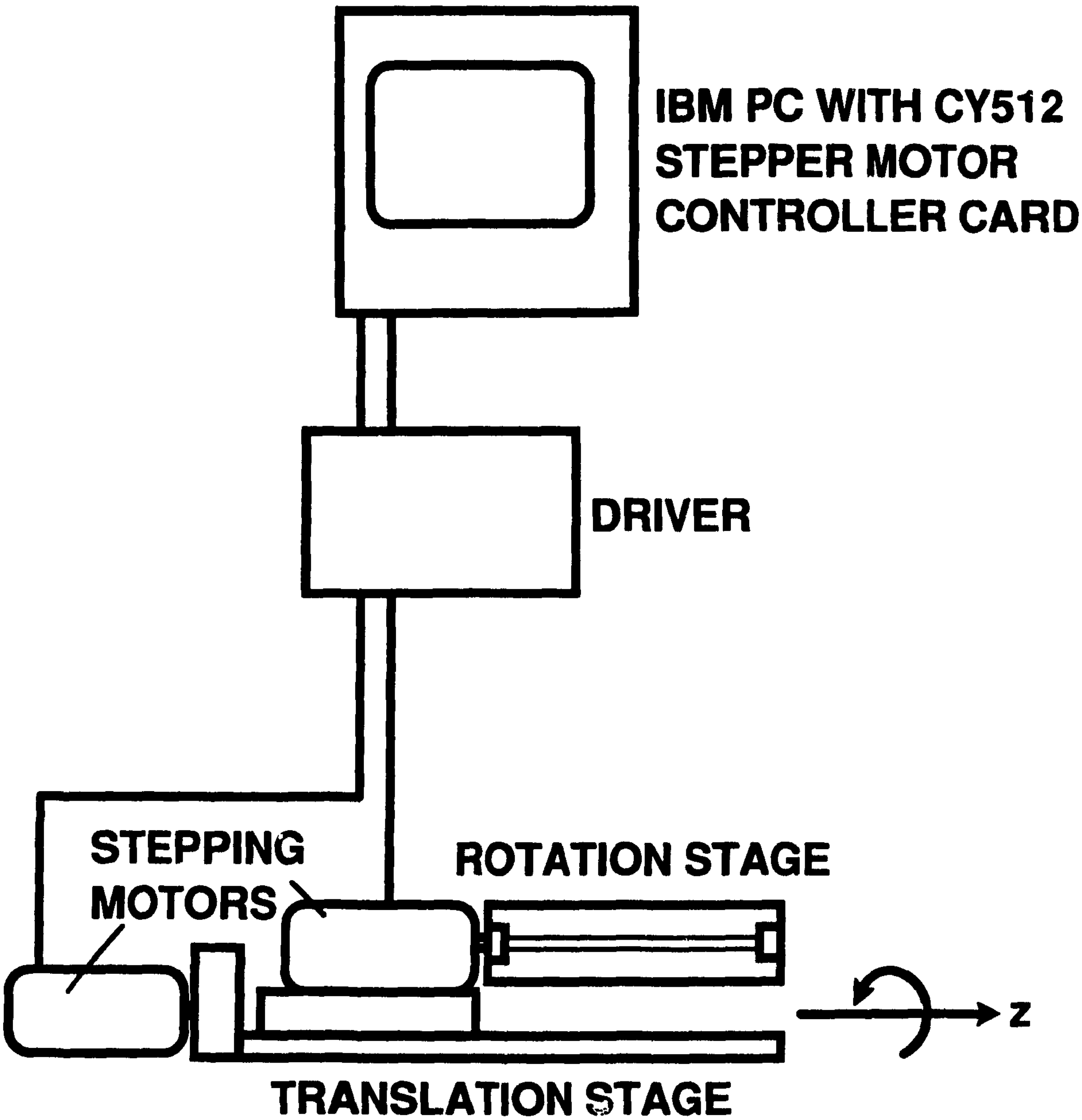

Figure 3.28 *Schematic of the computer controlled motion stages used in the laser ablation experiments.*

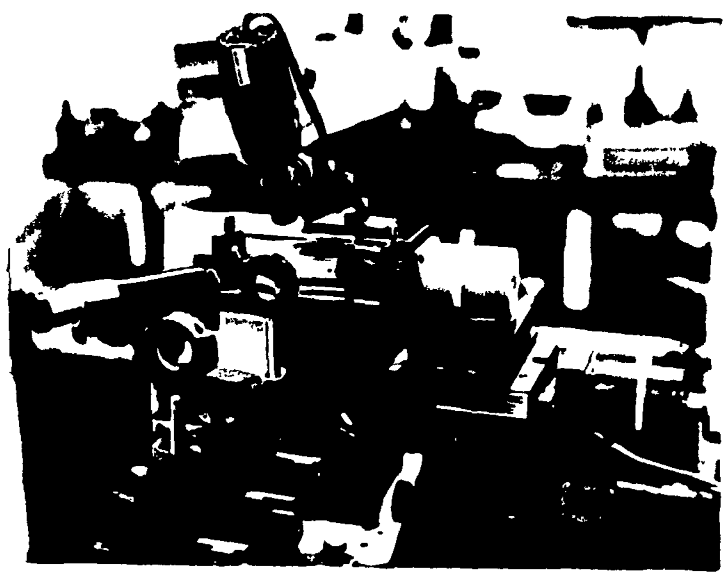

Figure 3.29 *Photograph of the motion stages and viewing microscope used in the laser ablation experiments.*

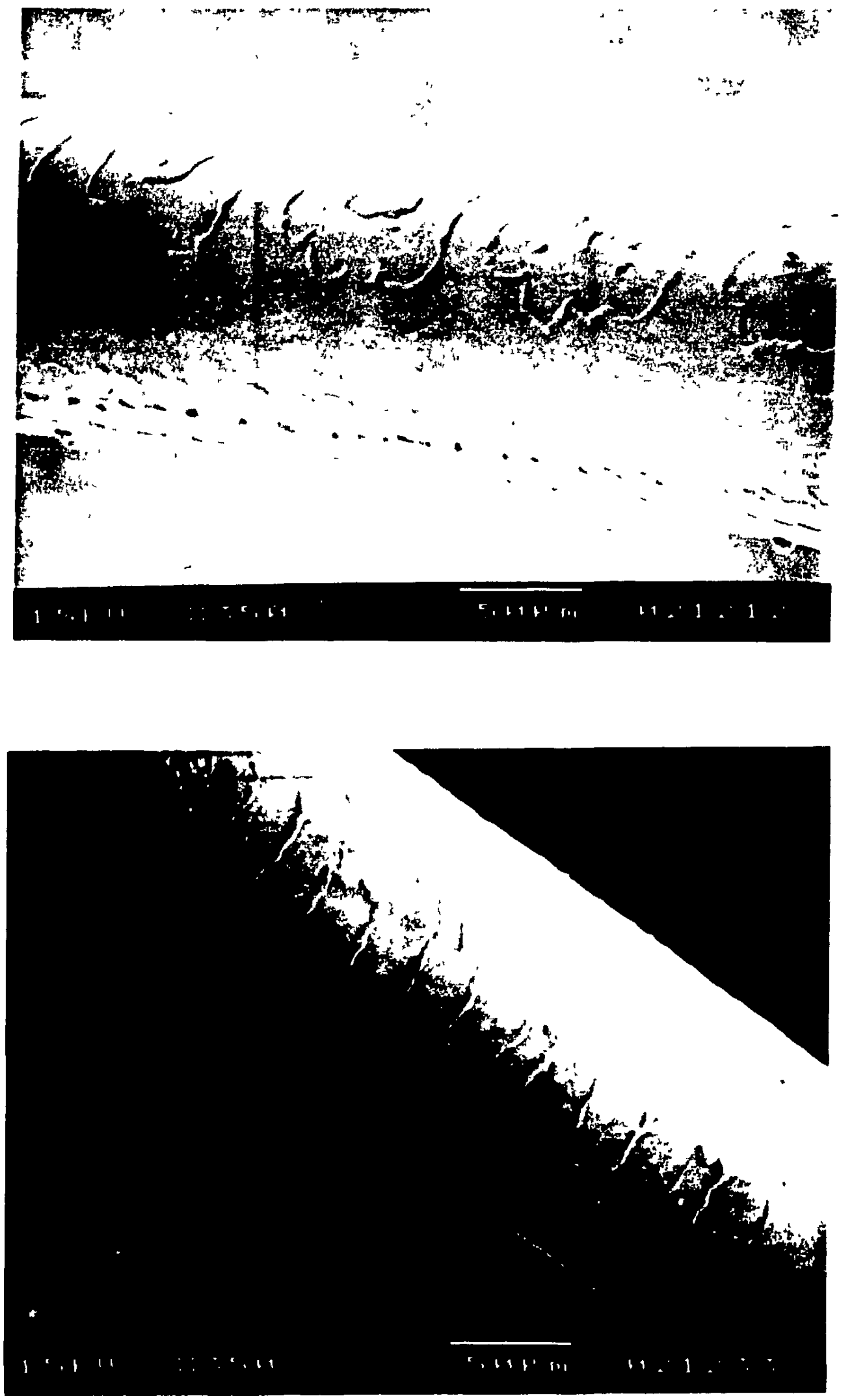

(a)

(b)

Figure 3.30 *Scanning electron microscope photographs of an IDT pattern on an optical fibre, (a) one of the buses and (b) the fingers.*

3.6 Potential applications:

As mentioned previously, PZT thin piezoelectric films coated on optical fibres act as focussed ultrasonic transducers which enable PZT coated optical fibres to be potentially used as high frequency (>100MHz) phase modulators for telecommunication applications. This geometry has already been exploited using a ZnO [17] piezoelectric film. However, it is relatively simple and convenient to use the sol-gel method [22] to fabricate PZT film which has high piezoelectric coupling constant.

Furthermore, the PZT coating length can be very long. If a proper IDT, as shown in Fig.3.26a, can be fabricated along the fibre coated with PZT film, even with a low voltage across the electrode pair of the IDT, the low frequency phase modulators (<10MHz), due to the length perturbation, for optical fibre sensor applications could be efficient and attractive as compared to the PVDF film coated optical fibre devices [15], [16]. In addition, an electronically controllable deflector may be also constructed with an outer electrode having an IDT as shown in Fig.3.26b. The other applications for the proposed geometry are miniature ultrasonic transducers.

3.7 Summary:

The fabrication and evaluation of a type of cylindrical lens made of PZT thin films deposited on optical fibres were presented. The PZT films were produced by Queen's University using a sol-gel process. Focussing mechanisms have been confirmed using a PZT coated alumel wire. A pulse-echo transmission measurement was used to demonstrate that miniature ultrasonic transducers are possible. Using a computer controlled Nd:YAG laser ablation set-up, an interdigital transducer pattern with fingers 20μm wide was successfully produced on an optical fibre. This pattern could produce axial strains along the fibre, making it bend. Optical fibre deflection up to 0.8mm was induced using a non-uniform PZT coating on the fibre.

Chapter 4: Conclusion

We have presented two novel ultrasonic lenses, that is, two lens geometries that focus acoustic waves. The first is a rod with a graded acoustic velocity profile in the radial direction. Following an optical analogy we name them acoustic graded-index (GRIN) lenses. The electron probe microanalyses, optical refractive index measurements, acoustic velocity measurements carried out by a 225MHz line-focus beam scanning acoustic microscope have been used to characterize the GRIN rods. It has been demonstrated that we can design, fabricate and verify the performance of GRIN lenses having different profiles. At present, the length of the GRIN rod made by MCVD method can be up to 40cm. At low frequencies, these GRIN rods with a proper cladding can be used as long acoustic buffer rods [14]. One of the potential application is to monitor the properties of molten metals [47].

It has been shown conclusively that longitudinal acoustic rays travelling in the rod will follow a sinusoidal path if the velocity profile is close to parabolic. This phenomenon was explained using an acoustic ray theory. We also showed that for the 17% GeO_2 doped GRIN rod as shown in Fig.2.12 the ray theory approximation is valid if the lens aperture is larger than 25 acoustic wavelengths. Such rods can be used as a lens having planar surfaces to focus the acoustic energy. Again, due to the experimental limitations, only longitudinal wave focussing was demonstrated. However, from our theory, we believe that shear acoustic waves will behave similarly to longitudinal acoustic waves in GRIN rods.

Since the liquid does not support shear acoustic waves, in order to observe shear waves, the water bath in the Schlieren set-up must be replaced by a solid and optically transparent isotropic medium with a high photoelastic constant. This task will be very important and interesting future work. However, we have learned through [48] that a small company in Tucson, Arizona, called Isotec Limited Partnership, fabricates GRIN blanks as shown in Fig.4.1 by fusing successive layers of glass with different indices of refraction, then heat treating to eliminate interfaces and provide a smooth index gradient [49], [50]. These blanks could be used to verify the focussing of shear and even surface acoustic waves [51], if the acoustic velocity profile follows the shape of the index of refraction profile as shown in Fig.4.1.

It is noted that the GRIN rod can be considered as a phase rod (or plate). It means that we may use a specific acoustic velocity profile to change the phase of the propagating wave inside the rod. Therefore, the acoustic profiles of those buffer rods used for the spherical [1] and cylindrical [2] concave lenses and those substrates used for planar lenses [4]-[9] could be designed in a way to improve their performance. For example, acoustic Fresnel zone plates (or lenses) [4]-[6] may be simply achieved by designing an acoustic velocity profile which satisfies the "Fresnel zone plate" conditions. Therefore, it is also suggested to conduct future work on an acoustic Fresnel lens made of a rod with a proper length and a proper acoustic velocity profile (dashed lines) as shown in Fig.4.2. In Fig 4.2 the relation of the radii of the successive zones are chosen as

$$r_n = \sqrt{\frac{n\lambda_w}{2}\left(F + \frac{n\lambda_w}{8}\right)} \qquad (n = 1,2,3,.....) \tag{4.1}$$

where F is the focal length and λ_w is the wavelength in water contacting the lens. The acoustic frequency f, velocity (V_1 and V_2) and the length (L) of the rod must satisfy the following condition:

$$2\pi f L\left(\frac{1}{V_1} - \frac{1}{V_2}\right) = (2m+1)\pi \qquad (m = 0,1,2,.....) \tag{4.2}$$

The second lens geometry studied was cylindrical. In fact, it is the thin piezoelectric lead-zirconate-titanate (PZT) film coated optical fibres and alumel wires. This PZT thin film has been fabricated and provided by Professor M. Sayer's research team. A sol-gel technology [22] which is simple and economical was used. We have demonstrated the focussing behaviors of these PZT films, the ultrasonic measurements of miniature transducers, and electronically controllable deflection. A novel laser ablation technique was developed to produce an interdigital transducer (IDT) pattern with a 20μm resolution on the outer electrode of the thin optical fibre. Such IDT fabricated on PZT coated optical fibres will improve the efficiency of the deflection, extension and contraction of the PZT coated optical fibres. The extension and contraction mechanism enable us to use the PZT coated single mode optical fibre as phase modulators.

At the present time, since there is no commercially available metal coated single mode optical fibre, the phase modulator application is not demonstrated in this thesis. Thus, to produce the PZT coating on single mode optical fibre is suggested to be the first priority for the future of this research. In addition to the proposed phase modulators, PZT coated single mode optical fibres can be also used as in-line optical fibre frequency shifters [43] and electric field sensors [44].

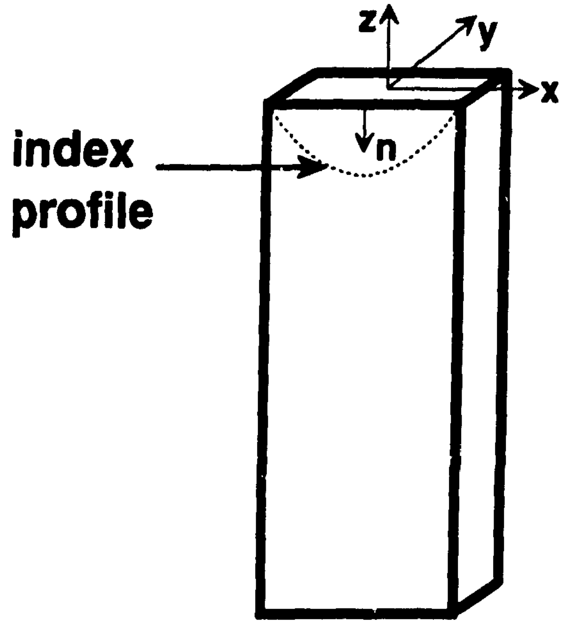

Figure 4.1 *Schematic of GRIN blanks.*

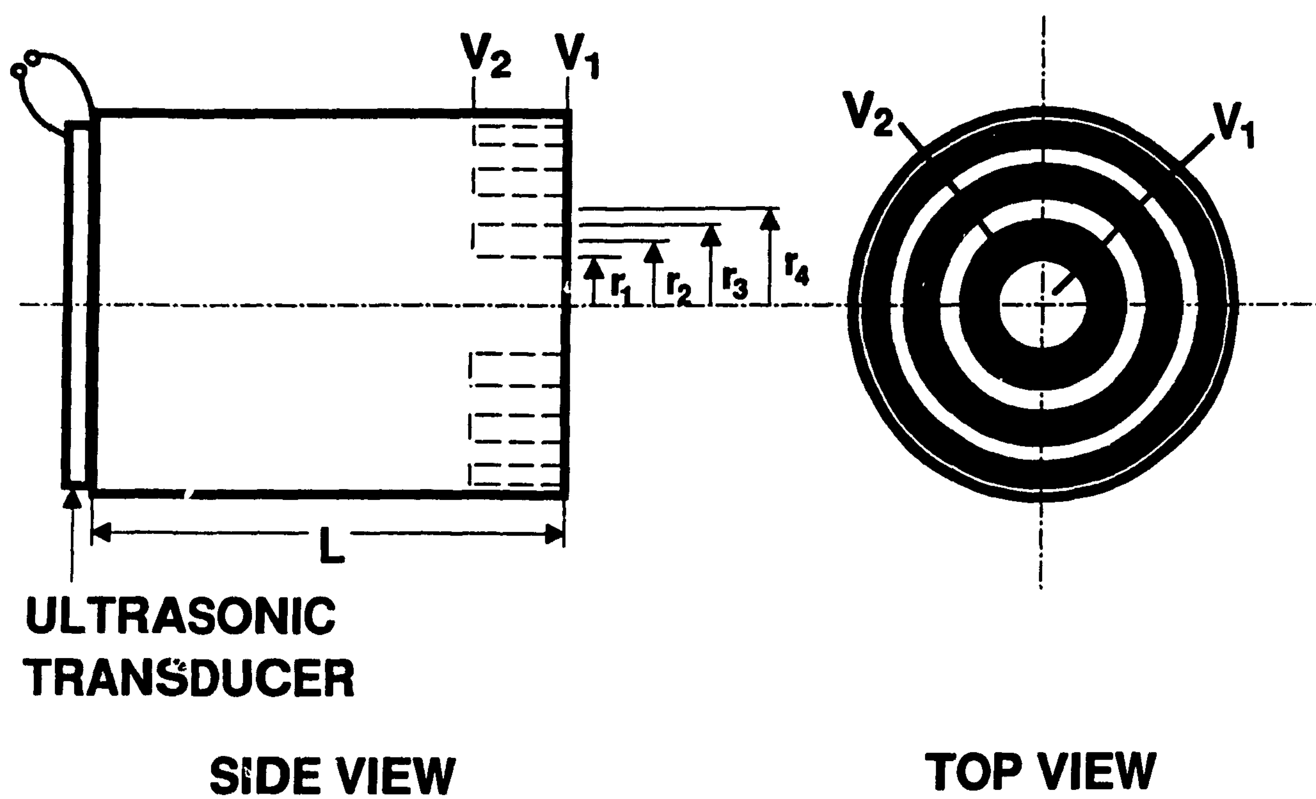

Figure 4.2 *Schematic of acoustic Fresnel lens made of a rod with a specified acoustic velocity profile.*

REFERENCES

[1] R.A. Lemons and C.F. Quate, "Acoustic microscopy", in *Physical Acoustics*. W.P. Mason and R.N. Thurston eds, New York:Academic Press, 1979, Vol.14, pp.2-92.

[2] Special issue on Acoustic Imaging, Proc. IEEE, Vol.67, pp.449-704, 1979.

[3] J. Kushibiki and N. Chubachi, "Material characterization by line-focus-beam acoustic microscope", IEEE Trans. Sonics and Ultrason., Vol.SU-32, pp.189-212, 1985.

[4] G. Chao, B.A. Auld and D.K. Winslow, Proc. IEEE Ultrasonics Symp., pp.140-141, 1972.

[5] S.A. Farnow and B.A. Auld, "Acoustic Fresnel zone plate transducers", Appl. Phys. Lett., Vol.25, pp.681-682, 1983.

[6] K. Yamada and H. Shimizu, "Planar-structure focusing lens for acoustic microscope", Proc. IEEE Ultrasonics Symp., pp.755-758, 1985.

[7] K. Toda and Y. Murata, "Acoustic focusing device with an interdigital transducer", J. Acoust. Soc. Am., Vol.62, pp.1033-1036, 1977.

[8]. G.W. Farnell and C.K. Jen, "Microscope lens using conversion of Rayleigh to compressional waves", Proc. IEEE Ultrasonics Symp., pp.673-676, 1980.

[9] K. Kikuchi, T. Nakamoto, S. Shiokawa, T. Moriizumi and T. Yasuda, "Ultrasonic imaging system using interdigital transducer", Proc. IEEE Ultrasonics Symp., pp. 618-622, 1982.

[10] B.A. Auld, *Acoustic Fields and Waves in Solids*. New York: John Wileys and Sons, 1973, Vol.I, Chap.4, pp.101-134.

[11] E.W. Marchand, *Gradient Index Optics*. New York: Academic Press, 1978.

[12] T. Uchida, M. Furukawa, I. Kitano, K. Koizumi and H. Matsumura, "Optical characteristics of a light-focusing fiber guide and its application", IEEE J. Quantum. Elect., Vol.QE-6, pp.606-612, 1970.

[13]. C.K. Jen, Z. Wang, A. Nicolle, C. Neron, E.L. Adler and J. Kushibiki, "Acoustic graded-index lenses", submitted to Appl. Phys. Lett., Feb. 1991.

[14] C.K. Jen, C. Neron, E.L. Adler, G.W. Farnell, J. Kushibiki and K. Abe, "Long acoustic imaging probes", to appear in Proc. IEEE Ultrasonics Symp., Hawaii, Dec.5-7, 1990.

[15] E.F. Carome and K.P. Koo, "PVF_2 phase shifters and modulators for fiber optic sensor systems", Proc. IEEE Ultrasonics Symp., pp.710-712, 1980.

[16] C.C. Ku, R.P. Depaula, J. Jarzynski and J.A. Bucaro, "High frequency response of a single mode fiber optical phase modulator utilizing a piezoelectric plastic jacket", SPIE, Vol.412, pp.178-184, 1983.

[17] D.S. Czaplak, J.F. Weller, L. Goldberg, F.S. Hickernell, H.D. Knuth and S.R. Young, "AO phase modulator for single mode fibers using cylindrical ZnO transducers", Proc. IEEE Ultrasonics Symp., pp.491-493, 1987.

[18] D.B. Patterson, A.A. Godil, G.S. Kino and B.T. Khuri-Yukub, "Detachable 400 MHz acousto-optic phase modulator for a single mode optical fiber", Opt. Lett., Vol.14, pp.248-251, 1989.

[19] H.F. Taylor, "Acousto-optic modulators for single mode fibers", IEEE J. of Lightwave Technology, Vol.LT-5, pp.990-992, 1987.

[20] R.H. Stolen and R.P. Depaula, "Single mode fiber components", Proc. IEEE, Vol.75, pp.1498-1511, 1987.

[21] F.S. Hickernell, C.M. Reese, H.D. Knuth T.P. Emmons, J.F. Weller and D.S. Czaplak, "Thin film zinc oxide bulk wave transducer structures for acousto-optic phase modulation of single mode fibers", Proc. IEEE Ultrasonics Symp., pp.715-718, 1986.

[22] G. Yi, Z. Wu, and M. Sayer, "Preparation of $Pb(Zr,Ti)O_3$ thin film by sol gel processing: electrical, optical, and electro-optic properties", J. Appl. Phys., Vol.64, pp.2717-2724, 1988.

[23] G. Yi, Z. Wu, K. Screenivas, M. Sayer, C.K. Jen and G. Perluzzo, "Ultrasonic experiments with lead zirconate titanate thin films fabricated by sol gel processing", Elect. Lett., Vol.25, pp.307-309, 1989.

[24] G. Yi, M. Sayer, Z. Wu, C.K. Jen and J.F. Bussiere, "Piezoelectric lead zirconate titanate coatings on metallic wires", Elect. Lett., Vol.25, pp.907-908, 1989.

[25] C.K. Jen, C. Neron, G. Yi, M. Sayer, M. Castonguay and J.D.N. Cheeke, "Acoustic microcope lenses employing PZT thin film transducers", Materials Sci. and Eng., Vol.A122, pp.21-25, 1989.

[26] G. Yi, M. Sayer, C.K. Jen, J.C.H. Yu and E.L. Adler, "Coaxial thin film transducers based on PZT", Proc. IEEE Ultrasonics Symp., pp.1231-1235, 1989.

[27] D.T. Moore, "Gradient-index optics: a review", Appl. Opt., Vol.19, pp.1035-1038, 1980.

[28] T. Miyazawa, K. Okada, T. Kubo, K. Nishizawa, I. Kitano and K. Iga, "Aberration improvement of Selfoc lenses", Appl. Opt., Vol.19, pp.1113-1116, 1980.

[29] T. Yamagishi, K. Fujii and I. Kitano, "Fabrication of a new gradient-index rod lens with high performance", J. Non-Cryst. Solids, Vol.47, pp.283-286, 1982.

[30] S. Ohmi, H. Sakai, Y. Asahara, S. Nakayama, Y. Yoneda and T. Izumitani, "Gradient-index rod lens made by a double ion-exchange process", Appl. Opt., Vol.27, pp.496-499, 1988.

[31] M. Yamane, A. Yasumori, M. Iwasaki and K. Hayashi, "Graded index materials by the sol-gel process", SPIE, Vol.1328, pp.133-144, 1990.

[32] T.M. Che, J.B. Caldwell and R.M. Mininni, "Sol-gel derived gradient index optical materials", SPIE, Vol.1328, pp.145-159, 1990.

[33] S. Konishi, "Sol-gel derived r-GRIN doped-silica lenses", SPIE, Vol.1328, pp.160-166, 1990.

[34] C.K. Jen, C. Neron, J.F. Bussiere, L. Li, R. Lowe and J. Kushibiki, "Characterization of cladded glass fibers using acoustic microscopy", Appl. Phys. Lett., Vol.55, pp.2485-2487, 1989.

[35] C.K. Jen, C. Neron, J.F. Bussiere, K. Abe, L. Li, R. Lowe and J. Kushibiki, "Acoustic microscopy of cladded optical fibers", Proc. IEEE Ultrasonics Symp., pp.831-835, 1989.

[36] C.K. Jen, "Similarities and differences between fiber acoustics and fiber optics", Proc. IEEE Ultrasonics Symp., pp.1128-1133, 1985.

[37] W.G. French, R.E. Jaeger, J.B. Macchesney, S.R. Nagel, K. Nassau and A.D. Pearson, "Fiber preform preparation", in *Optical Fiber Telecommunications*. S.E. Miller and A.G. Chynoweth eds, New York: Academic Press, 1979, pp.233-261.

[38] T. Sharpe, *Research Techniques in Nondestructive Testing*. New York: Academic Press, 1973, Vol.II, pp.317-321.

[39] M. Redwood, *Mechanical Waveguides*. New York: Pergamon, 1960, Chap.9, pp.191-207.

[40] C.K. Jen, A. Safaai-Jazi, J.C.H. Yu, C. Neron, G. Perluzzo and Z. Wang, "Long acoustic buffer rods with low spurious signals", Presented at Review of Progress in Quantitative NDE Conference, San Diego, California, July 15-20, 1990.

[41] D.A. Pinnow, G.D. Robertson Jr., and J.A. Wysocki, "Reductions in static fatigue of silica fibers by hermetic jacketing", Appl. Phys. Lett., Vol.34, pp.17-19, 1979.

[42] L. Li, G. Wylangowski, D.N. Payne, R.D. Birch, "Broadband metal/glass single-mode fibre polarisers", Elect. Lett., Vol.22, pp.1020-1022, 1986.

[43] H.F. Taylor, "Acoustooptic phase and frequency shifters for single mode fibers", SPIE, Vol.719, pp.87-91, 1986.

[44] M. Imai, H. Tanizawa, Y. Ohtsuka, Y. Takase and A. Odajima, "Piezoelectric copolymer jacketed single-mode fibers for electric-field sensor application", J. Appl. Phys., Vol.60, pp.1916-1918, 1986.

[45] J.-D. Aussel, J.-P. Monchalin, J.F. Bussiere, D. Malenfant, P. Roy, J.-F. Cusson, C. Carnois, "A PC-based data acquisition and signal processing package for non-destructive testing", CSNDT Journal, Vol.10, pp.18-27, 1989.

[46] K. Nakamura and H. Shimizu, "Poling of ferroelectric crystals by using interdigital electrodes and its application to bulk-wave transducers", Proc. IEEE Ultrasonics Symp., pp.527-530, 1983.

[47] C.K. Jen, Z. Wang, J.F. Bussiere, A. Nicolle and E.L. Adler, "Acoustic waveguiding rods of graded velocity profiles", to be presented in Ultrasonics Int'l Conf., Le Touquet, France, July 1-4, 1991.

[48] L. Belleville, "New process yields designer optics" in Laser Focus World, p.51, Oct. 1990.

[49] R. Blankenbecler, J.J. Hagerty and G.E. Rindone, "Prescribed profile gradient index glasses of macro dimensions and large Δn.", SPIE, Vol.1354, (6 pages), 1990.

[50] J.J. Hagerty, D.N. Pulsifer, "Glass plate fusion for macro-gradient refractive index materials", U.S. Patent No.4,929,065, May 29, 1990.

[51] G.W. Farnell, "Properties of elastic surface waves", in *Physical Acoustics*. W.P. Mason and R.N. Thurston eds, New York:Academic Press, 1970, Vol.6, pp.109-166.